2019-07-01

SNFing Glucose to PASs Mitochondrial Dysfunction: The Role of Two Sensory Protein Kinases in Metabolic Diseases

Kai Li Ong
Brigham Young University

SNFing Glucose to PASs Mitochondrial Dysfunction: The Role of Two Sensory Protein Kinases in Metabolic Diseases

Kai Li Ong

A dissertation submitted to the faculty of
Brigham Young University
in partial fulfillment of the requirements for the degree of

Doctor of Philosophy

Julianne H. Grose, Chair
Kim L. O'Neill
K. Scott Weber
David M. Thomson
Benjamin T. Bikman

Department of Microbiology and Molecular Biology

Brigham Young University

ABSTRACT

SNFing Glucose to PASs Mitochondrial Mitochondrial Dysfunction: The Role of Two Sensory Protein Kinases in Metabolic Diseases

Kai Li Ong
Department of Microbiology and Molecular Biology, BYU
Doctor of Philosophy

Mitochondria is no longer viewed as merely a powerhouse of the cell. It is now apparent that mitochondria play a central role in signaling, maintaining cellular homeostasis and cell fate. Mitochondrial dysfunction has been linked to many human diseases caused by cellular metabolic deregulation, such as obesity, diabetes, neurodegenerative disease, cardiovascular disease and cancer. Eukaryotic organisms have evolved an efficient way in sensing, communicating and responding to cellular stress and regulating mitochondrial activity correspondingly through a complex network of intercommunicating protein kinases and their downstream effectors. This dissertation focuses on the interplay of two of the master metabolic regulators in the cell: AMPK and PASK, and characterization of the functions of their downstream substrates: OSBP and MED13. AMPK is an energy sensing kinase that maintains energy homeostasis in the cell, whereas PASK is a nutrient sensing kinase that regulates glucose partitioning and respiration in the cell. Both kinases play important roles in mitochondrial function and regulation, and deficiency in either kinase has been found to associate with various human pathologies. Further characterization of the cross-talk and molecular mechanisms of both kinases in controlling mitochondrial health and function may aid in the identification of new targets for treating metabolic diseases.

Keywords: AMP-activated Kinase; SNF1; Oxysterol binding protein; OSBP; Osh6; Osh7; ORP5; ORP8; PAS Kinase; Med13; cyclin C; mitochondria function; mitochondria dynamic; mitophagy

ACKNOWLEDGMENTS

I would like to thank my advisor, Julianne Grose, who believed in my ability and gave me the opportunity to come and work with her back in September 2014, which has permanently changed my life. Without her faith in me, I would not be here today. Together we have been through thick and thin, the good times and the hard times, the laughter, the sweat, the blood and the tears. I have learned and grown so much from being in her lab and am forever grateful for her. I also want to give a big thank you to all my amazing committee members, for all their patience, support and guidance; for cheering me on for 5 years and helping me become the scientist I am today. I could not ask for a better committee. I also want to give special thanks to Kim O'Neill, for lifting my spirit whenever I felt discouraged and getting me through hard times from the very beginning. I am forever thankful to all the people that have supported me along the way, either physically, mentally or both—my husband, my mom, my brother, my mentors at BYUH: Shane Gold and Mark Cannon, all the wonderful friends that have been there for me—Evita Weagel, Edwin Velazquez, Stewart Morley, Deborah Johnson, Kiara Vaden, Nidhi Choksi, Ruchira Sharma, Denise Ng, Elise Melhado, Trevor Thurgood, Brooke Cozzens and all the present and past Grose lab members, O'Neill lab members, and the collaborators. I am thankful for everyone in the MMBIO Department who have let me borrow reagents/ instruments here and there in times of need. I am forever grateful for our friendships and grateful that we crossed paths during this time in our lives.

The list of people I would like to thank goes on. I would like to dedicate this work to all of you, because my life would not be the same without you.

TABLE OF CONTENTS

LIST OF FIGURES

LIST OF TABLES

CHAPTER 1: Role of Mitochondrial Dysfunction and Metabolic Diseases

1.1 Introduction

Mitochondria are powerhouses of the cell that generate the energy necessary for all cellular activity in the form of adenosine triphosphate (ATP), a high energy carrying molecule [1]. Although some ATP can be obtained through anaerobic glycolysis, most ATP derives from oxidation of carbohydrates and fatty acids in the mitochondria through a series of reactions in the Kreb cycle and the Electron transport chain (ETC). In addition to generation of cellular energy, mitochondria have also been recognized as an important signaling hub and a critical regulator of apoptosis about 2 decades ago due to two major discoveries: 1) cytochrome c, a protein previously known as only an electron transporter, was found to initiate apoptosis once it is released into the cytosol through association with apoptotic protease activating factors (Apaf) and activating signaling cascade of caspases [2]. 2) The discovery of Bcl-2 family's involvement in apoptotic signaling through controlling the release of cytochrome c into the cytosol [3]. It is now established (and still under rigorous, active research) that mitochondria communicate to the rest of the cells regarding its fitness through many pathways such as the release of metabolites, mitochondrial peptides, reactive oxygen species (ROS), activation of AMPK, changes in inner mitochondria membrane potential, calcium signaling and communication through mitochondria associated membrane (MAMs) [4-7]. Changes in mitochondria dynamic (fission and fusion) ensure delivery of appropriate signal to proper location in the cell, allow mitochondria fitness assessment by quality control mechanisms such as mitophagy and cellular stress adaptation [8, 9]. These mechanisms may function jointly—for instance, decreases in mitochondrial respiratory flux can result in reduced mitochondrial membrane potential, decreased output of ATP (and the corresponding increase in the AMP:ATP ratio), decreased ROS production, and alterations in

other TCA metabolites. These signals can activate AMPK and cause a switch from anabolic metabolism to a catabolic state; AMPK activation promotes mitochondria fission [10], hence mitochondria without adequate membrane potential are dissociated from healthy mitochondria and destroyed through mitophagy [11, 12]; decreases ROS levels thus reducing signaling pathway activation necessary for cell proliferation and metabolic adaptation [4]; decreases TCA metabolites which output may cause reduction in lipid production necessary for cell growth and reduced protein acetylation [5]; and inadequate mitochondria membrane potential also causes a decrease in Ca^{+} uptake hence improper calcium signaling [13]. Under starvation conditions, cells ensure adequate supply of substrates such as amino acids to the TCA cycle through autophagy in an effort to maintain mitochondria membrane potential or risk the release of cytochrome c. With mitochondria's importance to the overall cell health and role in many essential cellular processes, it is not surprising that mitochondrial dysfunction can lead to many diseases at the tissue and organismal level. Mitochondrial dysfunction has been associated with many diseases such as sarcopenia, type 2 diabetes mellitus (T2DM), neurodegenerative disease, cardiovascular disease, liver and kidney disease and cancer [14-17]. Furthermore, their regulation has been shown to be important in longevity in many different organisms from yeast to man [18, 19]. With mitochondria being at the center of cellular metabolism and signaling pathways, the difficulty in understanding and treating human diseases caused by mitochondrial dysfunction arises from the complex relationships between mitochondria and other cellular processes. Understanding of mitochondrial protein-protein signaling network, types of mitochondrial stressors, their interplay with mitochondrial dynamics and the mechanisms that orchestrate how cells respond to them is critical in better understanding the transition between health and disease.

1.1.1 Role of AMPK in mitochondrial function and metabolic diseases

AMP-activated kinase (AMPK) is an evolutionarily conserved protein kinase that regulates energy homeostasis in the cell. Cells need to manage their energy consumption depending on nutrient availability and on their capacity to produce ATP constantly by changing their metabolism, and AMPK is the key player in this process. AMPK is a heterotrimeric complex composed of a catalytic α-subunit and two regulatory subunits, β and γ (Figure 1-1 [20]). Humans possess multiple genes that encode for each subunit which results in different isoforms of AMPK complexes: two α-subunits, α1 and α2 encoded by the gene PRKAA1 and PRKAA2 [21]; two β-subunits, β1 an β2 encoded by the gene PRKAB1 and PRKAB2 [22]; and three γ-subunits, γ1, γ2 and γ3, encoded by the gene PRKAG1, PRKAG2 and PRKAG3 [23]. Each AMPK complex is only composed of one α, one β and one γ subunit at any given time, which gives rise to 12 possible combinations of AMPK complexes. Different complexes of AMPK seem to be functionally redundant with differences in tissue/ organ dependent expression levels [24]. When ATP is used in cellular processes, it is broken down into ADP and can be further broken down into AMP. AMPK senses changes in cellular AMP/ADP: ATP ratio by the binding of AMP, and to a lesser extent ADP to the γ subunit, which stimulates AMPK activity [25-27]. Binding of AMP/ ADP to the γ subunit promotes Thr172 phosphorylation in the activation loop in the kinase domain by upstream kinases such as LKB1 and protects Thr172 from dephosphorylation by protein phosphatases. Activation of AMPK can also be achieved in a non-AMP/ ADP sensitive fashion, by the phosphorylation of calcium-sensitive kinase CAMKK2 at Thr172.

AMPK has been identified as a central integrator of mitochondrial homeostasis by controlling multiple aspects of the mitochondrial life cycle: from mitochondrial biogenesis and

dynamics, to healthy removal by mitophagy [28]. Almost every mitochondrial insult or defect activates AMPK and given the function of mitochondria as the major source of ATP production in the cell, it makes perfect sense that AMPK, an energy homeostasis regulator in the cell would engage downstream effectors to ensure optimal mitochondrial function. AMPK promotes mitochondrial biogenesis through direct and indirect regulation of the peroxisome proliferator-activated receptor-γ co-activator 1 (PGC1) family— by affecting expression level of PGC1α [29], direct phosphorylation [30] or through AMPK-dependent modulation of p38 MAPK1 [31], HDAC5 [32, 33] or SIRT1 [34]. Understanding the effect of AMPK on mitochondrial biogenesis has important implications in multiple pathological states and processes, including Duchenne muscular dystrophy [35], mitochondrial myopathy[36], exercise capacity [37], muscle regeneration after injury [38] and protection from age-related myopathies [39]. AMPK is also a direct and crucial regulator of mitochondrial dynamics. As mentioned above, AMPK regulates a core component of the mitochondria fission pathway—mitochondrial fission factor (MFF) [40] through direct phosphorylation at Ser155 and Ser172 of MFF and promote DRP1 (a protein that mediates constriction of mitochondria during fission [41]) localization at mitochondria [10]. Therefore, AMPK controls the shape of the mitochondrial network in response to stress, in which fusion of mitochondria maximizes generation of ATP [42], distributes lipids and protects mitochondria from mitophagy [12, 43]; fission of mitochondria facilitates mitophagy of mitochondrial fragments lacking proper membrane potential, as well as allows timely apoptosis when necessary [44]. AMPK also regulates other pathways that control autophagy/ mitophagy through multiple downstream substrates such as mTORC1, ULK1, ATG9 and VPS34 to remove damaged/ depolarized mitochondria [45-48]. With AMPK's essential role in regulating energy

metabolism and mitochondria function, AMPK is currently at the center stage of interests in studies of diabetes and related metabolic diseases, as well as cancer [49, 50].

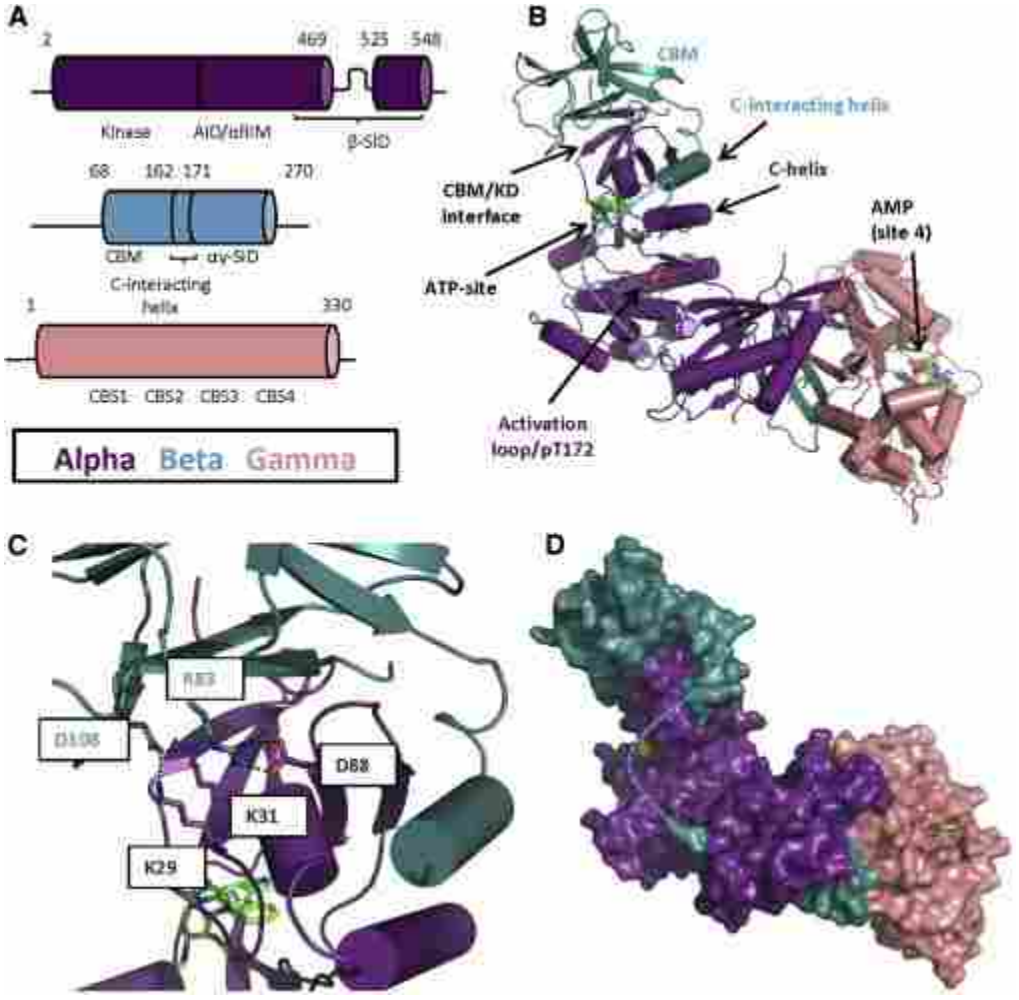

Figure 1-1 Crystal structure of AMPK complex (A) Schematic representation of the construct used for crystallization of AMPK α1β1γ1 (AMPKxtal), α (purple), β (cyan), and γ (pink). (B) Topology of near-full length AMPK α1β1γ1. Arrows indicate the location of the CBM-KD interface, αC-helix and C-interacting helix, ATP site, activation loop, and highest affinity AMP site (site 4). (C) Close-up view of the CBM-KD interface illustrating intersubunit electrostatics. (D) Surface representation of the structure shown in (B). The disordered segment between the β1 CBM and the C-terminal domain is shown as dotted lines. Adapted from Calabrese, M. F., et al. (2014). Structural Basis for AMPK Activation: Natural and Synthetic Ligands Regulate Kinase Activity from Opposite Poles by Different Molecular Mechanisms. Structure 22(8): 1161-1172.

The yeast ortholog of AMPK—SNF1 was identified in *Saccharomyces cerevisiae* (baker's yeast) in 1981 when the *snf1* mutation was found in a search for mutants unable to utilize sucrose (snf, sucrose-nonfermenting) [51]. SNF1/ AMPK pathways are highly conserved,

in which upstream kinases of AMPK— LKB1, CAMKK2, TAK1 were first identified in yeast [52-54]. Much like mammalian AMPK, SNF1 complex is a heterotrimeric protein kinase composed of one catalytic α subunit, one β subunit and one γ subunit. *Saccharomyces cerevisiae* genome possesses one gene that encodes for the catalytic α subunit Snf1, three genes encode for alternate β subunits Gal83, Sip1 and Sip2, and one gene encodes for the γ subunit Snf4 [55]. Crystal structure of SNF1 complexes are shown in Figure 1-2 [56]. The constitutively expressed α subunit Snf1is a 633 amino acid protein that phosphorylates its downstream targets. The α subunit consists of a N-terminal catalytic domain and a C-terminal regulatory region [57-59]. The regulatory region consists of a short autoinhibitory sequence (AIS) (380—415aa) and a region which facilitates the interactions with the β subunits of the complex (515—633aa) as sufficient for interaction with Sip2 [60]. The autoinhibitory domain interacts with both the regulatory subunit Snf4 and the kinase domain of Snf1 [61]. The interaction with Snf4 relieves the inhibition of the AIS allowing phosphorylation of Thr210 residue of Snf1 that results in activation of the catalytic subunit [62]. The β subunits direct the localization of α subunit, and exhibit overlapping function as each subunit alone is sufficient for growth under conditions in which SNF1 activity is required [63-65]. Under normal conditions, all three β subunits are cytosolic; however, the different N-termini of β subunits allows unique subcellular localization upon glucose depletion: Sip1 re-localizes to the vacuolar membrane, Gal83 re-localizes to the nucleus, and Sip2 remains cytosolic [64]. Sip1 is a 863 amino acids protein, Sip2 is a 415 amino acids protein and Gal83 is a 417 amino acids protein [55]. The β subunits contain conserved C-terminal sequences that mediate their interaction with the SNF1 complex [66]. Amino acids residue 198 to 350 of Gal83 and residues 154 to 335 of Sip2 are sufficient for interaction with Snf1; while residues 771 to 863 of Sip1 and residues 332 to 415 of Sip2 mediates interaction

with Snf4 [60, 66]. The sequence of glycogen binding domain (GBD) in Gal83 (161-243) and Sip2 (163-245) is conserved in the mammalian AMPK β1 subunit [67]. However, studies showed that GBD may affect SNF1 function through mechanisms independent of glycogen binding [67]. Despite all three β subunits having overlapping functions, the abundance of each beta subunit is differently regulated by glucose availability. Gal83 is the main beta subunit during glucose growth, while the level of Sip2 increases when switched to non-fermenting carbon sources. Sip1 is the least abundant amongst the three β subunits and its cellular level remained constant regardless of carbon sources [64]. Gal83 contributes the most to SNF1 activity in response to glucose depletion, while Sip2 has been implicated in aging [68]. SNF1 complexes with different β subunits also display preference for activation by Sak1, Tos3, and Elm1 in a stress-dependent manner [69]. Snf4 contains a Bateman domain that binds adenosine derivatives; however several studies showed that unlike AMPK, SNF1 is not allosterically activated by AMP *in vitro* [70-73].

1.1.2 Conserved signaling of AMPK-PASK from yeast to man

Like mammalian AMPK, SNF1 plays a central role in energy sensing, metabolism and stress response [74]. Per-Arnt-Sim kinase (PAS kinase) is a highly conserved nutrient sensing kinase that has recently been identified as being a downstream substrate of Snf1 in yeast [75]. PAS kinase is an emerging regulator of mammalian glucose and lipid metabolism, as shown by a wide range of studies [76]. Mice with PAS kinase deficiency display a hypermetabolic phenotype and are protected from high fat diet-induced obesity and insulin resistance [77]; PAS kinase is found to promote energy production by shifting metabolism towards respiration in both yeast and mammalian systems, through regulation of its substrate Cbf1/USF1 and perhaps through activation of AMPK pathways [78, 79] because the presence of PAS kinase is necessary

for AMPK activation in the nerve cells of the hypothalamus (N2A), as well as normal glucose-stimulated insulin production in cultured β-cells [78]. PASK also controls insulin secretion as it enhanced PDX-1 stability through inactivating glycogen synthase kinase 3β (GSK-3β); hence reducing blood glucose [80]. PAS kinase was also found to regulate glucose partitioning through phosphorylation of UDP-glucose pyrophosphorylase (Ugp1) [81]. With a large number of yeast PAS kinase (Psk1) interacting partners that are involved in cell growth (gene/ protein expression, replication/ cell division, and protein modification and degradation), vacuole function and stress tolerance identified [82], functions and regulation of PAS kinase remain to be explored.

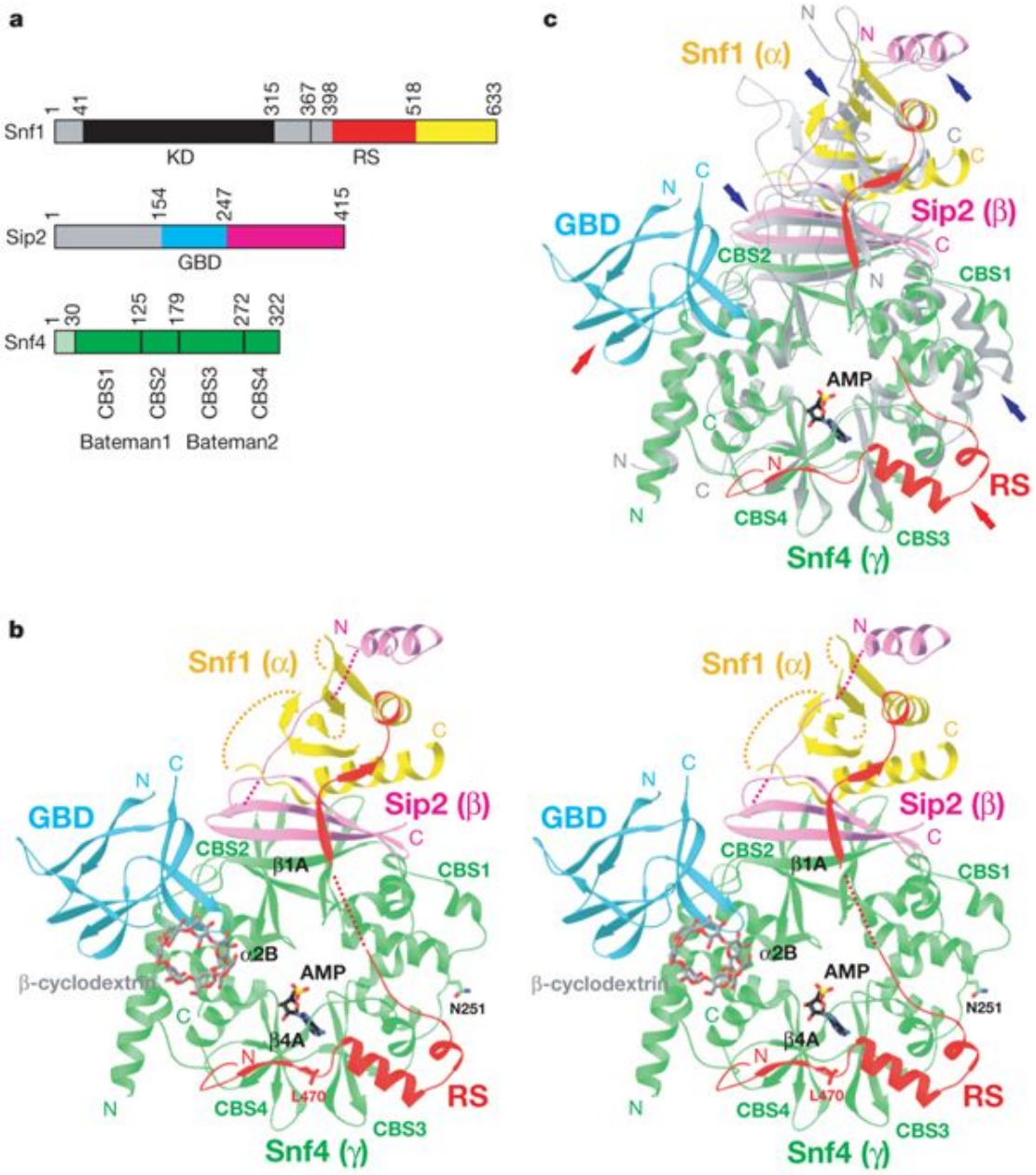

Figure 1-2 Crystal structure of SNF1 complex (A) Domain organization of SNF1 subunits. Residues that are included in the co-expression construct are shown in color, and the others are shown in grey or black. KD, protein kinase domain; RS, regulatory sequence. (B) Schematic representation (stereo view) of the heterotrimer core of SNF1. The regulatory sequence of the α-subunit (Snf1) is shown in red and the rest is in yellow; the GBD of the β-subunit (Sip2) is shown in cyan and the rest is in magenta; and the γ-subunit (Snf4) is shown in green. The positions of AMP (stick model in black), as observed from the S. pombe enzyme as well as that of β-cyclodextrin (in grey) as bound in the rat GBD10, are shown for reference. (C) Superposition of the structures of S. cerevisiae SNF1 (colored as in b) and S. pombe AMPK (in grey). The superposition is based on the γ-subunits only. Red arrows point to new features in the SNF1 structure, and blue arrows point to differences between the two structures. Produced with Ribbons30. Adapted from Amodeo, G. A., et al. (2007). Crystal structure of the heterotrimer core of Saccharomyces cerevisiae AMPK homologue SNF1. Nature 449: 492.

1.2 Conclusion

AMPK acts as the caretaker of mitochondria and this role is conserved from yeast to man [83]. Given the important role of mitochondria functions in cellular energetics, metabolism and survival, it is not surprising that there are more substrates dedicated to restoring mitochondria health waiting to be identified. Understanding the cross-talk of AMPK with other protein kinases and identifying new downstream targets of AMPK will help to unravel novel aspects of regulation in mitochondrial health and functions, which is of immerse therapeutic potential for metabolic diseases, neurodegenerative disorders and cancer. In Chapter 2, we report a novel downstream substrate of yeast AMPK (SNF1)—Osh7 and the regulation of mitochondrial function through this signaling pathway; in Chapter 3, we report a novel signaling pathway in which SNF1 regulates Med13 degradation and mitochondrial dynamic through PAS kinase.

CHAPTER 2: Differential Regulation and Function Support Paralogous Evolution of Yeast Osh6 and Osh7

Kai Li Ong[1], Sara Hanley[2], Daniel Arens[1], Katrina Cooper[2] and Julianne H. Grose[1]

2.1 Author information

[1]Department of Microbiology and Molecular Biology, Brigham Young University, Provo, UT, 84602, USA

[2]Department of Molecular Biology, Graduate School of Biological Sciences, Rowan University, Stratford, NJ, 08084, USA

*Correspondence: grosejulianne@gmail.com; Tel.: +01-801-422-4940

Kai Li Ong - jkm525@go.byuh.edu

Sara Hanley - hanleys2@rowan.edu

Katrina Cooper - cooperka@rowan.edu

Daniel Arens - danielarens09@gmail.com

Julianne Grose - julianne_grose@byu.edu

* The work described in this chapter has been submitted to the journal Molecular Biology of the Cell and is under review. It has been formatted for this thesis, but it is otherwise unchanged.

2.2 Abbreviations

ORP- Oxysterol binding protein related protein

OSBP- Oxysterol binding protein

LTP- Lipid transfer protein

ORD- OSBP-related protein domain

PI(4)P-Phosphatidylinositol 4-phosphate

PS- Phosphatidylserine

ESCRT- Endosomal sorting complexes required for transport

Vps4- Vacuolar protein sorting-associated protein 4

Osh- Oxysterol binding protein homolog

AMPK- AMP-activated protein kinase

AMP- Adenosine monophosphate

ADP- Adenosine diphosphate

ATP- Adenosine triphosphate

SNF1- Sucrose non-fermenting 1

2.3 Abstract

Gene evolution through duplication and divergence appears to be a common strategy for producing proteins with related but unique function. Herein we explore the evolution of two homologous oxysterol binding proteins (OSBPs) in yeast, Osh6 and Osh7. These proteins were previously found to have overlapping function, but evidence is provided herein for their differential regulation and function. First, Osh7, but not Osh6, is phosphorylated by the nutrient sensing protein kinase Snf1. This phosphorylation is required for Osh7 stability within the cell. Second, Osh7, but not Osh6, localizes to ER-mitochondrial contact sites. OSH6-deficient yeast, on the other hand, display a more pronounced respiratory-defect as well as a mitophagy defect. In addition, a double *osh6osh7* mutant suppresses the respiratory defect of OSH6-deficient yeast. These findings support differential but overlapping function for these OSBPs, explaining the selective pressures in the maintenance of both genes and providing pathways for the study of their mammalian homolog.

2.4 Introduction

Oxysterol binding proteins (OSBP) and OSBP-related proteins (ORP) are a large family of lipid transfer proteins (LTPs) conserved from yeast to man. The human genome encodes 12 ORP genes and a total of 16 ORP protein products generated from alternative splicing, whereas the *Saccharomyces cerevisiae* (baker's yeast) genome encodes seven ORP genes: Osh1-Osh7 [84, 85]. OSBP and ORP contain a conserved OSBP-related protein domain (ORD) at the C-terminal and were first discovered in the 1980's as the intracellular receptors of oxysterols [86]. Recent advances in the understanding of cellular OSBP revealed many lipids in addition to oxysterols may occupy the ORD, such as phosphatidylserine (PS), phosphoinositides, cholesterol and other anionic lipids [85, 87-90]. OSBP and ORP have been implicated in many cellular

functions such as sterol and lipid metabolism, cell cycle, calcium signaling, vesicular transport and apoptosis [91], with roles as lipid or signaling regulators at different membrane contact sites (MCS) [92-97]. OSBPs/ ORPs were also reported to play roles in various human diseases including dyslipidemia, amyotrophic lateral sclerosis (ALS) and many types of cancer [91]. Despite this importance, there is still much unknown about their individual functions and regulation.

Yeast Osh proteins collectively play a role in sterol homeostasis and share at least one essential function [84], however the unique functions of each Osh protein remain elusive. Together with their human homologs ORP5 and ORP8, respectively, Osh6 and Osh7 have been reported to mediate the counter transport of PI(4)P/PS between the endoplasmic reticulum (ER) and plasma membrane (PM) [98, 99]. Osh6 and Osh7 have also been reported to bind Vps4, an AAA ATPase that is essential for efficient transport in the multivesicular body (MVB) sorting pathway that functions to disassemble the ESCRT complexes, with no unique roles being ascribed to either [100-103]. ORP5 and ORP8 share approximately 80% similarity in sequence homology and constitute a unique group in human ORPs, as they are the only two ORPs to possess a C-terminal transmembrane domain (TMD) and both lack the FFAT motif [94]. ORP5 and ORP8 were found to localize at ER-mitochondria contact sites and affect mitochondria morphology and function [104]. Thus, experimental evidence and homology analysis have supported the model of overlapping functions between Osh6 and Osh7 as well as their human counterparts ORP5 and ORP8. In this study, we explored the conserved nature of Osh6 and Osh7, as well as evidence for differential roles and regulation of Osh6 and Osh7 through *in vivo* and *in vitro* studies.

2.5 Results

2.5.1 Evolutionary relationships of OSBP families supports a close relationship between Osh6 and Osh7

Phylogenetic analysis of amino acid sequence utilizing Maximum Likelihood methods [MegaX] showed that OSBP family proteins are grouped into four lineages among *S. cerevisiae*, *H. sapiens*, *C. elegans* and *D. melanogaster* (Figure 2-1). Osh6 and Osh7 are the most closely related yeast homologs, and their closely related human counterparts are ORP5 and ORP8. Sequence similarities between Osh6 and Osh7 (69.7% identity and 81.5% similarity) supports evolution by gene duplication, which often results in similar but disparate, selectable functions, yet only overlapping roles have been reported thus far.

2.5.2 AMPK/ Snf1 phosphorylates ORP8/ Osh7 directly but not Osh6

In our previous study of PAS kinase in yeast, Osh7 was identified as a substrate of a copurified kinase [82]. This contaminating kinase may be Snf1, an upstream regulator of PAS kinase. In support of this conclusion, purified yeast Snf1 or human constitutively active mammalian AMPK α1(1-312) is able to phosphorylate Osh7 or its human homolog ORP8 directly *in vitro* (Figure 2-2A -D). Kinase dead (KD) Snf1 was used in the assay to test for contaminating kinases copurifying with Snf1. These results confirm direct phosphorylation of Osh7 by Snf1.

As mentioned above, sequence homology suggests that Osh6 and Osh7 are close homologs of each other that arose during a yeast genome duplication event and are often treated as such. However, *in vitro* kinase assays suggest that Snf1 and AMPK α1(1-312) were able to differentiate between Osh6 and Osh7 as neither Snf1 nor AMPK phosphorylate Osh6 *in vitro*, suggesting differential regulation of Osh6 and Osh7 in yeast (Figure 2-2E & F).

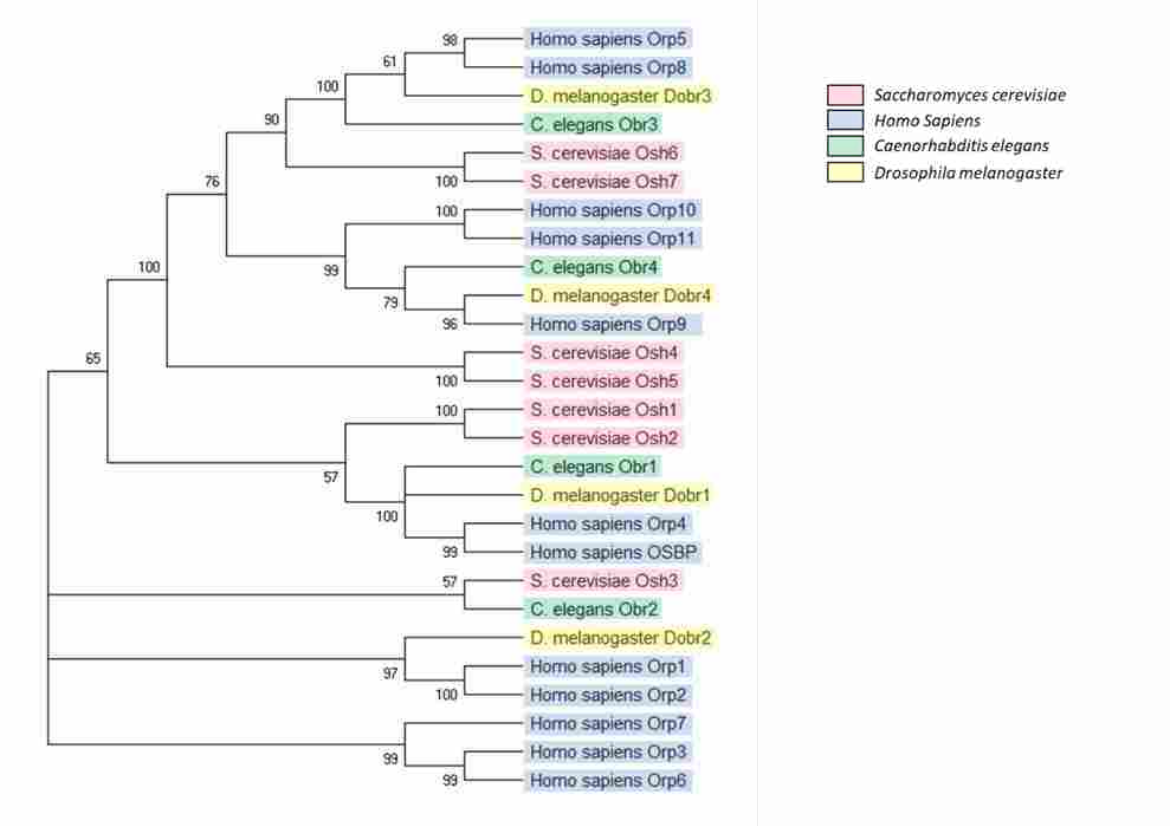

Figure 2-1 Evolutionary history and relationships of OSBP families in *S. cerevisiae*, *H. sapiens*, *C. elegans*, and *D. melanogaster* The phylogenetic tree was constructed using the Maximum Likelihood method and JTT matrix based model [105].The bootstrap consensus tree inferred from 2000 replicates is taken to represent the evolutionary history of the taxa analyzed [106]. Branches corresponding to partitions reproduced in less than 50% bootstrap replicates are collapsed. The percentage of replicate trees in which the associated taxa clustered together in the bootstrap test (2000 replicates) are shown next to the branches [106]. Initial tree(s) for the heuristic search were obtained automatically by applying Neighbor-Join and BioNJ algorithms to a matrix of pairwise distances estimated using a JTT model, and then selecting the topology with superior log likelihood value. This analysis involved 27 amino acid sequences. There were a total of 1669 positions in the final dataset. Evolutionary analyses were conducted in MEGA X [107].

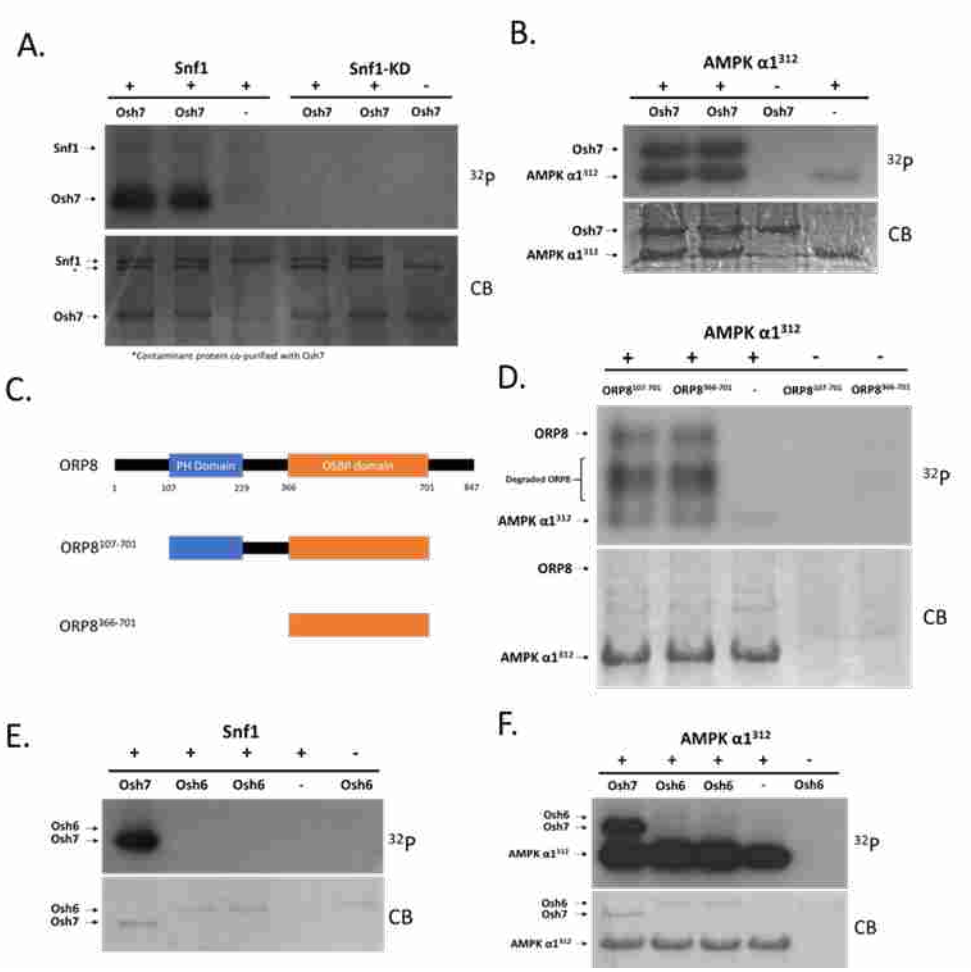

Figure 2-2 Evidence supporting the direct phosphorylation of Osh7 by Snf1 and direct phosphorylation of ORP8 by AMPK (A) Full length Osh7 (expressed in *E. coli* from pJG1054) was phosphorylated *in vitro* when incubated with wild type Snf1 (expressed in yeast from pJG1193) but not the kinase dead Snf1 (Snf1-KD, expressed in yeast from pJG1338). *In vitro* kinase assays were conducted using purified Snf1 incubated with radiolabeled ATP (32P) with or without purified Osh7. Reactions were visualized with 10% SDS-PAGE gel stained with coomassie brilliant blue (CB, bottom) followed by exposure on X-ray film (32P, top). Lane 1&2: WT Snf1+FL Osh7; Lane 3: WT Snf1 only; Lane 4&5 KD-Snf1+FL Osh7; Lane 6: FL Osh7 only. CB: Snf1 appear at the top of the double band in each lane. The bottom of the double band is a protein that co-purified with Osh7. (B) Full length Osh7 was shown to be phosphorylated by human AMPK α1(1-312) (AMPK α1312). Lane 1&2: FL Osh7 + AMPK α1312; Lane 3: FL Osh7 Only; Lane 4: AMPK α1312 only. (C) ORP8 (ORP8107-701: PH-OSBP domain, pJG1658; ORP8366-701: OSBP domain, pJG1659) were shown to be phosphorylated by AMPK α1312. ORP8 was purified from yeast (JGY91, Δsnf1) due to poor expression in *E. coli* BL21 and to prevent background phosphorylation from WT Snf1 (data not shown). Lane 1: ORP8107-701 + AMPK α1312; Lane 2: ORP8366-701 + AMPK α1312; Lane 3: AMPK α1312 only; Lane 4: ORP8107-701 only; Lane 5: ORP8366-701 only. (D) Diagram of ORP8 constructs utilized in this study. (E) Snf1 does not phosphorylate Osh6 *in vitro*. Purified Snf1 was incubated with radiolabeled ATP (32P) with or without purified Osh6/ Osh7. Lane 1: Snf1 + FL Osh7; Lane 2&3: Snf1+FL Osh6; Lane 4: Snf1 only; Lane 5: FL Osh6 only. (F) Purified AMPK α1312 was incubated with radiolabeled ATP (32P) with or without Osh6/ Osh7. Lane 1: AMPK α1312 + Osh7; Lane 2&3: AMPK α1312 + Osh6; Lane 4: AMPK α1312 only; Lane 5: Osh6 only.

2.5.3 Evidence for the direct interaction and stabilization of Osh7 by SNF1

The heterotrimeric *S. cerevisiae* SNF1 complex consists of a catalytic subunit Snf1, three inter-changeable beta subunits Gal83, Sip1 and Sip2, and a gamma subunit Sip4. Beta subunits of SNF1 bind Snf1 and Snf4 to form a functioning complex, and act as substrate binding domain [55, 108]. Direct interactions between Osh7 and Snf1, Gal83, Sip1 or Sip2 were investigated through the Yeast-2-Hybrid (Y2H) system. Full-length and/ or truncations of each SNF1 subunits mentioned above were cloned into bait and prey plasmids and tested against full-length Osh7, and the Osh7 OSBP domain (a.a. 53- a.a 392) or coiled-coil domain (CC domain, a.a. 366- a.a. 437) in the Y2H bait or prey plasmid (Figure 2-3A&B). The Y2H Gold yeast strain (Clontech) with 4 reporter genes (HIS3, ADE2, AUR1-C, MEL1) was transformed with bait and prey plasmids and spotted on synthetic minimum plates lacking leucine (LEU), tryptophan (TRP), histidine (HIS) and adenine (ADE) for selection of plasmid maintenance (LEU or TRP) or protein-protein interactions (HIS and ADE). All constructs were tested for autoactivation by transforming the bait or prey plasmid with target protein against an empty bait or prey plasmid to eliminate the possibility of false positive interactions. Direct interactions between the OSBP domain of Osh7 were observed with all beta subunits of SNF1 (Figure 2-3C), but not with the catalytic subunit Snf1 (data not shown). The Snf1/Snf4 binding domain of Gal83 (a.a 141- a.a. 417) [63, 109] is necessary for binding of the OSBP and CC domain of Osh7, but does not find full length Osh7; Full length Sip1 and Sip2 binds the OSBP domain of Osh7 directly, but not the CC domain or full length Osh7.

In addition to direct interaction via the yeast two hybrid, copurification supports an interaction between Snf1 and Osh7, but not Snf1 and Osh6 (Figure 2-3D). Lysates from yeast expressing Snf1-myc were incubated with equal amounts of purified Osh6 or Osh7, then

subjected to myc purification. Prominent bands are seen with Osh7, but only faint bands with Osh6.

Phosphorylation of Osh7 appears to stabilize the Osh7 protein in that the presence of wildtype Snf1 is necessary for maintaining intracellular Osh7. A wildtype (JGY1) or Δsnf1 (JGY91) strain harboring a plasmid containing Osh7-His under the GAL 1-10 promoter (pJG1357) were grown for 12 hours in SD-Trp and switched to SGal-Trp for 36 hours to induce Osh7 expression. Cells were then broken open and subjected directly to western blotting. Results indicate no detectable amount of Osh7 after 36 hours of induction in the Δsnf1 yeast (Figure 2-3E). In order to show that this deficit in Osh7 was due to Snf1 and not an adaptation of the Δsnf1 yeast, WT and Δsnf1 yeast were co-transformed with plasmids containing Snf1-Myc, Snf1 KD-Myc, or the EV-Myc control along with the Osh7-HIS, grown for 12 hours in SD-Ura-Trp followed by 36 hours growth in SGal-Ura-Trp to induce protein expression. Cells were then broken open and Osh7 was purified using His-tagged protein purification. Results indicate that Osh7-His can only be stably expressed when wildtype Snf1 is supplied, but not when Snf1 KD is present (Figure 2-3F).

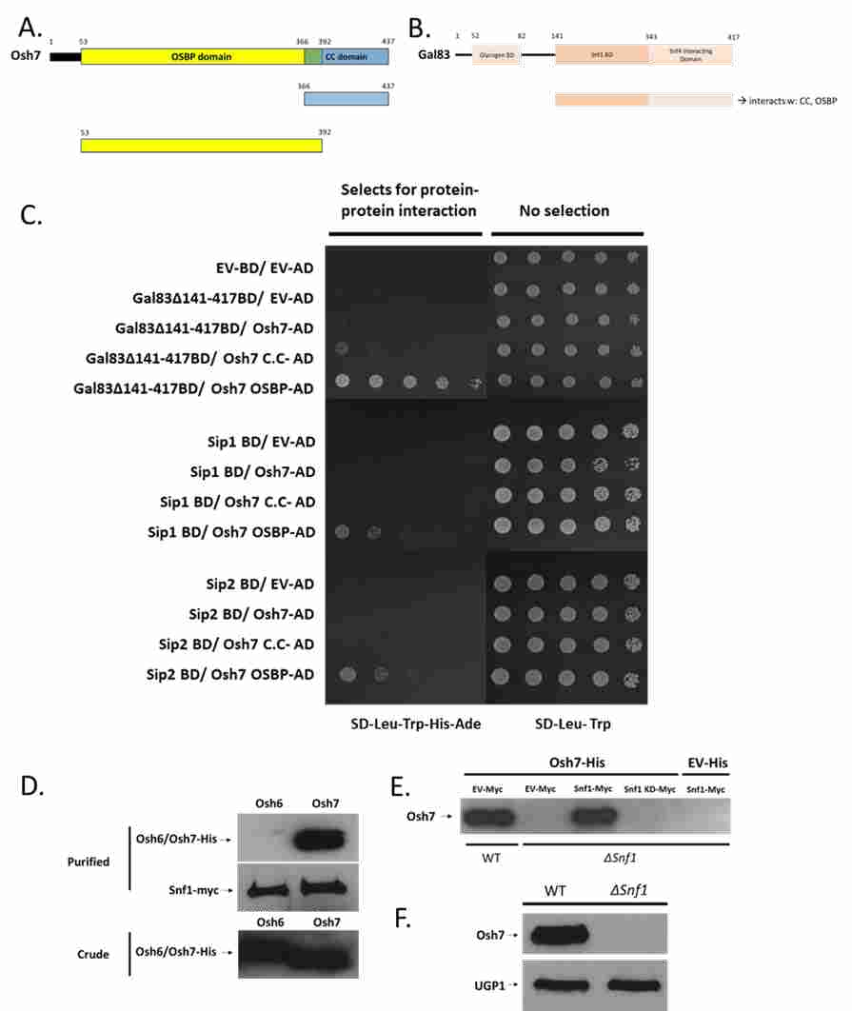

Figure 2-3 Evidence that direct interaction with SNF1 maintains the intracellular stability of Osh7 (A-C) Evidence that Osh7 directly interacts with the three beta subunits of the SNF1 complex (Gal83, Sip1 and Sip2). Constructs of Osh7 used in yeast-2-hybrid assays are diagrammed in (A) whereas interacting regions of Osh7 with Gal83 are shown in (B). The Snf1 binding domain of Gal83 and Snf4 interacting domain of Gal83 are necessary for recognizing OSBP domain of Osh7 (C, top). A weaker interaction of this truncation of Gal83 is also seen with coiled-coil domain of Osh7. Full-length Sip1 interacts with OSBP domain but not coiled-coil domain of Osh7 (C, middle). Full-length Sip2 interacts with OSBP domain but not coiled-coil domain of Osh7 (C, bottom). Y2HGold cells (Clontech) were co-transformed with OSBP domain/ coiled-coil domain of Osh7 (AD) and Gal83 Δ141-417 truncation/FL Sip1/ FL Sip2 (BD) and spotted on SD-Leu-Trp-His-Ade for selection of protein-protein interactions and SD-Leu-Trp as growth control. (D) Myc pull-down assay provides evidence that Osh7(His-tag) co-purifies strongly with Snf1(Myc-tag) from mixed cell lyastes, and Osh6 (His-tag) co-purifies with Snf1 to a lesser extent. Crude extract is shown to control for protein expression in the cell. (E) Overexpressed Osh7 is detected in wildtype yeast overexpressing Osh7-His (JGY1) but not Δsnf1 (JGY91) yeast. Anti-UGP1 antibody was used to probe UGP1 as loading control. (F) Overexpressed Osh7 is purified from WT but not Δsnf1 yeast. WT or Δsnf1 yeast strain transformed with Osh7-His or EV-His and Snf1-Myc, Snf1-KD-Myc or EV-Myc were subject to His-tagged purification followed by western blot. Lane 1: WT yeast with Osh7-His and EV-Myc plasmids; Lane 2: Δsnf1 strain with Osh7-His and EV-Myc plasmids. Lane 3: Δsnf1 Strain with Osh7-His and Snf1-Myc plasmids; Lane 4: Δsnf1 strain with Osh7-His and Snf1 KD-Myc. Lane 5: Δsnf1 strain with EV-His and Snf1-Myc plasmids.

2.5.4 Osh7, but not Osh6, co-localizes with mdm34; Snf1 does not affect Osh7 localization

In addition to the differential regulation of Osh6 and Osh7 by Snf1, the function of Osh6 and Osh7 was explored to investigate similarities and differences. The human homologs of Osh6 and Osh7, ORP5 and ORP8 were recently reported to localize at ER-mitochondrial contact sites and to affect mitochondria function [104], thus we looked at ER-mitochondrial contact site localization of these two proteins. In addition, the effects of Snf1 on this localization were investigated by varying the growth media to increase or decrease Snf1 activity, since Osh7 is degraded in Δsnf1 mutant and is not visible by microscopy. Snf1 becomes activated under low glucose conditions due to the increased AMP:ATP ratio, therefore glucose gradients were utilized [55]. Osh7 co-localized with Mdm34 at the ER-and mitochondria contact sites in WT yeast 45% of the time (Figure 2-4), while some remained cytosolic. This localization did not change with altered glucose levels. A small fraction of Δsnf1 mutant yeast also displayed some Osh7, and it was localized to the ER-and-mitochondria contact sites. Osh6 on the other hand remained cytosolic in both the WT and Δsnf1 strain, and its expression was not altered in response to Snf1. Thus, Snf1 does not appear to play a role in localization of Osh6 nor Osh7, but only a very low level of Osh7 was detected Δsnf1 mutant in the and usually seen as foci, which is consistent with the observation of Snf1 being necessary in maintaining Osh7 intracellular stability (see Fig. 2-3).

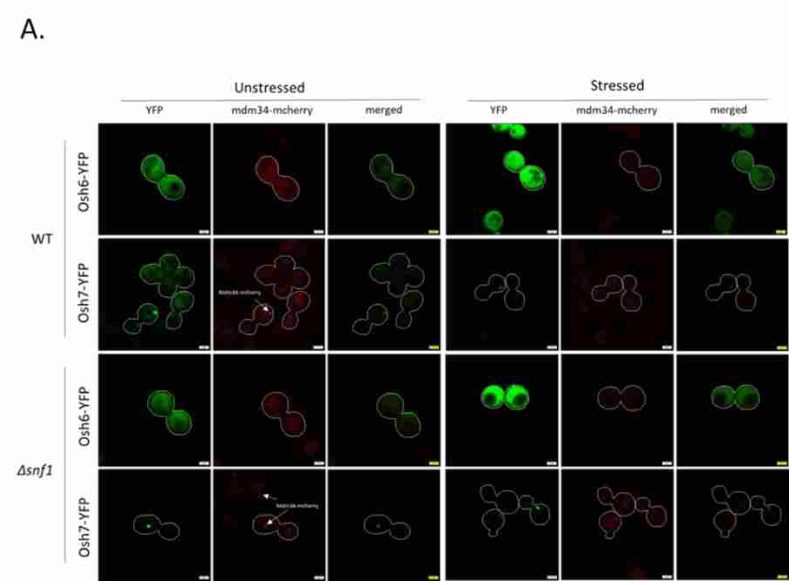

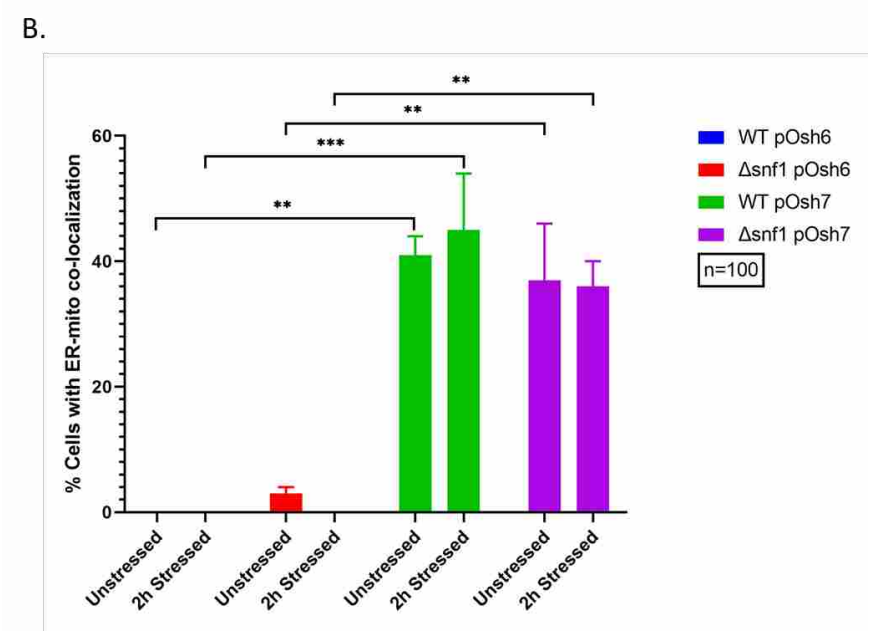

Figure 2-4 Osh7, but not Osh6, localizes to ER-mitochondrial contact sites in a Snf1 independent manner, and its stable expression is affected by Snf1 (A) WT and Δsnf1 cells with genome tagged Mdm34::mCherry harboring Osh6-YFP/ Osh7-YFP plasmid under ADH promoter were grown to log phase in SD-URA and then subject to low glucose/ nutrient stress in SD-URA for 2 hours. Cells were imaged before and after stress with Fluoview confocal microscope. B. Cell count and statistical analysis of Osh7-YFP co-localization with Mdm34-mcherry. (B) Statistical analysis of cells with or without at least 1 co-localizing foci of Osh6/Osh7-YFP with Mdm34 in WT/Δsnf1 strain, before and after 2 hours 0,05% glucose stress. Cells were visualized using Fluoview confocal microscope.

2.5.5 Both Osh6 and Osh7 plays a role in mitochondrial function; with Osh6 playing a more prominent role

To better understand the cellular functions of Osh6 and Osh7, including the Osh7 localization to ER-mitochondria contact sites, we examined the mitochondria morphology and functions in WT, Δosh6, Δosh7, Δosh6Δosh7 yeast. Our data showed that Δosh6 plays a more important role in mitochondria dysfunction compared to Osh7, as Δosh6 mutant cannot grow on media with non-fermenting carbon source (Figure 2-5A, 2% Glycerol-Ethanol in this experiment). The double mutant (Δosh6Δosh7) appeared to restore the mitochondria dysfunction observed in Δosh6 strain, consistent with differential rather than redundant functions for Osh6 and Osh7. On the other hand, the Δosh7 strain did not show obvious signs of mitochondrial dysfunction when grown on 2% Glycerol-Ethanol. We then subjected each strain of cells to Seahorse XFp OCR (oxygen consumption rate) analysis. Measurements were taken in basal, inhibited, and uncoupled respiratory environments and are represented as pmol O2 consumed/min/cell. Consistent with the plate assay (Figure 2-5B), Δosh6 yeast consumed significantly less oxygen than WT at all timepoints ($p<0.00001$) when normalized to cell number as shown in Figure 2-5E. However, as opposed to the plate assay it appears that some oxygen is consumed, which in conjunction with weak reactions to the inhibitory and uncoupling respiratory drugs TET and FCCP indicates low levels of respiratory carbon source utilization as opposed to non-mitochondrial oxygen consumption. The most surprising result is the respiratory defect observed in the Δosh7 knockout strain. The Δosh7 yeast consumed significantly less oxygen than WT, a divergence from the plate phenotype, at all timepoints ($p<0.001$). This may suggest a difference in carbon source utilization between solid and liquid media or truly represent a defective respiratory phenotype that does not affect growth. In accordance with the plate assay,

the Δosh6osh7 double mutant showed a recovery of respiratory function, although the OCR was lower than WT at all timepoints ($p<0.01$) indicating a potential genetic interaction between the two genes.

Further analysis of the respiratory data revealed differences in the strains response to the uncoupling drug FCCP, which transport H^+ across the inner mitochondria membrane. Respiratory rates between Δosh6 and Δosh7 were not significantly different during basal and inhibitory readings however upon the addition of FCCP the Δosh6 saw an increase of 40% while Δosh7 respiration increased by 100% resulting in significantly differences in uncoupled respiratory rates. For reference WT OCR increased by 99% and Δosh6osh7 increased by 61%. Florescent microscopy with plasmid containing mito-TFP was then used to examine mitochondria morphology in all four strains (Figure 2-5C). No obvious altered mitochondria morphology was observed suggesting the respiratory dysfunction of Δosh6 yeast is due to a mitochondrial dysfunction rather than deficit.

Mitophagy, the process of selectively degrading damaged mitochondria, was monitored using the OM45-GFP processing assay shown in previous study [110] and florescent microscopy with mitochondria-targeting TFP (Figure 2-6). Interestingly, the Δosh6 strain displayed no detectible mitophagy after 36 hours growth in YPL, much like Δatg32 control. Atg32 is a mitophagy specific receptor in yeast and mitophagy is completely inhibited in cells lacking ATG32 [111], therefore it serves as a negative control. Our data showed that Osh6 plays a significant role in mitophagy while Osh7, on the other hand, displayed only a decrease in mitophagy (Figure 2-6A&B). Once again the double mutant (Δosh6Δosh7) appeared to rescue the Δosh6 defect and phenocopied the less severe decrease in mitophagy of the Δosh7 strain.

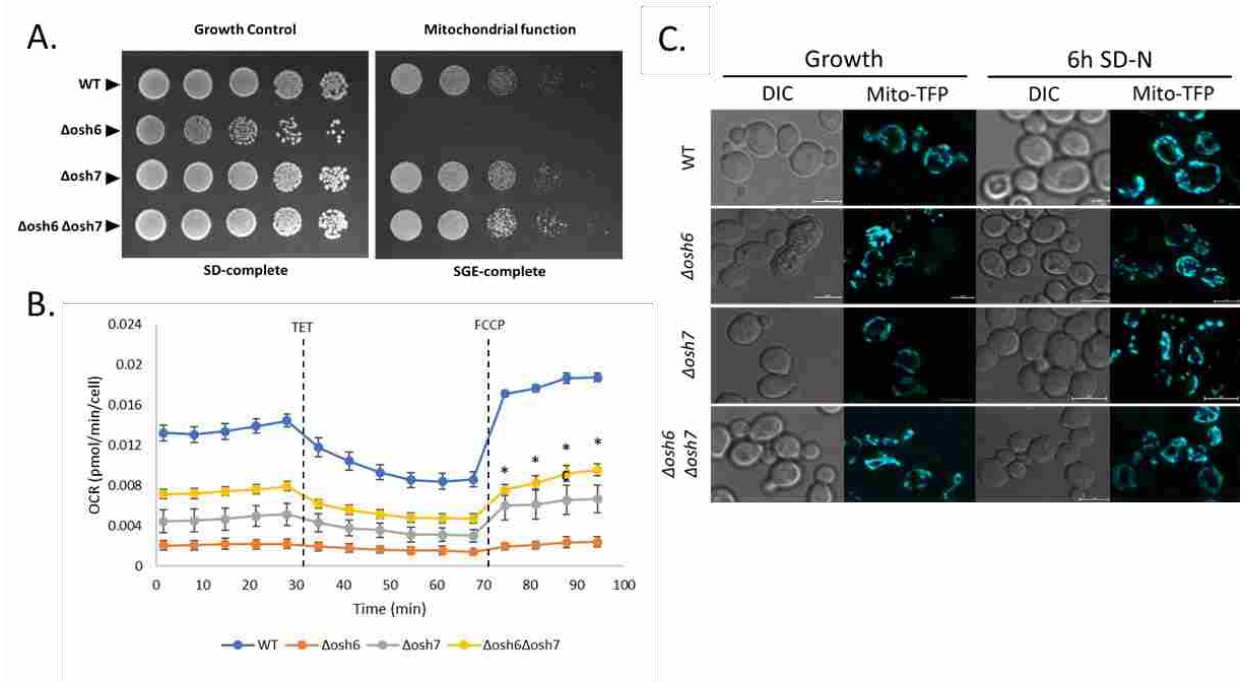

Figure 2-5 Both Osh6 and Osh7 plays a role in mitochondria function with Osh6 playing a more prominent role (A) An Δosh6 knockout display a respiratory-defect on synthetic media with glycerol/ethanol (SGE-complete) when compared with glucose (SD- complete) and Δosh6Δosh7 double knockout strains suppresses the mitochondria defect. Yeast were spotted in WT, Δosh6, Δosh7, Δosh6osh7 strain on SD-complete and SGE-complete plates. (B) Δosh6, Δosh7, and Δosh6Δosh7 knockouts were tested in Seahorse respiration assays in SGE-complete media after growth in SD-complete. OCR of both Δosh6 and Δosh7 are significantly lower than WT at all timepoints with $p<0.001$ and Δosh6Δosh7 at all timepoints with $p<0.01$. There were no significant differences in OCR between Δosh6 and Δosh7 up until FCCP was added and asterisk (*) represent where significant difference of OCR between Δosh6 and Δosh7 occur. Dotted lines represent injections of mitochondrial inhibitory and uncoupler drugs TET and FCCP. Error bars represent SEM. (C) Neither Osh6 nor Osh7 appears to affect mitochondria morphology. Mitochondria morphology were analyzed using florescent microscope. Cells were grown to logarithm phase in 0.5% glucose and switched to SD-N for 6h. Mitochondria morphology was visualized at growth phase and after 6h of nitrogen starvation.

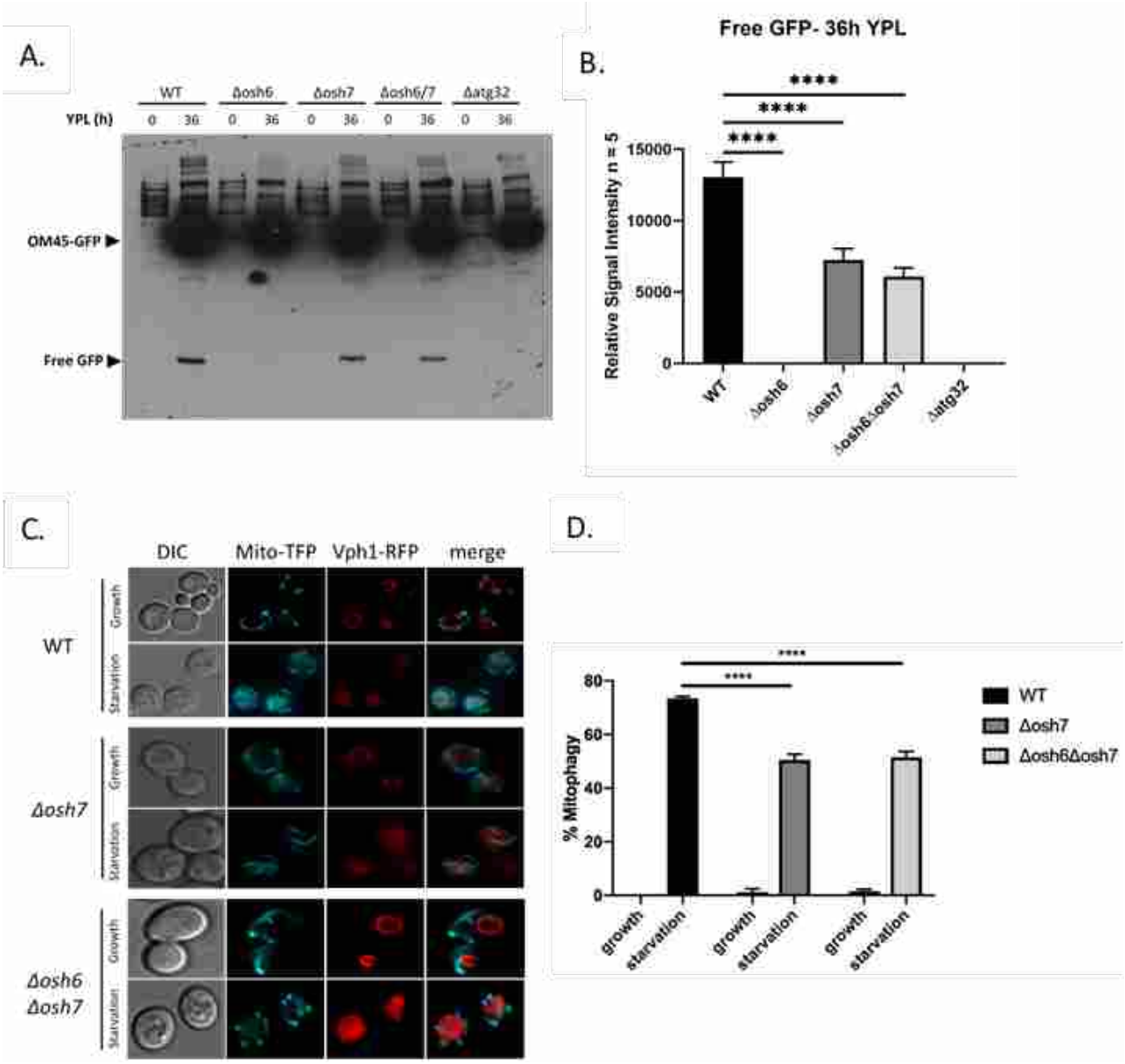

Figure 2-6 Osh6-deficient cells display mitophagy defects (A) Representative image of western blot analysis showed that Δosh6 strain has significant defects in mitophagy. Osh7 on the other hand, affects mitophagy to a lesser extent. Cells were grown to mid-log phase and switched to YPL for 36 hours. OD600 = 1 of cells were analyzed using western blotting. (B) Statistical analysis of free GFP relative signal intensity between WT, Δosh6, Δosh7, Δosh6Δosh7 and Δatg32 in A. (C) Cells expressing Mito-TFP and Vph1-mcherry were analyzed with florescent microscopy before and after 24 h nitrogen starvation. Mito-TFP construct contained mitochondrial leader sequence fused with TFP for mitochondria targeting, where Vph1-mcherry allows visualization of vacuole. Overlap of Mito-TFP and Vph1-mcherry following nitrogen starvation indicates mitophagy. Results for Δosh6 strain not shown due to cell death resulted under these conditions. (D) Statistical analysis of % mitophagy in C. was graphed with the indicated genotype (mean ± SEM, n ≥ 2). "****" indicates p-value < 0.0001 by one-way ANOVA followed by post-hoc Tukey analysis.

2.6 Conclusions

Gene duplication followed by divergence is a likely pathway for the evolution of novel protein functions. The first models for gene duplication were fairly simplistic, suggesting that gene duplication allowed for a wild type copy of the gene to be present while a second copy could evolve a side activity or novel function. A more accurate model for the evolution of paralogous genes may be the innovation, amplification, and divergence (IAD) model proposed by Bergthorsson, Andersson and Roth, which allows for selection at every step of the process [112]. In this model, a gene containing a side activity is amplified, sometimes in large duplicated arrays held by selection for the side activity. A copy of the gene may then acquire a mutation allowing for the side activity to predominate, and the amplified copies may collapse. In the case of the Osh6 and Osh7 paralogs, which may have evolved from a whole genome duplication of yeast, such homologous genes are often thought to have redundant function, where side activities are revealed following further investigation. Herein we present a further investigation into the Osh6 and Osh7 proteins, providing evidence for their divergent regulation and function as well as pathways for evolutionary selection.

Osh7 but not Osh6, appears to be directly phosphorylated by Snf1 and binds the SNF1 complex *in vivo* (Figure 2-2&3). To our knowledge, this is the first report of an OSBP as a substrate for SNF1, which regulation may be conserved from yeast to mammalian cells since the Snf1 homolog AMPK α1 (1-312) also phosphorylates the mammalian Osh7 homolog ORP8 *in vitro* (Figure 2-2). The Snf1-dependent phosphorylation appears to stabilize the Osh7 protein *in vivo* because yeast deficient in Snf1 or harboring a Snf1-KD mutant have no detectible Osh7 protein (Figure 2-3). Thus, Osh6 and Osh7 appear to be differentially regulated by Snf1.

In addition to the differential regulation of these two proteins, Osh6 and Osh7 also appear to have evolved disparate functions. Osh7 localized to ER-mitochondrial contact sites in this study but Osh6 remained cytosolic (Figure 2-3), only yeast lacking Osh6 displayed defects on respiratory media (Figure 2-4). Osh6 have a more significant role in mitochondria function according to Seahorse assay compared to Osh7 along with a severe defect in mitophagy (Figure 2-5&6). Remarkably, no difference was seen in yeast morphology of mitochondria from either yeast lacking Osh6 or Osh7, suggesting a defect in function rather than structure of the mitochondria from Δosh6 yeast. These results describe the first connection of Osh7 to yeast ER-mitochondrial contact sites as well as the first role for Osh6 in respiration and mitophagy.

Thus far the human homologs of Osh6 and Osh7, ORP5 and ORP8, have been shown to have overlapping function, being recruited to the ER-plasma membrane contact sites by phosphatidylinositol4-5 bisphosphate (PtdIns(4,5)P_2) and regulating PtdIns(4,5)P_2 at the plasmid membrane [88] . In addition, they have also been shown to affect respiratory function [104]. The results in the study of differential function for the yeast paralogs of Osh6 and Osh7 may provide a basis for the study of differential functions of the mammalian OSBP's, particularly with respect to mitophagy and the regulation by the Snf1 homolog AMPK. Mammalian ORPs have been linked to a wide variety of diseases from dyslipidemia to ALS and cancer, making the understanding of paralogous evolution particularly crucial.

2.7 Experimental procedures

2.7.1 Yeast Strains, plasmids and primers

Yeast strains, plasmids and primers used in this study is shown in Table 1. Yeast strains generated in this study were constructed using standard polymerase chain reaction (PCR) based

gene disruption followed by sporulation method as previously described [113, 114], unless otherwise stated.

Table 2-1 List of yeast strain used

Strain	Background	genotype	abbreviation	a/ α	Reference/ Source
JGY 1	W303	*his3, Leu2, lys2, met15, trp1, ura3*	WT	a	David Stillman, University of Utah
JGY 91	W303	*snf1::*hphMX4, *his3, Leu2, lys2, met15, trp1, ura3*	Δsnf1	a	Demille D, 2015
JGY 1031		LYS2::GAL1UAS-GAL1TATA-His3 GAL2UAS-Gal2TATA-Ade2 URA3::MEL1UAS-MEL1TATA, AUR1-CMEL1, ura3-52, his3-200, ade2-101, trp1-901, leu2-3, 112, gal4del, gal80del, met-	Y2H Gold	a	Clontech
JGY 1366	BY4742/BY4741	*osh6::*KanMX4, MATa *his3Δ1, leu2Δ0, met15Δ0, ura3Δ0* *MATα his3Δ1, leu2Δ0, lys2Δ0, ura3Δ0*	Δosh6 Diploid	a/α	GE Health Care (CloneID:25074)
JGY 1400	SGAY7039	*osh7::*hphMX4 *can1Δ::*STE2pr-Leu2*, lyp1Δ, ura3Δ0, leu2Δ0, his3Δ1, met15Δ0*	Δosh7	α	Joanna Zukowska-Kasprzyk. Gavini Research Group, EMBL
JGY 1410	BY4741	*mdm34::mCherry::KanMX4, his3Δ1, leu2Δ0, met15Δ0, ura3Δ0*	Mdm34-mCherry	a	Maya Schuldiner's Lab, Weizmann Institute of Science
JGY1416	BY4741	*his3Δ1, leu2Δ0, lys2Δ0, ura3Δ0*	WT	α	This study
JGY1418	BY4741	*osh6::*KanMX4, *his3Δ1, leu2Δ0, lys2Δ0, ura3Δ0*	Δosh6	α	This study
JGY1419	BY4741	*osh7::*hphMX4*, his3Δ1, leu2Δ0, lys2Δ0, ura3Δ0*	Δosh7	α	This study
JGY1425	BY4741	*osh6::*KanMX4*, osh7::*hphMX4*, his3Δ1, leu2Δ0, lys2Δ0, ura3Δ0*	Δosh6Δosh7	α	This study
JGY1547	BY4741	*atg32::*KanMX4	Δatg32		Tim Formosa, University of Utah
JGY1586	W303	OM45::GFP::HIS, *ade2, ade6, can1-100, his3-11,15, leu2-3,112, trp1-1, ura3-1*	OM45-GFP		Katrina Cooper, Rowan University

JGY1589	W303	*osh7:hphMX4, his3, leu2, lys2, met15, trp1, ura3*	Δosh7	a	This study
JGY1628	BY4741	*snf1::hphMX4, mdm34::mCherry::KanMX4, his3Δ1, leu2Δ0, met15Δ0, ura3Δ0*	Δsnf1	a	This study

Table 2-2 List of plasmids used

Plasmid	Gene	Backbone	Organism	Origin	selection	Reference/ Source
pJG124	Empty vector	pRS424	*S. cerevisiae*	2u	TRP	Jared Rutter, University of Utah
pJG485	Y2H BD Empty vector	pGBKT7	*S. cerevisiae*	2u	TRP	Clontech
pJG549	Y2H AD Empty vector	pGADT7	*S. cerevisiae*	2u	LEU	Clontech
pJG725	Empty vector	pRS416	*S. cerevisiae*	2u	URA	[82]
pJG1009	Empty vector	pET15b with James Y2H MCS	*E. coli*		Amp	[82]
pJG1054	Osh7	pET15b	*E. coli*		Amp	[82]
pJG1115	Osh7	pRS426	*S. cerevisiae*	2u	URA	This study
pJG1193	Snf1	pRS313	*S. cerevisiae*	CEN	URA	[75]
pJG1238	Sip2	YEp-GBD	*S. cerevisiae*	2u	TRP	[75]
pJG1260	Gal83 aa141-417	YEp-GBD	*S. cerevisiae*	2u	TRP	[75]
pJG1333	FL Osh7	pGADT7	*S. cerevisiae*	2u	LEU	This study
pJG1338	Snf1-KD	pRS313	*S. cerevisiae*	CEN	URA	This study
pJG1353	Osh7 c.c. domain	pGADT7	*S. cerevisiae*	2u	LEU	This study
pJG1355	Osh7 OSBP domain	pGADT7	*S. cerevisiae*	2u	LEU	This study
pJG1357	Osh7	pRS424	*S. cerevisiae*	2u	TRP1	This study
pJG1375	Sip1	YEp-GBD	*S. cerevisiae*	2u	TRP	This study
pJG1611	Osh7	pRS416	*S. cerevisiae*	CEN	URA	This study
pJG1656	Osh6	pET15b	*E. coli*		Amp	This study

pJG1657	ampk α1 a.a.312	pET30a+	*E. coli*		Amp	Dave Thomson, Brigham Young university
pJG1658	ORP8 (PH-OSBP)	pRS426	*S. cerevisiae*	2u	Amp	This study
pJG1659	ORP8 (OSBP)	pRS426	*S. cerevisiae*	2u	Amp	This study
pJG1660	ORP8	pCDNA4/TO	mammalian		Amp	Vesa Olkkonen, University of Helsinki
pJG1684	mito-TFP	pRS316	*S. cerevisiae*	CEN	URA	Katrina Cooper, Rowan University
pJG1685	Vph1-mCherry	pRS313	*S. cerevisiae*	CEN	HIS	Katrina Cooper, Rowan University
pJG1688	mito-TFP	pRS313	*S. cerevisiae*		HIS	Katrina Cooper, Rowan University
pJG1697	Osh7-YFP	pRS416	*S. cerevisiae*		URA	Katrina Cooper, Rowan University
pJG1698	Osh6-YFP	pRS416	*S. cerevisiae*		URA	Katrina Cooper, Rowan University

Table 2-3 List of primers used

Primers	Sequence
JG1000	CATGCGTCAATCGTATGTGAATGC
JG2184	CTGCAGCGAGGAGCCGTAAT
JG3185	GGCGAATTCATGGCTCTCAATAAACTAAAGAATATACC
JG3186	GCCTCGAGATTCTTTTGGATTCCATGCTTTTTATAAG
JG3207	GGC CATATGGCTCTCAATAAACTAAAGAATATACC
JG3209	GCCTCGAGTTAATTCTTTTGGATTCCATGCTTTTTATAAG
JG3398	CTTGAGTTTCCTAAAAATTTCGCTTTTGGCACAACAACTC
JG3996	GGCCCCGGGCTCTCCCTTAGTGCTTGTGAAATAAAC
JG3997	GGCGGATCCTATTCTTTTGGATTCCATGCTTTTTATAAGCC
JG3401	GTTCTTCTTATCTACTTTTTAACTTGTGTG
JG3402	GATGCGGAAACAACGGGTTGAACC
JG3592	GCCAAAAAGTTGCTCTAAGAATCATTAATAAGAAGG
JG3603	CAACTTTCTCTTCTTGGATCTCTCC

JG3604	GGGAAATTTCAAAGATTTTTTTAATAGAGGC
JG3763	ATTCATATGAATATTATTTCCCAGCTGAAGCCAGG
JG3764	TCCTCGAGCTACTTGTAAATATAATAATCTAAATCCTCAC
JG3765	GAACATATGGCCGAAGACGGCGTTGAATTTCATTC
JG3988	GGCGGATCCATGGGCTCCAAAAAACTGACCGTAGGATCTG
JG3989	CGGCTCGAGCTATTGTTTTGCTGGGTTCTGCTTTTCG
JG4442	GGCGTCGACTTATTTGTACAATTCATCCATACCATGGGTAATACC
JG4445	GGCCCCGGGATGTCTAAAGGTGAAGAATTATTCACTGGTGTT
JG4446	GGCCAATTGACACTATTGAAACAAGTCCGTCCTGGC
JG4447	GCCGTCGACGTAATGCCATTCTCCTGTGAGTGGATCAAG
JG4448	GGCCAATTGATTGTTATGGCTGATTGGTTAAAGATTCGTGG
JG4522	TTTGACTCTCCTGCCTGCATGGTG
JG4523	AATAGCCCTGCGTTCACAAACTCG
JG4524	CGTTATCTAAGGCGAAGGAGGACTTG
JG4525	CGCCGGCAAAGTTACCCATAG
JG4551	GTTCCCGGGTTTGTACAATTCATCCATACCATGGG
JG4552	GGCACTAGTATGTCTAAAGGTGAAGAATTATTCA
JG4605	GGCCCCGGGATGGGCTCCAAAAAACTGACCGTAG

2.7.2 Growth media

Yeast strains were grown aerobically at 30°C unless otherwise stated. Medium used: YPAD (1% yeast extract, 2% peptone, 2% glucose with adenine), synthetic minimal medium with glucose or galactose (SD-/ SGal-; 0.67% yeast nitrogen base without amino acids, 0.2% auxotropic amino acids with vitamins, 2% glucose or 2% galactose), YPD (1% yeast extract, 2% peptone, 2% glucose), YPL (1% yeast extract, 2% peptone, 2% lactic acid, pH 5.5), synthetic minimal medium lacking nitrogen (SD-N; 0.17% yeast nitrogen base without amino acids, 2% glucose), depleted synthetic medium with glucose (SDD-; 0.17% yeast nitrogen base without

amino acids, 0.6% of auxotrophic amino acids, 0.5% ammonium sulfate, 2% glucose or 0.05% glucose).

2.7.3 In vitro kinase assays

Yeast plasmids expressing human ORP8 were constructed by PCR amplifying from plasmid containing ORP8 cDNA (pJG1660)-- a kind gift from Dr. Vesa M. Olkkonen (University of Helsinki). Plasmid with ORP8 PH-OSBP domain (pJG1658) were amplified using JG4447/JG4448, plasmid with ORP8 OSBP domain (pJG1659) were amplified using JG4446/JG4447 and cloned into EcoRI/XhoI site of pJG859. Bacteria expressing full length Osh7 (pJG1054), constitutively active human AMPK α1 (PRKAA1) [115], full length Osh6 (pJG1656) was constructed by PCR amplifying Osh6 from JGY1 using JG3988/JG3989 and cloned into the BamHI and Sall site of pJG1009, were also used.

Yeast (JGY1 or JGY91) harboring wildtype Snf1-myc, Snf1 kinase dead Snf1 KD-myc (pJG1193) or ORP8-HIS (pJG1658, pJG1659) plasmids were grown in selective 2% glucose synthetic minimal medium (SD-Ura) overnight, diluted 1:100 into 500mL of SD-Ura and grown for 12 hours, pelleted and resuspended in 500mL of selective 2% galactose synthetic minimal media (SGAL-Ura) and grown for 36 hours.

BL21 (DE3) *Escherichia coli* harboring Osh7-HIS (pJG1054), Osh6-HIS (pJG1656) or PRKAA1-HIS (pJG1657) were grown overnight at 37°C in Luria Bertani broth supplemented with ampilicin (LB Amp), diluted 1:100 into 500mL of LB Amp and grown for 3 hours, followed by 5 hours induction in LB Amp supplemented with 0.5 mM of IPTG.

Cells were pelleted and resuspended in appropriate lysis buffer: Myc-tagged purification lysis buffer (20 mM HEPES, 10 mM KCl, 1 mM EDTA, 1 mM EGTA, 50 mM NaCl, 10%

glycerol, 1 mM β-mercaptoethanol, Pierce Protease Inhibitor Tablet, pH 7.4, with or without phosphatase inhibitor-- 50 mM NaF, 35mM glycerophosphate); and HIS-tagged purification lysis buffer (50 mM HEPES, 300 mM NaCl, 20 mM imidazole, 10 mM KCl, 1 mM β-mercaptoethanol, Pierce Protease Inhibitor Tablet, pH 7.8). Cell suspension were then lysed with Microfluidics M-110P homogenizer (Microfluidics, Westwood, MA). Cell debris were then pelleted by centrifugation at 12,000 rpm, 4°C for 30min twice, transferring supernatant to a new tube after the first and second centrifugation. For HIS-tagged purification, 300 µL of nickel-nitrilotriacetic acid (Ni-NTA) agarose beads (Qiagen, Valencia, CA) was added to each 500mL culture of cell lysate and incubated at 4°C for 3 hours with agitation; for Myc-tagged purification, 20-25 µl of Myc-conjugated magnetic beads (Cell Signaling, Danvers, MA) were added to each 500 mL culture of cell lysate and incubated at 4°C for 2 hours with agitation. After incubation, Ni-NTA beads for HIS-tagged purification were washed twice with 10-15 mL ice cold lysis buffer without protease inhibitor (centrifugation at 1000 rpm, 4°C), transferred to polypropylene column and washed with additional 50 ml of lysis buffer without protease inhibitor. Myc-conjugated magnetic beads were washed with 4 ml of ice-cold lysis buffer without protease inhibitor per 5 µl of beads, using magnetic field to separate liquid from the beads. HIS-tagged protein were then eluted 3 times with 300 µl of elution buffer containing 250 mM imidazole and 100 mM NaCl without protease inhibitors. HIS-tagged protein can then be stored in 15% glycerol at -80°C. Myc-tagged protein were used immediately after purification without eluting.

WT Snf1-Myc/ Snf1 KD-Myc/ PRKAA1 were incubated with Osh6/ Osh7/ ORP8 PH-OSBP/ ORP8 OSBP in total volume of 30 µl of reaction mixture containing 1X Snf1 kinase buffer (50 mM Tris-HCl, 10 mM MgCl2), 1 mM dithiothreitol (DTT), pH 7.5, 10 µM ATP, and

7.5 μCi of γ32P-ATP (MP Biomedicals) for 35 min at 30°C. Kinase assays were stopped by the addition of 6X SDS-PAGE sample buffer, analyzed by SDS-PAGE, stained with coomassie blue (30 min), destained for 2 h, soaked in water for 1 h, dried and exposed to film in -80°C.

2.7.4 Yeast-2-hybrid assays

Plasmid containing Osh7 OSBP domain (pJG1355) and coiled coil (CC) domain (pJG1353) were PCR amplified using JG3763/JG3764, JG3765/JG3209 from pJG1115 and cloned into pJG549. Bait plasmid with Gal83/Sip1/Sip2/EV control were co-transformed with prey plasmid with full length Osh7/ OSBP/ CC/ EV control into Y2H Gold strain (JGY1031) and selected on SD-Leu-Trp plates and grown for 2 days at 30°C. Transformants were inoculated into 5 mL liquid cultures in SD-Leu-Trp and grown overnight, then serial diluted 1:5- 3,125 fold and 5uL of each dilution were spotted on SD-Leu-Trp plates as growth control and SD-Leu-Trp-His-ade plates to select for protein-protein interaction. Each construct has been tested with corresponding EV bait/prey plasmid control to eliminate false positive results.

2.7.5 Co-IP of Osh6/ Osh7 with Snf1

His-tagged Osh6/Osh7 were purified from *E. coli* BL21 (DE3) using standard His-tagged protein purification as previously described. Yeast (JGY4) harboring plasmid with Snf1 under ADH promoter (pJG1193) were grown in SD-URA for 12 hours then transfer to SGal-Ura for 36 hours. Cells were then pelleted and resuspended in myc-tagged purification lysis buffer (20 mM HEPES, 10 mM KCl, 1 mM EDTA, 1 mM EGTA, 50 mM NaCl, 10% glycerol, 1 mM β-mercaptoethanol, Pierce Protease Inhibitor Tablet, pH 7.4, with phosphatase inhibitor-- 50 mM NaF, 35mM glycerophosphate) and lysed open using glass beads disruption. Cell lysate were then centrifuged at 14,000 rpm for 30 min twice to remove cell debris. Purified Osh6-HIS and Osh7-His were then added into JGY4-Snf1-myc lysate followed by Myc-tagged protein

purification using Myc-Tag mouse mAB conjugated magnetic beads (Cell Signaling Technology #5698) to pull down Snf1-myc. Protein bound beads were then washed multiple times and boiled in sample buffer before separation on 10% SDS-PAGE. Osh6/Osh7 were detected with western blotting using anti-His antibody (Proteintech #HRP-66005) at 1:10,000, 2.5% milk TBST, and Snf1 using anti-myc antibody at 1:1000, 5% BSA, TBST.

2.7.6 Stability assays

WT yeast (JGY1) and Snf1 knockout yeast (JGY91) harboring plasmids with WT Osh7/ WT Snf1/ Kinase dead (KD) Snf1/ EV-HIS and/ or EV-Myc control were grown overnight at 30°C, diluted 1:100 into 100mL of SD-Ura-Trp and grown for 12 hours. Cells were then pelleted and resuspended in SGal-Ura-Trp and induce protein expression for 36 hours. Cells were subject to standard His-tagged purification followed by western blotting or crude lysate analysis. Crude lysate analysis: OD_{600} =1 number of cells were resuspended in 10% Trichloroacetic acid (TCA; 10% final concentration) and incubated for 10 min on ice. Cells were then pelleted by centrifugation at 14,000 rpm at 4°C for 10 min. After washing the pellet twice with 1 ml of ice-cold acetone, the pellet is air-dried. Air dried pellet were then resuspended in 100 µl of sample buffer (150 mM Tris-HCl, pH 8.8, 6% SDS, 25% glycerol, 6 mM EDTA, 0.5% 2-mercaptoethanol, and 0.05% bromophenol blue) and lysed by vortex with glass beads for 4 min followed by boiling at 100°C for 3 min. Proteins in crude lysate were then resolved in 10% SDS-PAGE and subject to western blots analysis. Presence of Osh6/Osh7-His were detected with anti-His and anti-UGP1 (a kind gift from Jared Rutter's Lab) were used as a loading control.

2.7.7 Microscopy for Osh6-YFP and Osh7-YFP localization

Yeast harboring YFP-Osh7 (pJG1697) and YFP-Osh6 were grown overnight in 2% glucose SD-URA, diluted 1:100 in 10mL 2% glucose SD-Ura and grown to log phase (4 hours at

30°C). Cells were then pelleted and resuspended in 0.05% glucose SDD-URA for 2 hours. Cells were imaged before and after starvation using Fluoview confocal microscope. Osh7-YFP co-localization with Mdm34-mCherry were counted (n=100cells) and analyzed using Prism.

2.7.8 Florescent microscopy mitochondria morphology

Cells harboring Mito-TFP plasmid were grown to log phase in SDD-His and then starve in SD-N for 6 hours. Mitochondria morphology were analyzed using a Nikon microscope (model E800) before and after starvation.

2.7.9 Plate testing for respiration

WT, Δosh6, Δosh7 and Δosh6Δosh7 were grown for 2 overnights in 3mL SD-complete at 30°C. Saturated culture were then serial diluted to 1:5- 3,125 fold in water and 5uL of each dilution were spotted on SD-complete plate (growth control) and SGE-complete plate to test for mitochondria dysfunction. Plates were incubated at 30°C for 2-3 days.

2.7.10 Whole yeast seahorse respiration assay

Cell Culturing and Culture Plate Preparation. A detailed explanation for the entire Seahorse protocol is contained within the supplementary protocol but will be briefly explained here. Single and double knockout strains were streaked onto YPAD and then liquid cultures were started in SD-Complete. During this time a Seahorse Cell Culture Plate was also prepared for cell seeding on the day of the assay. Overnight cultures were diluted into SGE-Complete after which cells were plated and allowed to incubate until the beginning of the respiration assay.

Sensor cartridge and drug preparation. While preparing the cell culture plate the wells and moats of the sensor cartridge utility plate were filled with XF calibrant and placed in a non-CO2 humidified 37º C incubator overnight. Carbonyl cyanide-p-

trifluoromethoxyphenylhydrazone (FCCP) and triethyltin chrloride (TET) used to test different respiratory conditions were prepared the day of the assay. Injection ports A and C of the sensor cartridge were loaded with 20 µl of S-Complete, port B TET, and port D FCCP. The sensor cartridge and utility plate were loaded into the XFp Analyzer for initial calibration.

OCR Normalization and XFp Analyzer Settings. Measurement cycles were performed as a 3 min mix, no wait, and 3 min measurement. Basal respiration was measured three times, port A injection twice, port B four times, port C twice, and port D four times. OCR was normalized to viable cells by plating serial dilutions of cell cultures on YPAD and calculating CFU/µl.

2.7.11 Mitophagy assays

Mitophagy of WT, *Δosh6, Δosh7* and *Δosh6Δosh7* yeast were monitored using OM45-GFP processing assay as previously described [110] and microscopy using mitochondria targeting TFP and vacuole targeting Vph1-RFP assays. Mitophagy was induced using post-log phase method in OM45-GFP processing assays followed by detection of mitophagy using western-blotting with anti-GFP (Proteintech #66002-1).

Mitophagy studies using chimeric fusion proteins were performed in live cells and imaged using florescent microscopy. For all experiments, cells were grown to mid-log (5x106 cells/mL), spun down and washed with H2O and resuspended in SD-N media for 24 hours. Cells were then analyzed by fluorescence microscopy and images were obtained using a Nikon microscope (model E800) with a 60x objective (Plan Fluor Oil, NA 1.3) and a CCD camera (RETIGA Exi). Data were collected using Autoquant and processed using Image Pro software. All images were obtained using the same exposures for the course of the experiment. Plasmids used: RSB2598 ADH1-mitoTFP-CYC1, RSB2600 ADH1-Vph1-mCherry-CYC1.

2.8 Supplementary methods

2.8.1 Cell culturing and culture plate preparation

The knockout yeast strains were streaked on YPAD solid media and grown for 54 hours at RT. Different growth times and temperatures were tested with varying degrees of success. Room temperature was chosen because we wanted to avoid gaining suppressors in the knockouts and hiding interesting phenotypes. Using a growth time of 54 hours allowed the colonies to become large enough to pick but minimized suppressor acquisition. Less time also yielded poor growing liquid cultures in the next step, which failed to respire. We inoculated 5 ml of SD-Complete liquid media in triplicate (to make sure at least one would reach saturation) with single colonies and grew them at 30º for 42 hours while rotating. At this stage 30º was chosen because room temperature cultures yielded erratic oxygen rates and sometimes would not respire despite the cells being alive when tested later. Approximately 18 hours before the assay the wells of the cell culture plate were coated with 50 µl of 0.25 mg/ml concanavin A, add 400 µl of water per moat, and store at 4º. After the 42 hours we then diluted 100 µl of saturated cell culture into 5 ml of SGE-Complete, made day of experiment, and let them grow at 30ºC for 6 hours while rotating. If the cultures don't look saturated then there is a good chance it won't respire. While it is possible for a strain to be so slow growing it doesn't get saturated but can still respire we often saw that lack of saturation correlated with no respiration or it was erratic. The cells were then centrifuged at 3000 rpm for three minutes and the pellets resuspended in fresh SGE-Complete to an OD600 between 0.2 and 0.3. Seeding the proper number of cells for a Seahorse respiration assay is important as the machine has an optimal OCR range where the readings can be normalized correctly. Using saturated cultures as described above for these strains will put them close to the 0.2 to 0.3 OD600 range. Most strains are optimal for seeding near 0.25. However, it

should be noted that strains used in other experiments while this protocol was designed were optimal near 0.2 and 0.35. We seeded 50 µl of cell suspension into wells B-G and 50 µl of SGE-Complete into wells A and H of the cell culture plate. The plate should be washed with water prior to seeding to remove unbound concanavin A. After seeding the plate was centrifuged at 300 rpm for 1 min with no brakes and cell adherence was verified under a microscope. The volume of the wells was brought up to 180 µl with SGE-Complete, the moats filled with 200 µl of water, and the plate was placed in a 30º incubator for 40 min until loading into the Seahorse XFp Analyzer.

2.8.2 Sensor cartridge and drug preparation

While preparing the cell culture plate the day before the assay. We filled the wells and moats of the sensor cartridge utility plate with 200 and 400 µl of XF calibrant, respectively and placed it in a non-CO2 humidified 37º incubator overnight. Three hours prior to beginning the assay we prepared a 260 µM carbonyl cyanide-p-trifluoromethoxyphenylhydrazone (FCCP) and 10% ethanol solution in S-Complete. At this stage ethanol is the primary carbon source for the yeast and minimizing the amount added is ideal. To make the FCCP got into solution it was incubated in a 45º water bath. It should have a transparent very light-yellow color when ready. After the cell culture plate has started its 40 min incubation we prepared an 806.3 uM solution of triethyltin chloride (TET) in S-Complete in a chemical fume hood. Warnings on the bottle included fatal when inhaled, fatal when ingested, and fatal when in contact with skin. Keep reagent bottle wrapped in absorbent material and in a sealed secondary container. TET has a damp earth and musty or moldy smell to it. If the smell is strong or present for a long time something is wrong with containment. The smell is occasionally detectable when the resealed container is taken from the fumehood but it isn't detectable when diluted and is safe to handle.

We then loaded injection ports A and C of the sensor cartridge with 20 µl of S-Complete, port B TET, and port D FCCP. The sensor cartridge and utility plate were inserted into the XFp Analyzer for calibration. Once the calibration was over the cell culture plate was inserted.

2.8.3 OCR normalization and XFp analyzer settings

Measurement cycles were performed as a 3 min mix, no wait, and 3 min measurement. Basal respiration was measured three times, port A injection twice, port B four times, port C twice, and port D four times. OCR was first normalized to viable cells by plating serial dilutions of cell cultures on YPAD and calculating CFU/µl. Using the strains in the OD600 range described above in serial dilutions and plating has yielded easy counting when 50 µl of a 10-3 and 100 µl of a 10-4 dilution is plated. Cells started appearing after two days but an official count was taken after four days because some strains will have many colonies appear later.

CHAPTER 3: PAS kinase Regulates Cyclin C Localization in Yeast Through Direct Phosphorylation

Kai Li Ong[1], Katrina Cooper[2], Julianne Grose[1]

3.1 Author information

[1]Department of Microbiology and Molecular Biology, Brigham Young University, Provo, UT, 84602, USA

[2]Department of Molecular Biology, Graduate School of Biological Sciences, Rowan University, Stratford, NJ, 08084, USA

*Correspondence: grosejulianne@gmail.com; Tel.: +01-801-422-4940

Kai Li Ong - jkm525@go.byuh.edu

Katrina Cooper - cooperka@rowan.edu

Julianne Grose - julianne_grose@byu.edu

*The work described in this chapter has been submitted to a scientific journal and is under review. It has been formatted for this thesis, but it is otherwise unchanged.

3.2 Abbreviations

SSN2- Suppresor of SNF1

MED13- Mediator complex subunit 13

Cdk8- Cyclin dependent kinase 8

PASK- Per-Arnt-Sim (PAS) kinase

Psk1- Pas domain-containing Serine/threonine protein Kinase 1

Psk2- Pas domain-containing Serine/threonine protein Kinase 2

CWI- Cell wall intergrity

MAPK- Mitogen-activated protein kinases

CKM- Cdk8 Kinase module

Slt2- Suppressor of the LyTic phenotype 2

IDR- Intrinsic disordered region

Rho1- Ras Homolog 1

USF1- Upstream stimulatory factor 1

Pkc1- Protein kinase C 1

3.3 Abstract

Per-Arnt-Sim (PAS) kinase is an important nutrient sensing kinase that is evolutionarily conserved from yeast to man. It is known to increase lipid production in response to nutrients while decreasing respiratory metabolism. Herein we describe a novel function of PAS kinase in the regulation of cell death. SSN2 (MED13) was previously retrieved from a yeast two-hybrid screen for direct PAS kinase binding partners. Together with cylin C, Med13 is part of the CDK8 Kinase Module (CKM) in the multi-subunit mediator complex that acts as an interface between DNA bound transcription factors and RNA polymerase II. In yeast, Med13 is degraded in response to unfavorable cellular stress and triggers nuclear release of cyclin C into the cytoplasm where it promotes mitochondrial fragmentation and programed cell death. Herein we provide evidence for the direct phosphorylation and stabilization of Med13 by PAS kinase, the corresponding inhibition of nuclear cyclin C release, and the regulation of mitochondria fragmentation upon carbon or oxidative stress.

3.4 Introduction

Cells have developed complex mechanisms for sensing their cellular environment and control key metabolic processes appropriately. At the heart of these mechanisms are sensory protein kinases, capable of regulating many interrelated pathways through the phosphorylation of tens of substrates. Per-Arnt-Sim (PAS) kinase is a conserved sensory protein kinase that regulates glucose homeostasis in yeast, mice and humans.

PAS kinase controls a pivotal point in glucose allocation, the partitioning of glucose to lipid biosynthesis versus respiratory metabolism. In mice, PAS kinase-deficiency has been shown to protect against weight gain, hepatic triglyceride accumulation, and insulin insensitivity when mice are placed on a high-fat diet [77]. These mice are also hypermetabolic in that they

display increased whole-animal CO_2 output and O_2 uptake when compared to their wild-type littermates. This protection from hepatic triglyceride accumulation was also seen in PAS kinase-deficient mice placed on a high-fat high-sugar diet, which more closely resembles the western diet [116]. In addition, liver and muscle tissue from these mice displayed increased respiratory rates when compared to the wild type littermates. These effects on triglyceride and respiratory metabolism appear to be evolutionarily conserved in that yeast PAS kinase also controls lipid biosynthesis and respiration, in part through the phosphorylation of its substrate Cbf1 [82].

In addition to the regulation of triglyceride biosynthesis and respiratory metabolism, PAS kinase is regulated by nutrient status. PAS kinase activity increases upon fasting and refeeding, as well as by the addition of glucose [78]. In addition, PAS kinase has also been shown to control pancreatic B-cell insulin and glucagon production in response to glucose in both humans and mice studies [117-120].

Herein we describe a novel function for PAS kinase in regulating mitochondrial fragmentation and cell death through the phosphorylation and subsequent stabilization of Med13 (also known as SSN2 in yeast). Med13, together with cyclin C, is part of CDK8 Kinase Module (CKM) in the multi-subunit mediator complex that acts as an interface between DNA bound transcription factors and RNA polymerase II. In yeast, Med13 is degraded in response to unfavorable cellular stress such as peroxide stress [121, 122]. This degradation triggers nuclear release of cyclin C into the cytoplasm, where cyclin C associates with the mitochondria to promote mitochondrial fragmentation and programed cell death. The glucose responsive kinase Snf1 has recently been shown to regulate Med13 degradation in response to reactive oxygen species [122]. Herein we describe a novel, direct role for a second sensory kinase in this pathway, placing PAS kinase as a regulator of cell death in response to glucose.

3.5 Results

3.5.1 PAS kinase 1 (Psk1) interacts with Med13 in vivo

A previous large-scale yeast-2-hybrid (Y2H) screen for PAS kinase binding partners identified Med13 as putative direct binding partner of Psk1 [82]. The interaction between Med13 and PAS kinase was further studied through truncation analysis, with amino acids 571-650 being required (Figure 3-1). This region is part of the intrinsic disordered region (IDR) of Med13 and has been previously identified as the Med13 degron, the region required for Med13 degradation. IDR's are defined by a continuous stretch of flexible, disorder-promoting residues that are key to cellular control in that they facilitate the relay of macromolecular decisions as they transition to more ordered states.

3.5.2 Psk1 phosphorylates Med13 in vitro

The relationship between Med13 and Psk1 has not been previously explored and there are many possible outcomes from their protein-protein interaction. For example, Med13 could be a binding partner that regulates Psk1 activity, such as by localizing it to the CKM, or it could serve as a substrate of Psk1. We therefore purified Psk1 as well as Med13 and assayed for direct, Psk1-dependent phosphorylation through *in vitro* kinase assays (Figure 3-2). Psk1 phosphorylated $Med13^{571-650}$ *in vitro*, while the kinase dead (KD) mutant of Psk1 showed only weak phosphorylation, suggesting that Med13 is directly phosphorylated by Psk1. Note that Psk1 has been previously show selectively for only certain phosphorylate substrates under the in vitro kinase conditions utilized herein [82].

A.

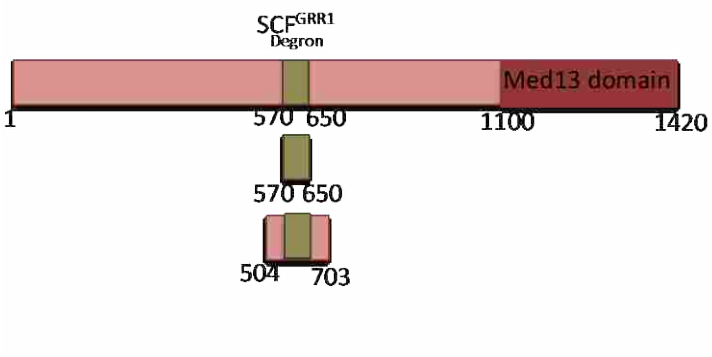

B.

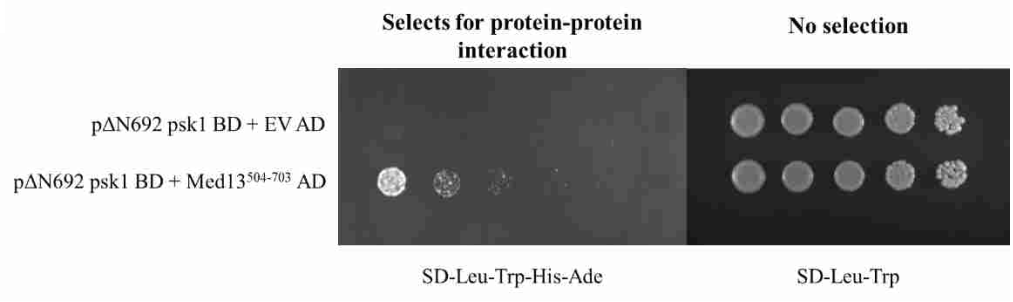

Figure 3-1 PAS kinase directly binds to Med13 as found in a yeast two-hyrid assay (A) A diagram of the full length Med13 protein, indicating the region of the SCFGRR1 degron and the mediator complex subunit 13 (Med13) domain. The two yeast two-hybrid constructs that bind to PAS kinase 1 (Psk1) are indicated below the full-length protein. Both contain the degron. (B) A dilution series showing the strength of the interaction between Psk1 and Med13$^{504-703}$.

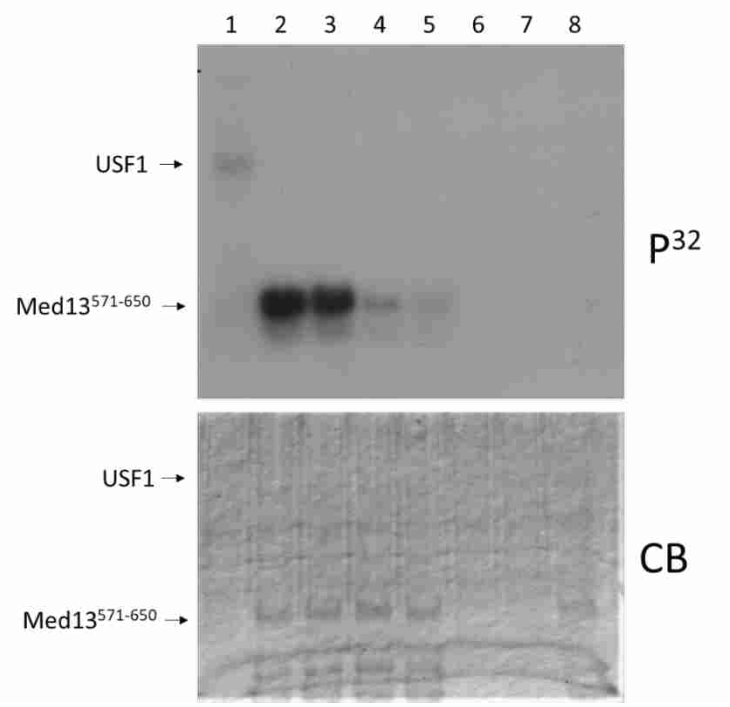

Figure 3-2 Psk1 phosphorylates Med13 *in vitro* Purified Med13$^{571-650}$ was incubated with radiolabeled ^{32}-P ATP in the presence or absence of purified Psk1/ Psk1-KD for 12 min at 30°C. Samples were then resolved in 12% SDS–PAGE, followed by staining with Coomassie blue. Gels were then dried and imaged on x-ray film. Lane 1: Psk1+USF1; Lane 2&3: Psk1+ Med13$^{571-650}$; Lane 4&5: Psk1-KD+ Med13$^{571-650}$; Lane 6: Psk1 only; Lane 7: Psk1-KD only; Lane 8: Med13$^{571-650}$ only. Psk1 is not visible in the Coomassie Blue stained gel due to low protein concentration.

3.5.3 Psk1 is required for Med13 degradation in response to carbon stress

In order to determine the effects of Psk1-dependent Med13 phosphorylation *in vivo*, the stability of cyclin C was assessed in response to carbon source, a known regulator of Psk1 activity [123]. As shown in Figure 3-3B, Med13 is degraded upon switching from high glucose to low glucose (0.5%). This degradation is dependent upon PAS kinase as it is not seen in the Δpsk1Δpsk2 yeast.

Cyclin C nuclear release before and after glucose stress was also examined with Fluoview confocal microscope. PAS kinase appears to play a role in the nuclear release of cyclin

C as well upon 2 hours of 0.05% glucose stress in that cyclin C remains nuclear in many of the PAS kinase-deficient (Δpsk1Δpsk2) yeast (Figure 3-3B).

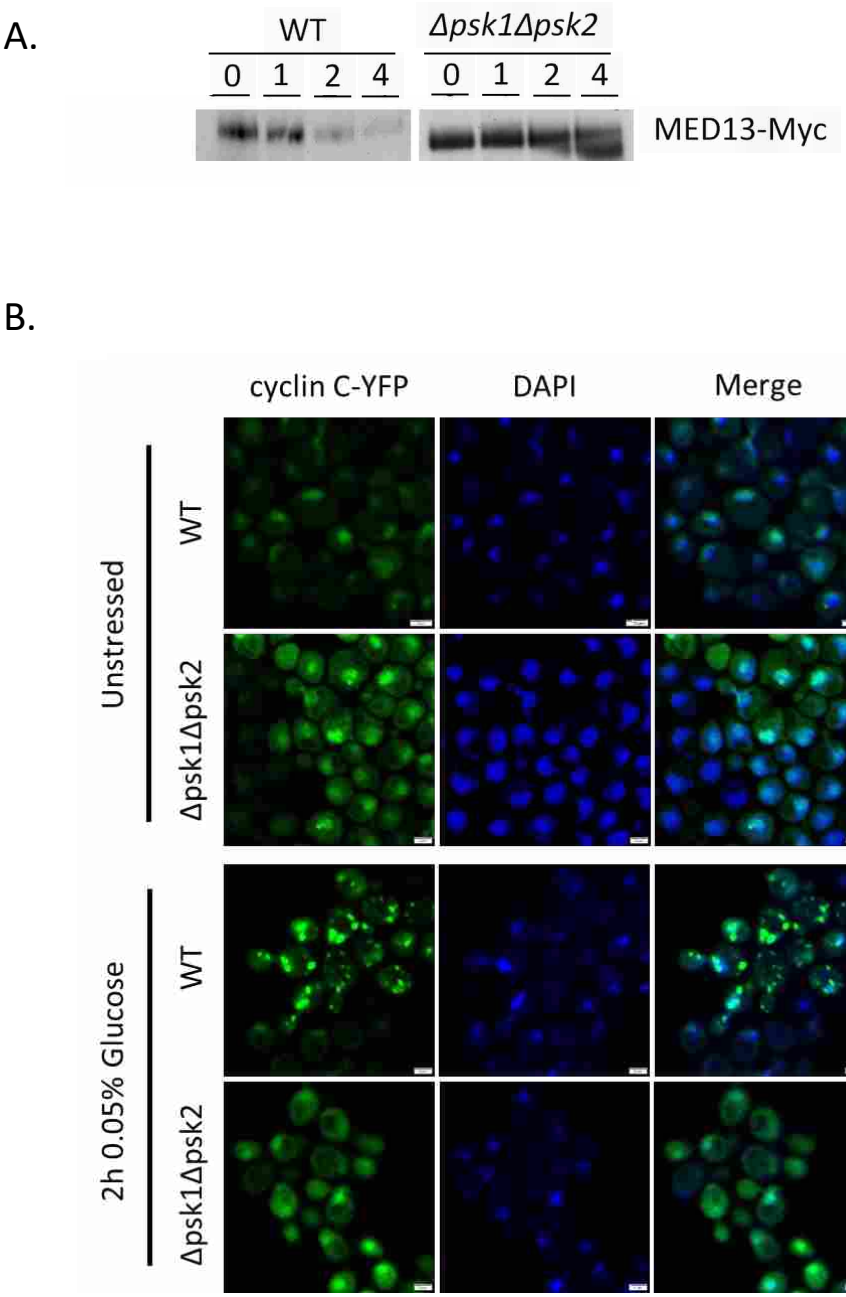

Figure 3-3 PAS kinase is required for Med13 degradation in response to carbon stress (A) Wild type and Δpsk1Δpsk2 yeast overexpressing Med13-Myc were transferred from 2% glucose to 0.5% glucose for 0, 1, 2 and 4 hours, and yeast extracts were analyzed by western blot using anti-myc antibody for MED13-Myc detection (cell signaling). (B) Cyclin C localization in WT and Δpsk1Δpsk2 knockout strain were observed with Fluoview confocal microscope before and after 2 hours 0.05% glucose stress. Yeast harboring plasmids with cyclin C-YFP, mito-mCherry were used in this study and NucBlue™ Live ReadyProbes™ was used to visualize the nucleus.

3.5.4 Psk1 affects localization of cyclin C and its nuclear release upon oxidative stress

The degradation of Med13 has been shown to promote the export of cyclin C from the nucleus into the cytoplasm, where it binds mitochondria to initiate fragmentation and subsequent cell death. The localization of cyclin C was therefore used as a readout for Med13 activity in wild type versus PAS kinase-deficient yeast (Δpsk1Δpsk2). As previously shown, cyclin C is exported to the cytoplasm in response to 1mM H_2O_2 stress (Figure 3-3). This localization was inhibited to an extend by PAS kinase deficiency. In Δpsk1Δpsk2 yeast, a single peri-nuclear foci of cylin C-YFP is seen under normal growth condition and upon 2h oxidative stress, with lesser nuclear release of cyclin C after 2h oxidative stress compared to wild type.

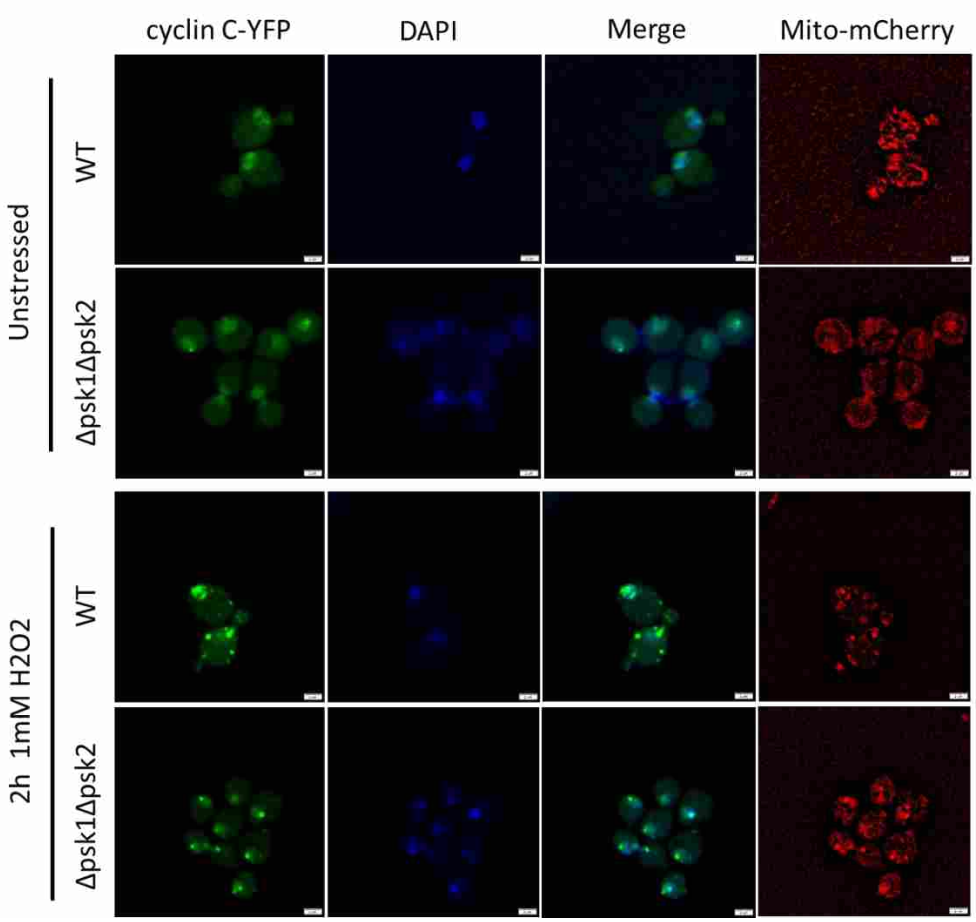

Figure 3-4 PAS kinase plays an important role in cyclin C nuclear release upon oxidative stress Localization of cyclin C-YFP in wild-type or Δpsk1Δpsk2 cells before and following 2 h treatment with H_2O_2 (1 mM) was visualized through Fluoview confocal microscope. Perinuclear foci of cylin C-YFP is seen in Δpsk1Δpsk2 cells and psk1/ psk2 affected nuclear release of cyclin C upon oxidative stress.

3.6 Conclusions

Cell death pathways are intimately tied to external cues, containing many check points in order to avoid unnecessary destruction. One such cell death pathway is the cyclin C pathway in which is translocation from the nucleus to the cytoplasm results in mitochondrial fragmentation and, ultimately, cell death. We have previously shown cyclin C translocation to be dependent on two critical pathways (Figure 3-5). First is the Cell Wall Integrity (CWI) MAPK pathway. In this pathway, cell wall sensors including Wsc1, Mtl1 and Mid2 are activated by stresses such as

hydrogen peroxide, leading to the activation of Rho1 which phosphorylates protein kinase C (Pkc1), initiating the CWI MAPK cascade. Slt2 is activated by this cascade, and phosphorylates cyclin C, which in turn phosphorylates Med13 in a priming event. Med13 is then phosphorylated by Slt2, targeting it for destruction by the ubiquitin-mediated SCF^{GRR1} pathway. Recently, the SNF1 complex was shown to be required for this pathway, but the molecular mechanisms of this pathway have not been described. Herein we provide evidence that PAS kinase, a known downstream target of SNF1, directly phosphorylates Med13 and is required for its degradation in response to carbon or hydrogen peroxide stress. A model for the regulation of cyclin C localization through a cascade including PAS kinase (Psk1) is shown in Figure 3-5.

First, yeast Psk1 directly interacts with Med13 *in vivo*, specifically at the previously identified degron (amino acids 571-650, Figure 3-1), and phosphorylates Med13 *in vitro* (Figure 3-2). PAS kinase is also required for the degradation of Med13 by the SCF^{GRR1} pathway in response to carbon stress. And finally, PAS kinase-deficiency leads to cyclin C retention in the nucleus.

The complexity of two signaling cascades involving several protein kinases allows for careful control of the cell death pathway in response to several external stimuli. The CWI pathway has been shown to be activated by many cell membrane perturbing agents, including chlorpromazine. Interestingly, PAS kinase is also activated by cell integrity stress [123], including the cell membrane perturbing agent chlorpromazine. In addition to cell integrity stress, PAS kinase is well-known to respond to nutrient status, particularly glucose, in both yeast and mammalian cells [75, 78, 123]. Herein we provided the first evidence for Med13 degradation and cyclin C export in response to glucose depravation (Figure 3-3).

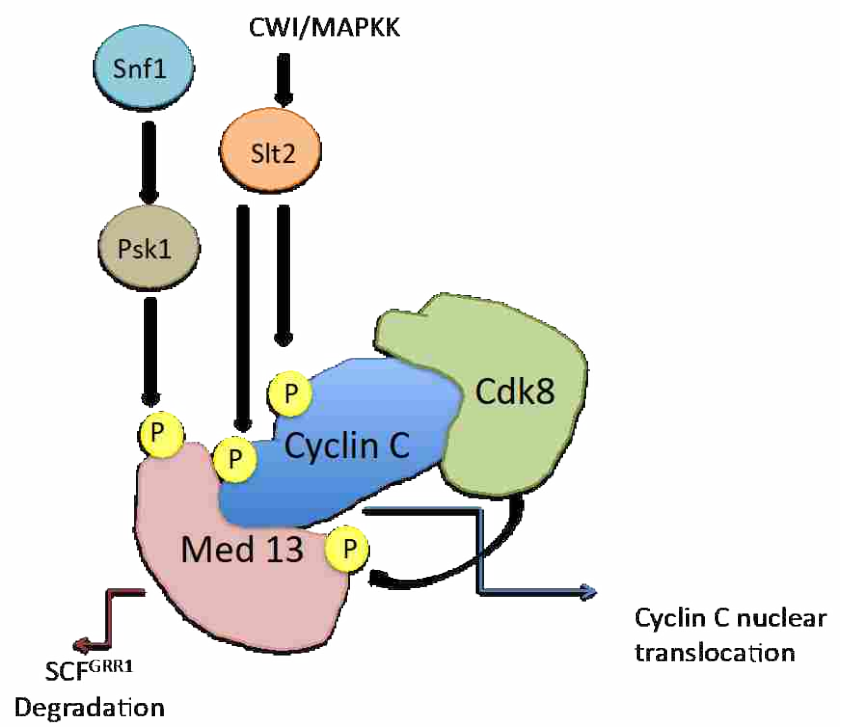

Figure 3-5 A model for the regulation of cyclin C localization through a cascade including PAS kinase (Psk1) Cell wall stress (such as peroxide) stimulates cell wall sensors (Wsc1, Mtl1 and Mid2) to activate Rho1 which in turn activates protein kinase C (Pkc1) which triggers the SWI MAPK cascade, leading to the activation of Slt2. Slt2 directly phosphorylates cyclin C, which then primes the degron through cyclin C/Cdk8 phosphorylation of Med13. A second phosphorylation event is required. Snf1 kinase, in response to peroxide or carbon stress, activates PAS kinase and phosphorylates Med13, targeting the degron for ubiquitin-mediated SCF^{Grr1} degradation.

In addition to Med13, three other yeast PAS kinase substrates have been characterized. First, UDP-glucose pyrophosphorylase (UGP1), a key enzyme in glucose utilization for glycan biosynthesis, a component of the yeast cell wall. Phosphorylation of Ugp1 results in increased increased cell wall biosynthesis, necessary for growth, and decreased glycogen storage. This pathway is consistent with the role of PAS kinase described herein in-conjunction with the cell wall integrity pathway. Second, PAS kinase phosphorylates yeast Cbf1, shifting cellular metabolism from respiration and toward lipid biosynthesis, which lipids are also required for the cell membrane. And finally, PAS kinase phosphorylates yeast Pbp1 to activate stress granule formation and TORC1 inhibition at stress granules [124]. In addition to these two substrates, yeast Psk2 has been shown to activate Rho1 by an unknown mechanism, suppressing the growth

defect of a tor2 temperature-sensitive mutant [125]. Each of these roles appears to be a cell survival role, promoting cell growth and proliferation. At first glance, they are strikingly juxtaposed to the cell death pathway described herein. However, it is likely that these sensory pathways play a two-fold role in the cell. First, they alert the cell to the need for increased glucans and lipids necessary for cell growth or to repair cell damage. And second, they initiate cell death when this damage is too severe. This is supported by the ability of Psk2 to activate Rho1, an upstream kinase in the Med13 pathway, suggesting PAS kinase regulates the Med13/cyclin C/Cdk8 pathway by two mechanisms. The Med13/cyclin C/Cdk8 pathway described herein requires several inputs and priming events, ensuring that cell death is not initiated without several inputs.

3.7 Experimental procedure

3.7.1 In vitro kinase assay

Yeast (JGY142 or JGY4) harboring wildtype Psk1-HIS (pJG1089), kinase dead Psk1 KD-HIS (pJG1170) or were grown in selective 2% glucose synthetic minimal medium (SD-Trp/Ura) overnight, diluted 1:100 into 500mL of SD-Trp/ Ura and grown for 12 hours, pelleted and resuspended in 500mL of selective 2% galactose synthetic minimal media (SGAL-Trp/Ura) and grown for 36 hours.

BL21 (DE3) *Escherichia coli* harboring Med13-HIS were grown overnight at 37°C in Luria Bertani broth supplemented with ampilicin (LB Amp), diluted 1:100 into 500mL of LB Amp and grown for 3 hours, followed by 5 hours induction in LB Amp supplemented with 0.5 mM of IPTG. Cells were pelleted and resuspended in HIS-tagged purification lysis buffer (50 mM HEPES, 300 mM NaCl, 20 mM imidazole, 10 mM KCl, 1 mM β-mercaptoethanol, Pierce Protease Inhibitor Tablet, pH 7.8) with or without phosphatase inhibitor (50 mM NaF, 35mM

glycerophosphate). Cell suspension were then lysed with Microfluidics M-110P homogenizer (Microfluidics, Westwood, MA). Cell debris were then pelleted by centrifugation at 12,000 rpm, 4°C for 30min twice, transferring supernatant to a new tube after the first and second centrifugation. For HIS-tagged purification, 300 µL of nickel-nitrilotriacetic acid (Ni-NTA) agarose beads (Qiagen, Valencia, CA) was added to each 500mL culture of cell lysate and incubated at 4°C for 3 hours with agitation. After incubation, Ni-NTA beads for HIS-tagged purification were washed twice with 10-15 mL ice cold lysis buffer without protease inhibitor (centrifugation at 1000 rpm, 4°C), transferred to polypropylene column and washed with additional 50 ml of lysis buffer without protease inhibitor. HIS-tagged protein were then eluted 3 times with 300 µl of elution buffer containing 250 mM imidazole and 100 mM NaCl without protease inhibitors. HIS-tagged protein were then be stored in 15% glycerol at -80°C.

WT Psk1-His/ Psk1 KD-HIS were incubated with Med13-HIS in total volume of 30 µl of reaction mixture containing 1X kinase buffer (pH 7.5), 0.2mM ATP, and 0.2 µCi of γ32P-ATP (MP Biomedicals) for 12 min at 30°C. Kinase assays were stopped by the addition of 6X SDS-PAGE sample buffer, separated by SDS-PAGE, stained with coomassie blue (30 min), destained for 2 h, soaked in water for 1 h, dried and exposed to film in -80°C.

3.7.2 Cyclin C-YFP nuclear release microscopy

WT (JGY1) and Δpsk1Δpsk2 (JGY4) yeast strain were transformed with cyclin C-YFP (pJG1703) and mitochondria targeting mCherry plasmid- Mito-mCherry (pJG1691). 50 µL of overnights from each transformant were transferred to 25mL of SD-URA-TRP (2% glucose) and cultures were grown to late log phase (OD_{600} = 0.8~1.3), followed by 2 h of 1mM H_2O_2/ switching to 0.05% glucose SD-URA-TRP treatment. Cells were then fixed immediately in 70% ethanol and store in 4°C for >12 h. Before imaging with Fluoview confocal microscope, cells

were pelleted, washed twice in 1mL ddH_2O and stained with NucBlue™ Live ReadyProbes™ at the concentration of 1 drop/ml for 20 minutes under room temperature.

3.7.3 Yeast-2-Hybrid Assay

Prey plasmid containing Med13$^{570\text{-}650}$ (pJG1465) were co-transformed with bait plasmid containing psk1(pJG598)/ EV control (pJG421) into Y2H Gold strain (JGY1031) and selected on SD-Leu-Trp plates and grown for 2 days at 30°C. Transformants were inoculated into 5 mL liquid cultures in SD-Leu-Trp and grown overnight, then serial diluted 1:5- 3,125 fold and 5uL of each dilution were spotted on SD-Leu-Trp plates as growth control and SD-Leu-Trp-His-ade plates to select for protein-protein interaction. Each construct has been tested with corresponding EV bait/prey plasmid control to eliminate false positive results.

CHAPTER 4: Concluding Remarks

Metabolic diseases are a global epidemic and deregulation of cellular metabolism can lead to a wide variety of disease including metabolic syndrome, obesity, neurodegenerative disorder and various types of cancer. They occur when cells allocate too many of their primary resources towards one pathway at the expense of another pathway, or simply due to improper response to cellular stress leading to deregulation of cellular processes, organellar dysfunction, or even cell death. My research focused on the understanding of interplay between key metabolic regulators: AMPK/SNF1, PASK/PSK1, identifying novel downstream targets of these kinases: MED13/SSN2, OSBP/(OSH6/OSH7) and characterizing their role in mitochondrial function as well as regulation of mitochondria signaling. With the central role of mitochondria in cellular energy homeostasis as well as the regulation of key cellular processes such as proliferation, growth and cell death, understanding how cells control mitochondrial respiration and maintain mitochondrial health through cross-talk between metabolic regulators is key to developing effective treatments for many common diseases resulting from metabolic dysfunction, particularly mitochondrial dysfunction.

Sensory protein kinases are a major way in which the cell regulates central metabolism. They can phosphorylate tens of substrates to control entire metabolic pathways, shifting the metabolism of the cell depending on nutrient availability, cellular energy level or different stressors. AMP-activated kinase (AMPK) and Per-Arnt-Sim kinase (PASK) are two of the main metabolic regulators in the cells. Both kinases regulate critical metabolic nodes of central metabolism: lipid versus respiratory metabolism, anabolic versus catabolic metabolism and control mitochondria function and health. In Chapter 2, we explored the regulation of the oxysterol binding protein Osh7 by SNF1— the yeast AMPK ortholog and provided evidence for

conservation of this regulation in mammalian cells. As part of this study, we investigated the localization and function of Osh7 and its close homolog, Osh6. Deficiency of either Osh6 or Osh7 both causes a mitochondrial phenotype, with Osh6-deficeincy being more severe. We provide evidence that this mitochondrial defect may be due to defects in mitophagy, a pathway for clearing damaged mitochondrial which is commonly disrupted in many diseases including heart disease, diabetes, cancer, and neurodegeneration. Although previously thought to have redundant cellular roles, evidence is displayed herein for the preferred localization of Osh7 at ER-mitochondria contact sites, whereas Osh6 remains primarily cytoplasmic. In addition, the regulation by Snf1 is specific for Osh7. Thus, we have uncovered a major pathway for the regulation of mitochondrial health, under the control of the master and commander SNF1/AMPK through oxysterol binding protein.

In Chapter 3 and appendix chapters 1 and 2, we investigated the role of both SNF1 and PAS kinase in mitochondrial and cell death regulation through the phosphorylation of Med13, a key regulator of cyclin C. Med13 controls cyclin C export from the nucleus, when Med13 is inactivated cyclin C is exported to the cytoplasm. In the cytoplasm cyclin C associates with the mitochondria to induce fragmentation and ultimately, cell death. In collaboration with the cyclin C experts at Rowan University (Katrina Cooper's Laboratory), we have shown that Snf1 is required for Med13 activity in response peroxide stress, whereas PAS kinase directly phosphorylates Med13 and controls its activity in response to both peroxide and carbon stress. In a Snf1 mutant or a PAS kinase mutant, cyclin C is trapped in the nucleus. Nuclear release of cyclin C is known to promote mitochondria fission and timely apoptosis when necessary. Combined these results support a model in which Snf1 and PAS kinase control cell death in

response to both AMP and glucose levels. Each of these proteins are conserved from yeast to man, suggesting that these pathways may be key in metabolic diseases in human as well.

The complexity of these metabolic pathways is only matched by the complexity of their regulation, requiring exquisite control by sensory proteins that can regulate entire processes. Herein we have further characterized two key metabolic controllers, AMPK and PAS kinase, and their control of mitochondrial health and cell death. Further characterization of these signaling pathways involving mitochondrial signaling, mitochondria health and functions may provide novel therapeutic targets in treating metabolic diseases, neurodegenerative disorders and cancer.

APPENDIX 1: Snf1 Cooperates with the CWI MAPK Pathway to Mediate the Degradation of Med13 Following Oxidative Stress

Stephen D. Willis[1], David C. Stieg[1], Kai Li Ong[2], Ravina Shah[1,3], Alexandra K. Strich[1,4], Julianne H. Grose[2] and Katrina F. Cooper[1, 5.]

Microb Cell. 2018 Aug 6; 5(8): 357–370.

A1.1 Author information

[1]Department of Molecular Biology, Graduate School of Biomedical Sciences, Rowan University, Stratford, NJ, 08084, USA.

[2]Department of Microbiology and Molecular Biology, Brigham Young University, Provo, UT 84602, USA.

[3]Current address: Department of Biological Sciences, Rowan University, 201 Mullica Hill Rd, Glassboro, NJ 08028. USA.

Current address: Shawnee High School, Medford, New Jersey 08055, USA.

Stephen D. Willis - willis58@rowan.edu

David C. Stieg - stiegdc@rowan.edu

Kai Li Ong - jkm525@go.byuh.edu

Ravina Shah - shahr8@rowan.edu

Alexandra Strich - 210619@lrstudents.org

Julianne Grose - julianne_grose@byu.edu

*This work described in this chapter was published in the journal Molecular Biology of the Cell in 2018. It has been formatted for this thesis but is otherwise unchanged.

A1.2 Abbreviations

PCD - Programmed cell death

ROS - Reactive oxygen species

SCF - Skp1, Cullin, F box E3 ligase

IDR - intrinsic disordered region

Cdk - cyclin dependent kinase

PKA - Protein Kinase A

MAPK - MAP Kinase

AMPK - 5' adenosine monophosphate-activated protein kinase

AMPKK - 5' adenosine monophosphate-activated protein kinase kinase

ORF - Open reading frame

ßME - ß-mercaptoethanol

CKM – cyclin C/Cdk8 kinase module

ROS - Reactive Oxygen Species

Y2H –Yeast Two Hybrid

A1.3 Keywords

Cyclin C; Cdk8; Med13; SCFGrr1; AMPK; Snf1; ubiquitin mediated destruction; signal transduction; H2O2 stress: MAPK

A1.4 Abstract

Eukaryotic cells, when faced with unfavorable environmental conditions mount either pro-survival or pro-death programs. The conserved cyclin C-Cdk8 kinase plays a key role in this decision. Both are members of the Cdk8 kinase module that, along with Med12 and Med13, associate with the core Mediator complex of RNA polymerase II. In *S. cerevisiae,* oxidative stress triggers Med13 destruction, which releases cyclin C into the cytoplasm to promote mitochondrial fission and programmed cell death. The SCF^{Grr1} ubiquitin ligase mediates Med13 degradation dependent on the cell wall integrity pathway MAPK Slt2. Here we show that the AMP kinase Snf1 activates a second SCF^{Grr1} responsive degron in Med13. Deletion of Snf1 resulted in nuclear retention of cyclin C and failure to induce mitochondrial fragmentation. This degron was able to confer oxidative-stress-induced destruction when fused to a heterologous protein in a Snf1 dependent manner. Although *snf1*Δ mutants failed to destroy Med13, deleting the degron did not prevent destruction. These results indicate that the control of Med13 degradation following H_2O_2 stress is complex being controlled simultaneously CWI and MAPK pathways.

A1.5 Introduction

All eukaryotic cells are continually exposed to changing environmental conditions. Consequently, they have evolved elaborate mechanisms to both sense damage and transmit this signal to the nucleus. The resulting response varies dependent upon the stress encountered but in gross terms cells have to decide whether to activate pro-survival or pro-death programs. Despite this being a critical decision point, what remains understudied are the molecular details of how cells decide their fate upon encountering unfavorable environments. Previous studies revealed that the conserved cyclin C protein plays a key role in this decision in response to increased

environmental reactive oxygen species (ROS) [126-134]. Cyclin C, together with its kinase partner Cdk8, Med12 and Med13, form the Cdk8 Kinase Module (CKM) of the multi-subunit Mediator complex. This complex acts as an interface between DNA bound transcription factors and RNA polymerase II (RNAP-II [135-137])When the CKM module is bound, it predominantly negatively regulates expression of a subset of stress response genes[126, 138-141]. Following an increase in environmental ROS (induced by H_2O_2 treatment), this repression is relieved by the nuclear release of cyclin C to the cytoplasm[127, 129, 134, 142]. Intriguingly, here cyclin C plays a second role directing stress-induced mitochondrial fission as well as promoting programmed cell death (PCD) [127, 132, 143, 144]. Consistent with this function, cells lacking cyclin C cells are less able to execute stress-induced mitochondria fission and are more resistant to oxidative stress [127, 143]. Taken together, these results argue that cyclin C nuclear release must be carefully controlled as it signals a commitment to PCD.

Our previous studies have revealed that a complex molecular mechanism that controls cyclin C nuclear release. In response to environmental ROS, cyclin C is directly phosphorylated by Slt2, the MAP kinase of the Cell Wall Integrity (CWI) signal transduction pathway ([131] and Figure A1-1A). This canonical pathway is characterized by a family of cell-surface sensors (Wsc1, Mid2 and Mtl1[144]) that transmit the stress to a small G protein Rho1, which thereafter activates protein kinase C (Pkc1)[145, 146]. Once activated, Pkc1 transmits the intracellular signal to the MAPK Slt2/Mpk1 [147] as well as to the pseudo-kinase Kdx1/Mlp1 via the MAPK module. In addition to cyclin C[131], Slt2 directly phosphorylates two other transcription factors (Rlm1, Swi4/Swi6) that stimulate the expression of other stress response genes[148-151]. More recently, Slt2 has also been shown to regulate gene expression by phosphorylating tyrosine-1 of the RNAP II carboxy-terminal domain[146, 152]. This event is

associated with pause/termination processes in mammals[153]. Intriguingly, it is required for the loss of cyclin C and Cdk8 from target genes following stress in yeast [152].

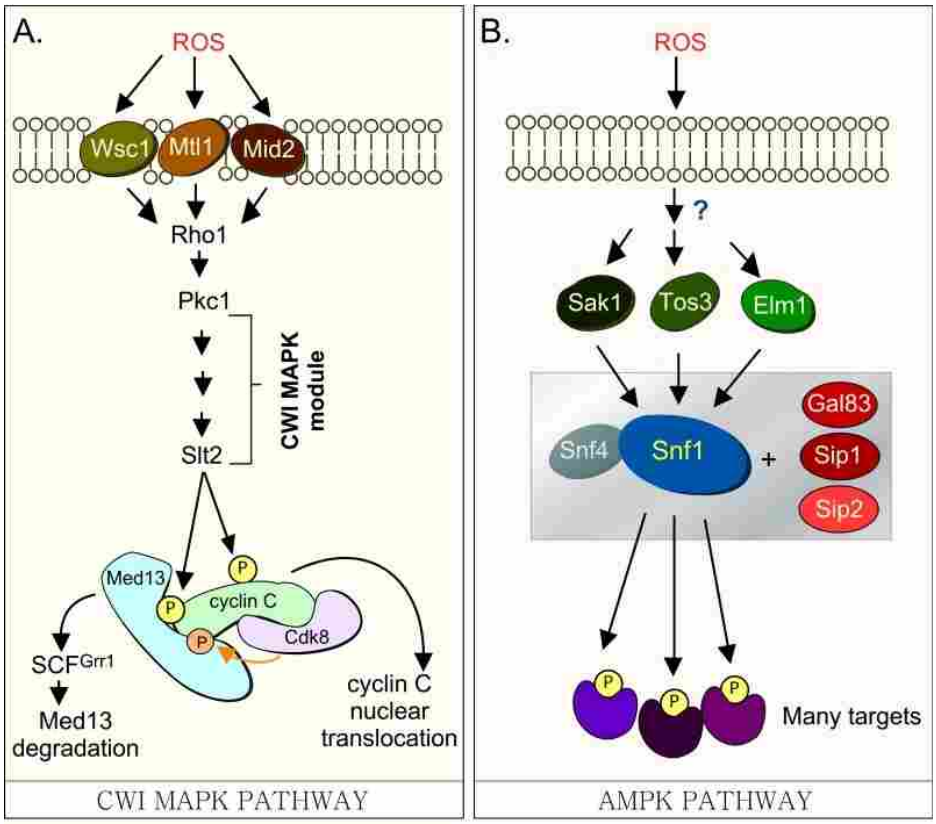

Figure A1-1 Cdk8 module regulation by the CWI MAPK pathway (A) H_2O_2 stimulates cell wall sensors Wsc1, Mtl1 and Mid2, leading to activation of Rho1 that in turn triggers the cell wall integrity (CWI) MAPK pathway by activating Protein Kinase C (Pkc1). Activation of this cascade triggers the MAPK, Slt2, to directly phosphorylate cyclin C, an event required for the 1st step towards its release from the nucleus. The second step requires Slt2 to directly phosphorylate Med13-degron742-844, which targets it for ubiquitin mediated degradation by SCFGrr1. Cyclin C-Cdk8 activity is needed to prime the degron before it is recognized by SCFGrr1 9. (B) Outline of the AMPK pathway in yeast. It remains unknown how this pathway is activated in response to H_2O_2 stress. The gray box represents the Snf1 kinase complex (see text for details).

In *S. cerevisiae,* Med13 destruction is required for cyclin C nuclear release[154]. Consistent with this, cyclin C is cytoplasmic in unstressed *med13*Δ and the mitochondria are predominantly fragmented[154]. More recently we identified SCF^{Grr1} as the E3 ligase that mediates Med13 destruction[133]. Like other SCF targets[155], recognition of this phospho-degron requires it first to be primed by one kinase (cyclin C-Cdk8) and then activated by another

(Slt2). These studies also revealed that phosphorylation of cyclin C by Slt2 is required for the SCF^{Grr1} to recognize Med13 ([133] and Figure A1-1A). Like the Slt2-degron, this domain lies within the large intrinsic disordered region (IDR) of Med13 (Figure A1-2A). IDR's are defined by a continuous stretch of disordered promoting residues which easily transition into more ordered states. These structural transitions afford IDR's great flexibility and as such these regions are known to play key roles in macro-molecular decisions including signaling pathways[156, 157].

In addition to Slt2, the highly conserved 5' adenosine monophosphate-activated protein kinase (AMPK), which plays a major role in the utilization of alternative carbon sources after glucose depletion[158], is also activated in response to various environmental stresses including oxidative stress[159]. In *S. cerevisiae*, the catalytic subunit of the heterotrimeric AMPK complex is encoded by *SNF1*. Other members of the complex (outlined in Figure A1-1B) include two regulatory subunits, the γ subunit Snf4 and one of the three alternative β subunits, Sip1, Sip2, or Gal83[158]. The three β isoforms determine the respective cellular addresses after activation of Snf1, with the Snf1-Gal83 isoform being enriched in the nucleus[160-162]. The catalytic activity of Snf1 is regulated by phosphorylation at Thr-210 that is located in the activation loop of its kinase domain[163]. This is executed by one of three upstream kinases, Sak1, Tos3, and Elm1[159, 164, 165]. These in turn are activated by an unknown mechanism in response to a variety of stresses which lends specificity to the system[159].

In this report we show that Snf1, Sak1 and at least one β isoform are required for the H_2O_2 induced degradation of Med13. Using yeast two-hybrid analysis the Snf1-interacting domain on Med13 was identified. This domain lies in the large IDR region of Med13 and is recognized by SCF^{Grr1} after Snf1 directed phosphorylation. Consistent with this, Snf1 is required

for efficient cyclin C nuclear release following H_2O_2 stress. Taken together, this reveals that Med13 degradation is regulated by two SCF^{Grr1} degrons that are regulated by three different classes of kinases, a Cdk, a MAPK and an AMPK. As all three kinases are required for Med13 degradation, this complex molecular mechanism ensures that cyclin C nuclear release is tightly controlled and prevents its untimely release into the cytoplasm.

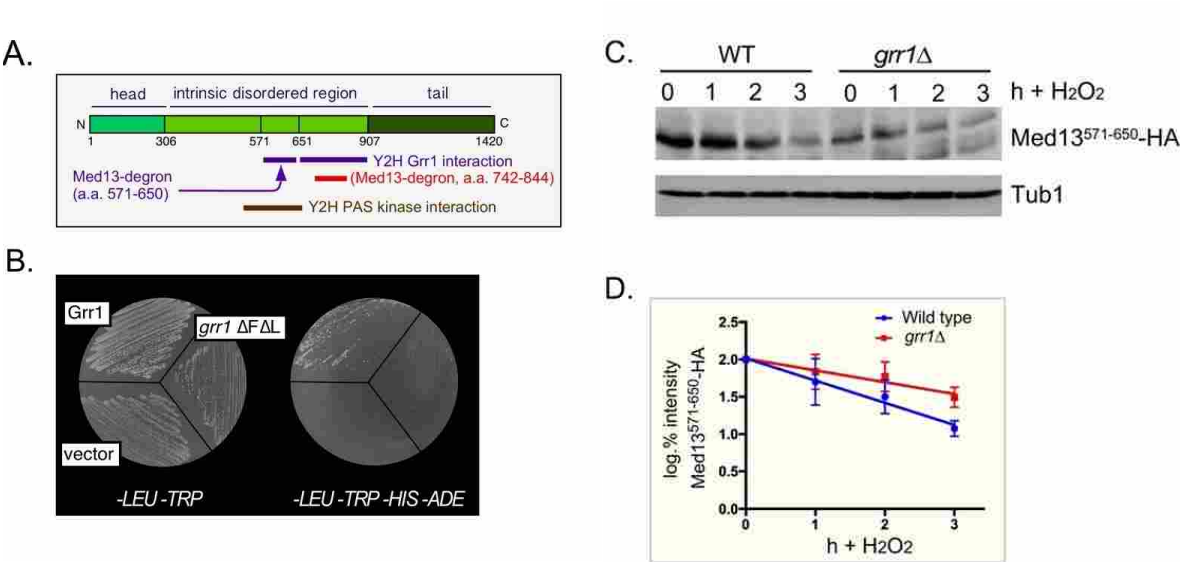

Figure A1-2 Med13 contains two H_2O_2 stress responsive degrons (A) Cartoon of the results from ProteinPredict® 89 analysis of yeast Med13. The amino and carboxyl terminal domains are structured and separated by a large intrinsic disordered region. The positions of the two degrons are indicated. (B) Yeast two hybrid analysis of degron571-650 and Grr1 derivatives. Yeast PJ69-4a cells harboring Med13-activating domain plasmid (pDS15) and either pAS2, pAS-Grr1 or pAS2-Grr1ΔFΔL binding domain plasmids were grown on -LEU, -TRP drop out medium to select for both plasmids (left panel) and -TRP, -LEU, -HIS -ADE (right panel) to test for Med13-Grr1 interaction. (C) Wild-type (RSY10) or grr1Δ cells (RSY1770) harboring degron571-650 (pDS15) were treated with 0.4 mM H_2O_2 for the timepoints indicated and Med13571-650-HA levels analyzed by Western blot. Tub1 levels were used as loading controls. (D) Degradation kinetics of the degron571-650 constructs shown in C. Values represent averages ± SD from a total of at least two Western blots from two independent experiments.

A1.6 Results

A1.6.1 Med13 contains two SCF^{Grr1} phospho-degrons

We have previously shown that SCF^{Grr1} is the E3 ligase responsible for mediating Med13 degradation following H_2O_2 stress [121, 133]. This degron (amino acids 742-844, Figure A1-2A,) is primed by cyclin C-Cdk8 and activated by Slt2. In these studies we also observed that

another Med13 domain (amino acids 571-650) can also bind to Grr1 using the Gal4 yeast two hybrid (Y2H) assay[166]. These results were repeated using two baits, wild-type Grr1 and a *grr1ΔFΔL* mutant, which can neither bind to the SCF or recognize substrates[167, 168]. As anticipated, the Gal4 activating domain Med13$^{571\text{-}650}$ fusion protein (hereon out referred to as degron$^{571\text{-}650}$) can associate with wild-type Grr1 as an interaction is detected selecting for the dual *HIS3* and *ADE2* reporter genes (Figure A1-2B). The vector control and mutant bait were unable to grow on this media suggesting that the interaction is specific.

To confirm that degron$^{571\text{-}650}$ is responsive to SCF^{Grr1} we examined its degradation, via Western blot analysis, following 0.4 mM H_2O_2 treatment in wild-type and *grr1*Δ cells. This concentration of H_2O_2 induces mitochondrial outer membrane permeabilization (MOMP) dependent regulated cell death response in yeast [169-171] and triggers cyclin C nuclear release[127, 129, 131, 154]. The results show that although less degron$^{571\text{-}650\ is}$ present in unstressed *grr1*Δ cells, the protein is more stable following H_2O_2 stress (Figure A1-2C and quantified in A1-2D). Taken together with the Y2H data, these results argue that degron$^{571\text{-}650}$ is a SCF^{Grr1} responsive degron. They are also consistent with our previous published work demonstrating that Grr1 is required for H_2O_2 induced degradation of Med13 [133].

A1.6.2 Snf1 is required for stress-induced degradation of Med13

We next addressed if the H_2O_2 mediated destruction of degron$^{571\text{-}650}$ required Cdk8 kinase activity. To execute this, the degradation of degron$^{571\text{-}650}$ was monitored as described above in cells deleted for cyclin C harboring either functional myc-tagged cyclin C or a vector control. The results revealed that the degron$^{571\text{-}650}$ is degraded with the same kinetics in the presence or absence of cyclin C (Figure A1-S1A and quantified in Figure A1-S1B). These results suggest that another kinase phosphorylates degron$^{571\text{-}650}$. One candidate is the PAS kinase. This kinase is

required for glucose homeostasis and is encoded by two orthologs Psk1 and Psk2[172]. Intriguingly, previous Y2H studies have revealed that a domain of Med13 (amino acids 505-703), that encompasses the degron$^{571-650}$, interacts with Psk1 [173]]. The Y2H assay was repeated using Psk1 as bait and the smaller degron$^{571-650}$ as prey and again an interaction was observed (Figure A1-S2A). We next tested if the PAS kinase plays a role in the degradation of full length Med13. Wild-type and *psk1*Δ *psk2*Δ cells harboring a functional HA-tagged Med13 plasmid [133] were treated with H_2O_2 and Med13 degradation monitored by Western blot analysis. The results show that Med13 is degraded with similar kinetics in the mutant and wild-type cells (Figure A1-S2B and quantified in Figure A1-S2C). These results indicate that although the PAS kinase can interact with degron$^{571-650}$, it is not required for Med13 degradation following H_2O_2 stress.

PAS kinase activation by carbon sources is dependent on the Snf1 complex [124, 174]. Since Snf1 has many targets [175], we next tested if Snf1 mediates Med13 degradation following H_2O_2 stress as just described. The results show that Med13 is significantly more stable in *snf1*Δ cells (Figure A1-3A and quantified in Figure A1-3C). Similar results were obtained when the Snf1 kinase dead mutant (K84R, [176]) was the only source of Snf1 (Figure A1-3B and quantified in Figure A1-3D). Taken together, these results indicate that Snf1 activity is required for Med13 degradation following H_2O_2 stress.

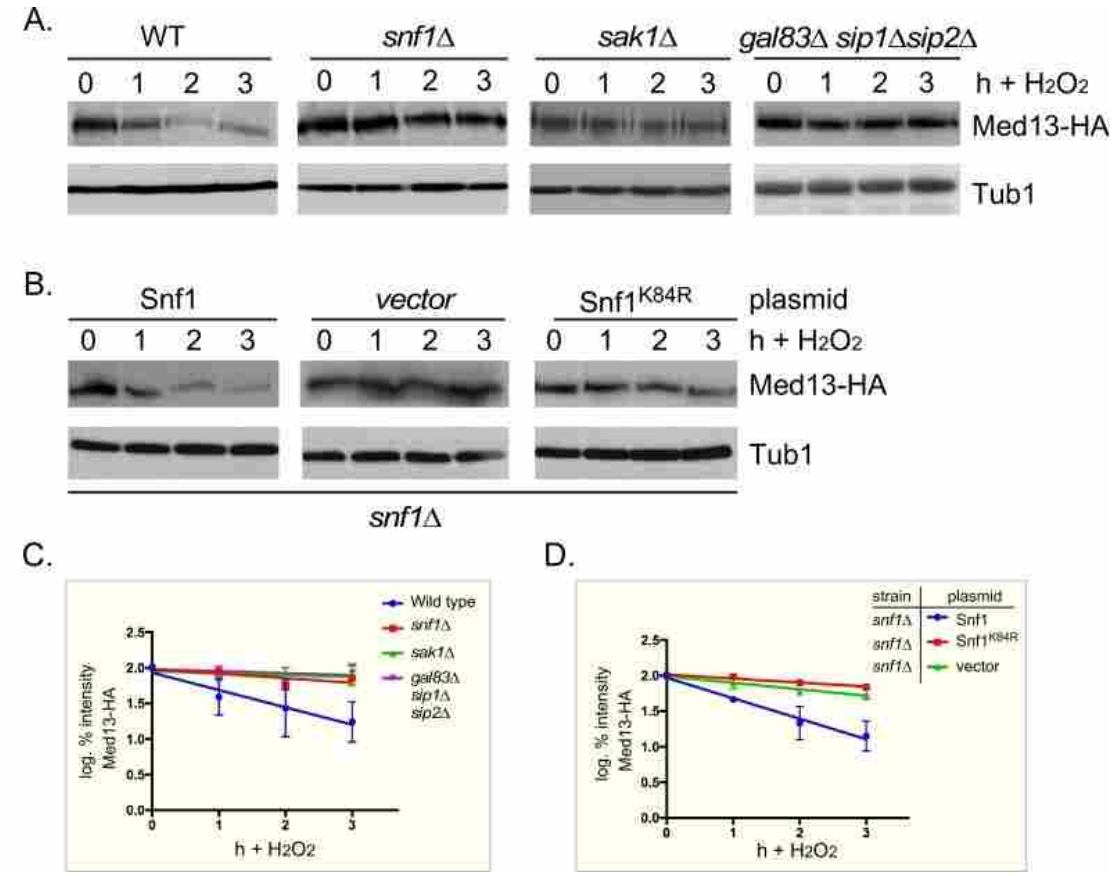

Figure A1-3 Snf1, Sak1 and at least one β subunit are required for degradation of Med13 following H2O2 stress (A) Wild-type (RSY10), snf1Δ (RSY2080), sak1Δ (YPDahl17) and gal83Δ sip1Δ sip2Δ (MSY557) cells harboring full length Med13-HA (pKC801) were treated with 0.4 mM H2O2 for the timepoints indicated and Med13-HA levels analyzed by Western blot. Tub1 levels were used as a loading control. (B) snf1Δ cells harboring Med13-HA (pKC803) and either wild- type Snf1 (JG1193), a vector control (pRS316) or snf1K84R (JG1338) were treated and analyzed as described in A. (C and D) Degradation kinetics of the Med13-HA shown in A and B. Values represent averages ± SD from a total of at least two Western blots from independent experiments.

Sak1 has been identified as the AMPK kinase that is activated in response to oxidative stress [177]. Therefore, we next addressed if Sak1 is required for H_2O_2 induced Med13 degradation. The degradation assays described above were repeated in *sak1*Δ cells and results revealed that Med13 was again significantly more stable in *sak1*Δ than wild type (Figure A1-3A and quantified in Figure A1-3C). This result supports the previously proposed model that Sak1 is the AMPKK that activates Snf1 in response to oxidative stress [159]. We next addressed if the nuclear enriched isoform, Snf1-Gal83 [143, 160-162], is required for Med13 degradation under

similar circumstances. Unexpectedly, the results show that Med13 is still degraded in *gal83*Δ cells (Figure A1-S3A). Likewise, similar results were obtained when Med13 degradation was monitored in a *sip1*Δ *sip2*Δ strain (Figure A1-S3A). However, deletion of all three β subunits significantly inhibited the degradation of Med13 to a similar extend as observed in *snf1*Δ (Figure A1-3A and quantified in Figure A1-3C). Taken together, this suggests at least one of the β subunits of the Snf1 complex is required for Med13 degradation following H_2O_2 stress.

A1.6.3 Snf1 activation alone is not sufficient to mediate Med13 degradation

We next addressed if Snf1 activation was sufficient to mediate Med13 degradation in the absence of H_2O_2 stress. To execute this Med13 levels were examined in wild-type cells after they had been switched from 2% to 0.05% glucose which, is sufficient to activate Snf1 (Figure A1-4A and [159]). No differences in Med13 levels were observed following glucose deprivation (Figure A1-4B). Taken with the results presented in Figure A1-3, this suggests that Snf1 activation is necessary but not sufficient to mediate the degradation of Med13 following H_2O_2 treatment.

A1.6.4 The CWI pathway sensors proteins are not required for Snf1 activation

It is known that both the CWI and AMPK pathways are activated in response to oxidative stress but how these two pathways communicate is not well understood [178]. Importantly, although it is known how the signal is transmitted to the CWI pathway, it is unclear how the AMPK pathway is activated (Figure A1-1B). One possibility is that the pathways cross talk, through the cell wall sensor proteins. To test this, we examined Snf1 phosphorylation status in a strain lacking the three cell wall sensors (Wsc1, Mid2 and Mtl1[144]). Consistent with previously published work [159], Snf1 is phosphorylated following H_2O_2 treatment in a Sak1 dependent manner (Figure A1-4C). Likewise the cell wall sensor triple mutant is also able to activate Snf1 following H_2O_2 treatment (Figure A1-4C). These results suggest that the activation

of the CWI pathway is not required to transmit the stress signal to the AMPK pathway. Others have demonstrated that Snf1 is not required for activation of Slt2 [179]. Consistent with this, we observed that the Med13 degron$^{571\text{-}650}$ is still degraded following H_2O_2 stress when a mutant of cyclin C, that cannot be phosphorylated by Slt2 (S266A [131]), is used as the sole source of cyclin C (Figure A1-S1C&D). Taken together, these results argue that the AMPK and MAPK signaling pathways act independently of each other. The extension of this conclusion is that both pathways contribute independently to regulating Med13 destruction following H_2O_2 stress.

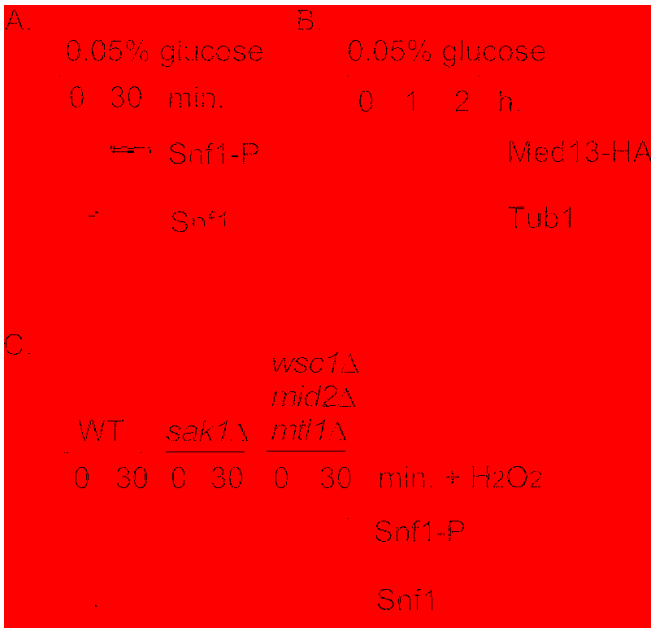

Figure A1-4 Snf1 activation does not mediate Med13 degradation (A) Mid-log -type cells (RSY10) growing in 2% glucose (T=0) were switched to media containing 0.05% glucose. Snf1 phosphorylation and Snf1 itself were detected as described in materials and methods for the timepoint indicate. (B) Wild-type cells harboring Med13-HA (pKC801) were switched to media containing 0.05% glucose. Med13-HA levels were detected by Western blot analysis for the timepoints indicated. Tub1 was used as a loading control. (C) As in (A) except that Snf1 phosphorylation was monitored after 0.4 mM H_2O_2 treatment in the strains indicated.

A1.6.5 The Snf1 degron lies within the IDR of Med13

Snf1 has previously been shown to phosphorylate an SCF^{Grr1} phospho-degron in Pfk27, a key regulator of glycolysis [180]. Taking this into account, we asked if the Gal4 activating domain Med13$^{571\text{-}650}$ fusion protein (degron$^{571\text{-}650}$) is an Snf1 responsive degron by monitoring its H_2O_2

mediated degradation *snf1*Δ cells. The results show that degron$^{571\text{-}650}$ is more stable in *snf1*Δ cells compared to wild type following H_2O_2 stress (Figure A1-5A and quantified in Figure A1-5B). This suggests that degron$^{571\text{-}650}$ is a Snf1 responsive degron. To further support this conclusion, we examined the degradation kinetics of a degron mutated for either of the potential Snf1 phosphorylation sites previously identified in proteomic screens (S587 [181] and S636 [182], Figure A1-6A) although none of these sites perfectly fit the Snf1 consensus sequence [183, 184]. The studies revealed that both mutants were degraded following H_2O_2 treatment with kinetics similar to wild type (Figure A1-S3B). We also noted that serine 634 could potentially be phosphorylated by Snf1 (see Figure A1-6A). As it lies very close to serine 636, we made a double mutant (S634A, S636A) and repeated the assay. Again this mutant degron was degraded following H_2O_2 treatment (Figure A1-S3B). However, the triple mutant (S587A, S634A, S636A) exhibited enhanced stability following H_2O_2 stress (Figure 5C and quantitated in Figure 5B). Taken together, these results suggest that Snf1 phosphorylates Med13 following H_2O_2 stress targeting S587, S634 and S636. Consistent with this model, we (Figure 5D and S3C) and others [185] have shown that Snf1 can co-immunoprecipitates with Cdk8 both before and after H_2O_2 stress. As cyclin C directly binds to the adjacent degron$^{742\text{-}844}$ (Figure 2A and [133]) this places Snf1 in close proximity to degron$^{571\text{-}650}$. In addition, these data also support the notion suggested by others that a subpopulation of Snf1 is nuclear in unstressed cells [143, 162, 185].

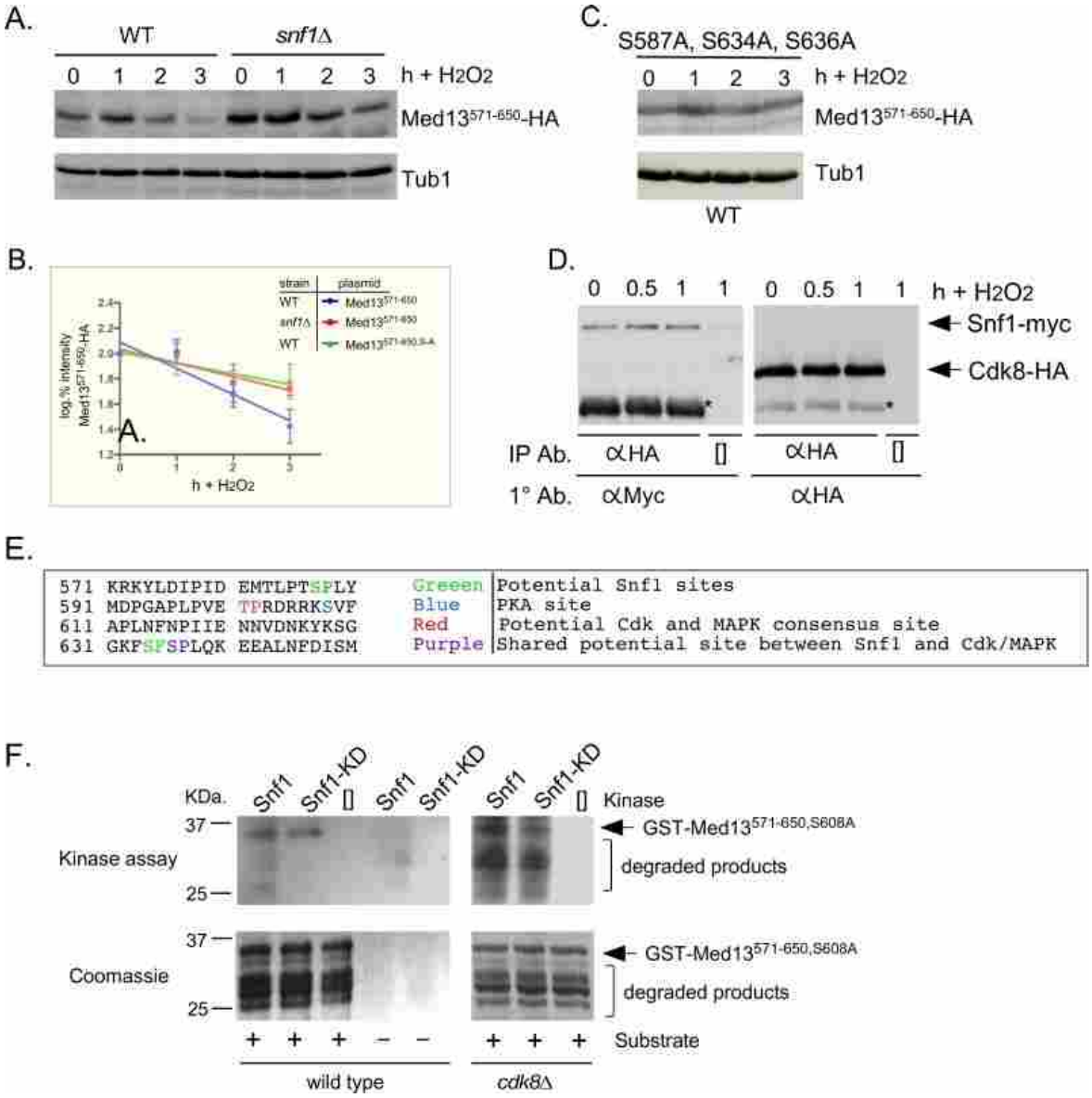

Figure A1-5 Snf1 phosphorylates degron$^{571\text{-}650}$ (A) Mid-log wild-type (RSY10) or *snf1*Δ cultures (RSY202) harboring degron$^{571\text{-}650}$ (pDS15) were subjected to an H_2O_2timecourse experiment and protein extracts analyzed by Western blot. Tub1 levels were used as loading controls. (B) Degradation kinetics of degron$^{571\text{-}650}$ shown in (A) and (C). Values represent averages ± SD from a total of at three Western blots from independent experiments. (C) As in (A) except that degron$^{571\text{-}650,S587A,\ S634A,\ S636A}$ (pDS56) was analyzed in wild-type cells. (D) Co-immunoprecipitation analysis of Snf1-myc and Cdk8-HA. Mid log wild-type cells harboring Snf1-myc and Cdk8-HA on single copy plasmids were treated with 0.4 mM H_2O_2 for the timepoints shown. Protein extracts were immunoprecipitated with anti-HA, separated by SDS-PAGE Western analysis and the membrane probed with the antibodies shown. [] represents no IP antibody and the asterisk represents the heavy chain. See Figure A1-S3C for vector control. (E) Potential phospho-sites in Med13$^{571\text{-}650}$. (F) Upper panels: Kinase assays using Snf1 and Snf1^{K84R}-myc (kinase dead) immunoprecipitated from yeast protein extracts prepared from either wild type (left panel) or *cdk8*Δ cells (right panel) and Med13-degron$^{571\text{-}650}$ (GST-Med13$^{571\text{-}906,S608A}$ purified from *E. coli*) as the substrate. The reactions were separated by SDS PAGE and subject to autoradiography. Lower panels: Coomassie stained gels showing the input used in the kinase assays.

To address if Snf1 directly phosphorylates Med13 kinase assays were performed with wild-type and kinase dead Snf1 (K84R). The activated kinase was immunoprecipitated from yeast extracts and incubated with GST-Med13$^{561\text{-}650,\ S608A}$ purified from *E. coli.* Serine 608 was mutated to alanine as it is a potentially contaminating PAS kinase site (Figure A1-5E and [124]). In addition, although this site has also been identified as target of PKA mediated phosphorylation [186], we have previously shown that this site does not play a role in Med13 degradation in response to oxidative stress [133]. Lastly, it is documented that Snf1 does not phosphorylate GST so this control was not included here [187]. The results (Figure A1-5F) show that Snf1 is able to directly phosphorylate degron$^{571\text{-}650}$. However, despite taking the precautions listed above, kinase activity was also observed using the kinase dead version. This suggests that another kinase that immunoprecipitates with Snf1 is able to phosphorylate this degron. One strong possibility is Cdk8, which is a proline directed kinase that can phosphorylate the minimal consensus sequence S/T-P [188]. Med13$^{571\text{-}650}$ contains one such site (Figure A1-5E). Therefore the kinase assays were repeated using Snf1 extracts isolated from a *cdk8*Δ strain. The result show that degron$^{571\text{-}650}$ was phosphorylated by Snf1 and this activity was reduced in the kinase dead control (Figure A1-5F). Taken together, these results are suggestive that Snf1 directly phosphorylates Med13$^{571\text{-}650}$. However, as some phosphorylation of degron$^{571\text{-}650}$ was observed when Snf1^{K84R} was used, we cannot rule out the possibility that an intermediary kinase may be playing a role.

A1.6.6 Other potential Snf1 sites on Med13 are not needed for its degradation following H_2O_2 stress

The Snf1 proteomic screen mentioned above also identified 5 additional potential Snf1 sites in Med13 [182]. Intriguingly, these sites all lie within the large IDR of Med13 (Figure A1-

6A). As IDR regions provide ideal environments for post-translational modifications which effect signaling events [189], we asked if these additional sites also play a role in Med13 degradation. To address this question, Med13-HA fragments were fused to the SV40 nuclear localization sequence (NLS) and assayed for H_2O_2 mediated destruction. The results revealed that the construct that contains both degrons as well as all the potential Snf1 sites (amino acids 306-906) is degraded. However, the Med13$^{306\text{-}570}$ construct, that contains the remaining potential Snf1 sites but not the two SCF^{Grr1} responsive degrons, was significantly more stable. This suggests that these other potential Snf1 sites do not play a role in the H_2O_2-stress mediated degradation of Med13. To address if the head and tail regions of Med13 contain unidentified Snf1 sites, Med13 constructs spanning these regions (amino acids 1-306 and 907-1420) were also tested as described above for stability following H_2O_2 stress. The results (Figure A1-6C) demonstrate that these constructs are not destroyed under these conditions. This supports our conclusion that the Snf1 degron lies within amino acids 571-650. Degron$^{742\text{-}844}$ also contains a potential Snf1 target site (Figure A1-6A). However, this degron fused to the Gal4 activating domain is destroyed following H_2O_2 stress in wild-type and *snf1*Δ cells alike (Figure A1-6D). Taken together, these results support the above conclusions that the Snf1 phosphorylation sites lie within degron$^{571\text{-}650}$.

A1.6.7 Snf1 is necessary for cyclin C nuclear release and stress-induced mitochondrial fission

As Med13 degradation is required for cyclin C nuclear release [133, 154] we next tested if Snf1 was also required for this event. To address this, the location of a functional cyclin C-YFP reporter protein [130] before and after stress in wild-type and *snf1*Δ cells was examined (Figure A1-7A and quantified in FigureA1-7B). The results show that a majority of cyclin C-

YFP is cytoplasmic in wild-type cells whereas it remains significantly more nuclear in *snf1*Δ cells. These data indicate that Snf1 is required for the oxidative stress induced nuclear release of cyclin C. We next examined the mitochondrial morphology in *snf1*Δ cells as cyclin C nuclear release initiates stress-induced mitochondrial fission [127, 129, 134]. As previously reported, unstressed wild-type cells exhibited mainly reticular mitochondrial morphology (Figure A1-7C) that switched to a predominantly fragmented phenotype after 3 hours of 0.4 mM H_2O_2 treatment. In *snf1*Δ cells, significantly less fragmented mitochondria are seen after H_2O_2 treatment. Taken together, these results indicate that activation of Snf1 is required for stress-induced mitochondrial fragmentation through C nuclear release.

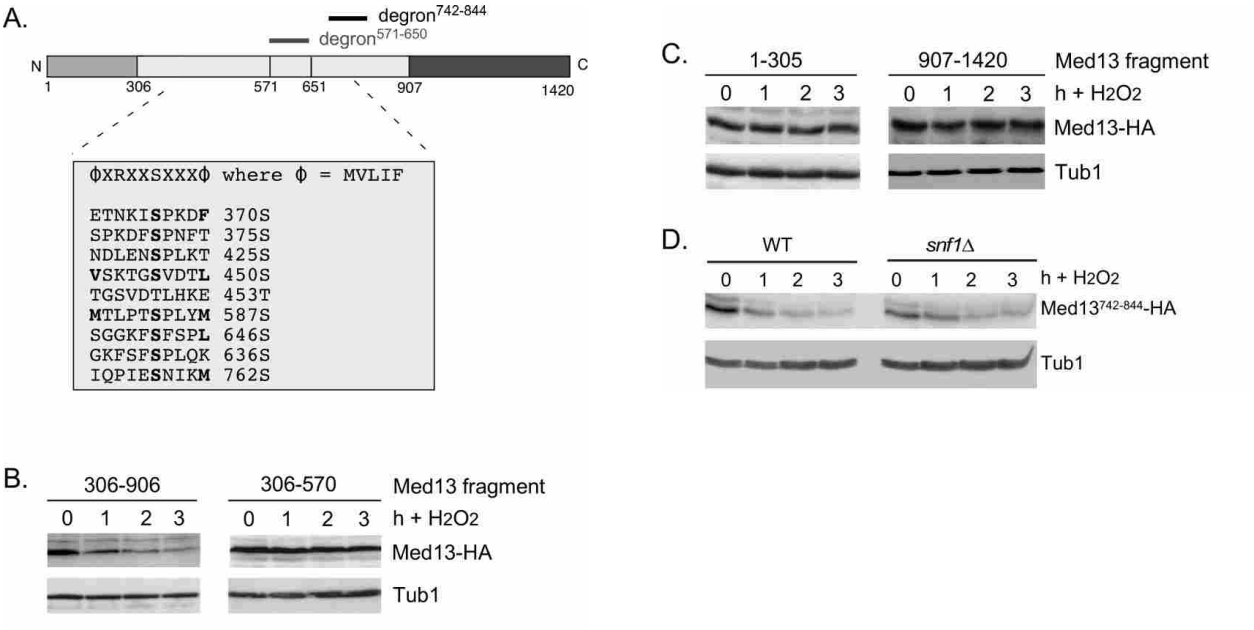

Figure A1-6 Other potential Snf1 sites in Med13 are not required for its degradation following H_2O_2 stress (A) Map of Med13 outlying the positions of the two Med13 degrons, the consensus Snf1 target site 57 and potential Snf1 sites, identified by published proteomic screens. (B) and (C) Wild-type (RSY10) cultures harboring the NLS-Med13-HA constructs shown were grown to mid-log phase (0 h) then treated with 0.4 mM H_2O_2 for the indicated times. Med13-HA levels were determined by Western blot analysis. Tub1 levels were used as a loading control. (D) Mid-log wild type or *snf1*Δ cultures (RSY202) harboring HA tagged Med13 degron742-844 (pDS32) were subjected to an H_2O_2 timecourse experiment and protein extracts analyzed by Western blot. Tub1 levels were used as loading controls.

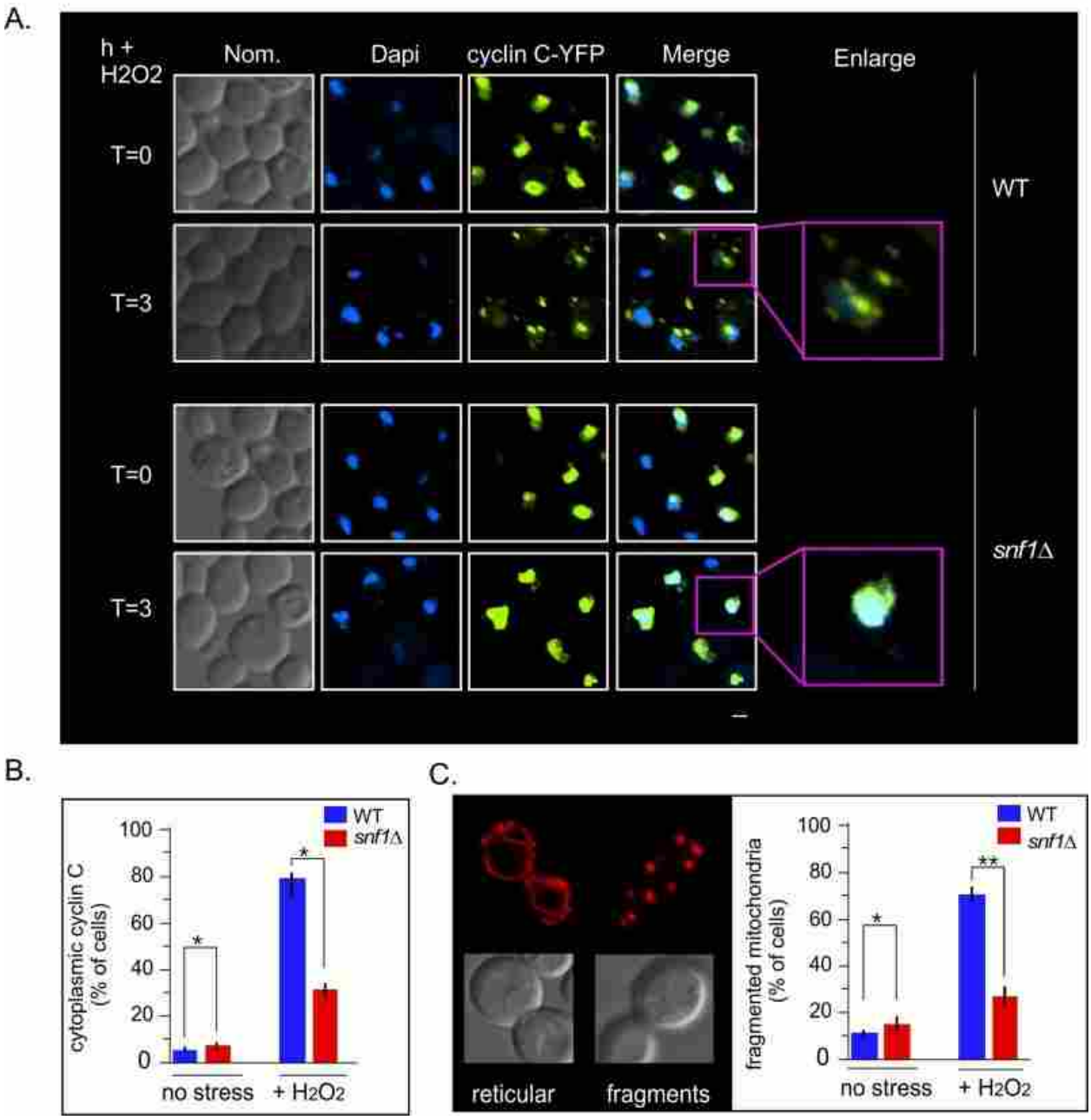

Figure A1-7 Cyclin C remains predominantly nuclear following H_2O_2 stress in *snf1*Δ (A) Fluorescence microscopy of mid-log phase wild-type and *snf1*Δ cells harboring a cyclin C-YFP expression plasmid (pBK38). Cells were stained with Dapi to visualize the nucleus. (B) Quantification of the results obtained in (A). At least 200 cells were counted per timepoint from 3 individual isolates. The percent of cells (mean ± SEM) within the population displaying cytoplasmic cyclin C is given. * $p < 0.05$ difference from wild type. (C) Right panel: representative images of the two mitochondrial morphologies scored. Left panel: as in (B) except that percent of cells displaying fragmented mitochondria was scored. Representative images of the mitochondrial morphologies scored are shown in the left hand panel. The percent of cells (mean ± s.e.m.) within the population displaying fragmented mitochondria is given. * $p < 0.05$ difference from wild type. ** $p < 0.01$ difference from wild type. Bar = 13 μM.

A1.6.8 Med13-degron$^{571\text{-}650}$ is not required for the degradation of Med13 following H_2O_2 stress

We next addressed if Snf1 mediated phosphorylation of Med13 is required for Med13 degradation. Degron$^{571\text{-}650}$ was deleted from full length Med13 and the degradation kinetics of this construct (Med13$^{deg\Delta 571\text{-}650}$) was examined in *med13*Δ cells. The results show that Med13$^{deg\Delta 571\text{-}650}$ was degraded with kinetics similar to wild type (Figure A1-8A upper two panels, quantified in Figure A1-8B). We also observed that this construct retained cyclin C in the nucleus in unstressed cells and released it into the cytoplasm following H_2O_2 stress (Figure A1-S5). These results were unexpected as deletion or inactivation of Snf1 results in Med13 stabilization following H_2O_2 stress (Figure A1-3). Similarly, deletion of the Slt2 responsive degron (amino acids 742-844) only partially rescued the deletion (Figure A1-8A, bottom two panels) whereas Med13 is significantly stabilized in *slt2*Δ cells following H_2O_2 stress [133]. These results suggest a complex model in which the function of either Snf1 or Slt2 is only required when their respective degron is present. If correct such a model would predict that the degron impeaches degradation when not phosphorylated. Moreover these studies predict independent roles for these two signaling pathways that ultimately direct in the same outcome of Med13 degradation.

A1.7 Discussion

Our previous work has shown that nuclear release of the yeast and mammalian cyclin C predisposes cells to initiate PCD following stress [127, 134]. In *S. cerevisiae,* this nuclear release requires the destruction of Med13 [154] mediated by the E3 ligase complex SCF^{Grr1}, which requires Slt2 and Cdk8 activity [133]. In this current work, we provide evidence that Sak1 activated Snf1 is also required for H_2O_2 induced Med13 degradation and cyclin C nuclear

release. In the absence of this kinase, Med13 degradation following H_2O_2 stress is inhibited and cyclin C remains predominantly nuclear. Consistent with this model, we showed that Snf1 is required for the degradation of the Med13 degron$^{571\text{-}650}$. Paradoxically, deletion of this degron did not prevent H_2O_2 induced destruction of Med13. Instead this mutant exhibited H_2O_2 induced Med13 degradation and cyclin C nuclear release. Intriguingly, deletion of the Slt2-resonsive degron (Med13$^{742\text{-}844}$) also did not protect Med13 from H_2O_2 induced degradation although the protein was slightly more stable than wild type. Taken together, this study indicates that Slt2 and Snf1 pathways cooperate to trigger Med13 destruction. The use of two required pathways may help insure the proper signals are in place to target Med13.

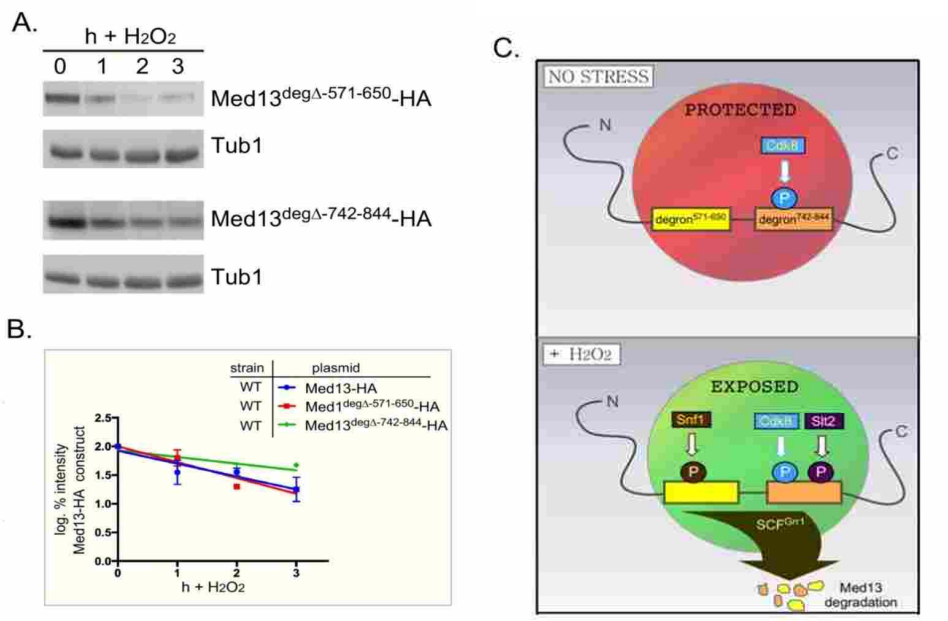

Figure A1-8 Either Med13 degron is sufficient for Med13 degradation (A) *med13*Δ (RSY1701) cells harboring either Med13$^{571\text{-}650\text{deg}\Delta}$-HA (pKC805, upper panels) or Med13$^{742\text{-}844\text{deg}\Delta}$-HA plasmids (pKC814, lower panels) were treated with 0.4 mM H_2O_2 for the timepoints indicated and Med13$^{\text{deg}\Delta}$-HA levels analyzed by Western blot. Tub1 levels were used as a loading control. (B) Degradation kinetics of the results shown in (A). Values represent averages ± SD from a total of at least two Western blots from independent experiments. For clarity, the degradation kinetics of wild-type Med13-HA from previous experiments was included. (C) Model depicting how two SCF^{Grr1} phospho-degrons mediate the destruction of Med13 following H_2O_2 stress. In unstressed cells cyclin C-Cdk8 phosphorylates degron$^{742\text{-}844}$ 9 but both degrons are protected by an unknown mechanism from Snf1 and Slt2 kinase activity (depicted by the red circle). Following H_2O_2 stress Snf1 and Slt2 are activated and permitted access to the now exposed degrons. This results in SCF^{Grr1} mediated degradation of Med13 and cyclin C nuclear release (not shown).

To accommodate these two results the following model that best fits the data is proposed (outlined in Figure A1-8C). In unstressed cells the IDR region of Med13, which encompasses both degrons, is protected from SCF^{Grr1} activity (depicted by red circle in Figure A1-8C) by an unknown mechanism. Following H_2O_2 stress, two events happen, the hierarchy of which is unknown. The protection is lost (depicted by green circle in Figure A1-8C) and the activated kinases Snf1 and Slt2 phosphorylate their respective degrons, triggering SCF^{Grr1} mediated degradation of Med13. Although we currently favor the hypothesis that Snf1 directly phosphorylates Med13, we could not definitively exclude the possibility that Snf1 may promote Med13 phosphorylation indirectly via an intermediary kinase another kinase. That being said, the model presented in Figure A1-8C could accommodate this possibility. More importantly however, the model supports the observation that both the AMPK and MAPK pathways act independently of each other (Figure A1-4), and are required for Med13 degradation. However, in the absence of either the Snf1 or Slt2 degron, this protection is lost, allowing SCF^{Grr1} to recognize either activated degron. This model also accounts for the observation that when either degron is expressed in isolation then it would require its kinase to render it recognizable by SCF^{Grr1}.

If this model is correct, then how could this region be protected from AMPK and MAPK activity in unstressed cells? One strong possibility could be connected to the fact that both degrons lie within the very large IDR domain of Med13 (Fig 2A). IDR's are known to endow proteins with highly malleable structures that undergo disorder-to-order transitions [190]. It has been proposed that the IDR domains can have different binding partners that transiently associate [142]. In some cases, this can lead to proteins binding the same region that possess unrelated, or even opposite functions [191]. Thus proteins that contain IDR regions are frequently involved in

signaling as they can easily change their conformational state in response to changing environmental conditions. Taken together, it is feasible to propose that in unstressed cells, the IDR region of Med13 is in one conformational state that, by associating with an unknown protein, protects this region. Upon stress, the confirmation changes and the degron becomes exposed. This model is also consistent with the observation that IDR regions are notorious for being regulated by multiple kinases [189, 192]. This has led to the idea that IDRs and multiple phosphorylation events together provide structural variability [193] resulting in ultra-sensitive molecular switches that are triggered at a threshold level of phosphorylation. Thus our results suggest a model in which Med13 degradation is regulated by three types of different kinases, a cyclin dependent kinase, a MAPK and AMPK.

Lastly, here we show that Snf1 phosphorylates Med13, either directly or by an intermediary kinase, as well as being able to associate with the CKM before stress (Figure A1-5D). These results are consistent with a growing number of papers that have shown that a sub-population of the Snf1-Gal3 isoform is present in the nucleus under normal conditions [143, 185, 194], as well as enriched in the nucleus upon glucose starvation [65, 160, 162]. In addition, Sak1 is needed for Snf1 nuclear localization [195]. In support of this model, Snf1, Gal83 and Sak1 localize to the *SUC2* promotor under non-starvation conditions [143]. This promotor is also negatively regulated by the CKM [196]. Repression is relieved by Snf1 mediated phosphorylation of two proteins known to repress *SUC2* expression, the DNA binding protein Mig1 [197] and the glucose kinase Hxk2 [143, 198], causing them to be released into the cytoplasm [199, 200]. Likewise, carbon starvation results in the degradation of cyclin C [128], an event that occurs in the cytoplasm [129]. Surprisingly we found that although Sak1 is needed for Med13 destruction following H_2O_2 stress, deletion of Gal83 has no effect (Figure A1-3A and

A1-S2A). However, deletion of all three β-subunits does inhibit Med13 degradation. This would suggest that in the absence of Gal83 either Sip1 or Sip2 are able to activate nuclear Snf1. However, the Snf1-Sip1 and Snf1-Sip2 isoforms have not been reported to be nuclear, either dispersing to the vacuolar membrane (Sip1) or remaining cytoplasmic following carbon deprivation (Sip2) [65, 160, 162]. Further studies need to be executed to address if Sip1 or Sip2 can translocate into the nucleus in the absence of Gal83. Intriguingly, just recently the Mitochondrial Voltage-Dependent Anion Channel Protein Por1 (yVDAC1) has been shown to enhance Snf1 nuclear enrichment by promoting the nuclear enrichment of Gal83 [194]. This unexpected finding serves to emphasize that there is much still to learn about the role Snf1 kinase plays in response to changing environmental conditions.

A1.8 Materials and methods

A1.8.1 Yeast strains and plasmids

Most experiments were performed in the *S. cerevisiae* W303 strain [201] and are listed in Table S1. Exceptions to this are the *sak1*Δ (YPDahl17, a gift from S. Hohmann [202]), the *sip1*Δ *sip2*Δ (MML1445, a gift from E. Herrero) and *psk1*Δ *psk2*Δ strains which are W303-1A strains. The *sip1*Δ *sip2*Δ *gal83*Δ strain (MSY557, a gift from M. Schmidt [203]) is an S288c strain. Finally, the Y2H assays were performed in PJ69-4a [166] that was obtained from the Yeast Resource center, a gift from S. Fields. In accordance with the Mediator nomenclature unification effort [204], we use *CNC1* and *CDK8* gene designations for cyclin C (*SSN8*/*UME3*/*SRB11*) and Cdk8 (*SSN3*/*UME5*/*SRB10*) respectively. The *snf1*Δ and *gal83*Δ strains (RSY1949 and RSY2080 respectively) were constructed using gene replacement methodology as described [205]. The *sak1*Δ (RSY1976) was a gift from S. Hohmann [202]. All cells were grown at 30°C.

All plasmids used in this study are listed in Table S2. The wild-type epitope tagged plasmids pKC801, pKC803 (*MED13*-HA), pBK38 (*ADH1*$_{Pro}$-*CNC1*-YFP), Snf1-Myc and *ADH1*$_{Pro}$-*CNC1*-MYC (pKC337) are functional and have been previously described [126, 129, 130, 133, 206, 207]. All other plasmids were constructed using PCR cloning techniques and details are available upon request. In short, all constructs were amplified from plasmid DNA using Phusion Taq (Thermo) digested using Thermo fast digest restriction enzymes and ligated using Thermo fast ligase into their respective vectors. Site directed mutagenesis (New England Bio-Labs Q5) was used to create plasmids harboring amino acid mutations and the change confirmed by sequencing (Eurofins Genomics). The *MED13* Y2H plasmids were constructed by PCR cloning regions of Med13 in frame with the Gal4 activating domain of pACT2. The NLS-Med13 fusion constructs were made by first creating a backbone vector (pNLS-HA) that contains the SV40 nuclear localization sequence (NLS) in frame with a single HA epitope tag under the control of the *ADH1* promotor. PCR-cloning was then used to place fragments of Med13 in frame with NLS. All in frame fusion proteins were verified by sequence analysis. Other plasmids that were used in this study that have been previously described are listed in Table S2.

A1.8.2 Cell growth

Yeast cells were grown in either rich, non-selective medium (YPDA) or synthetic minimal medium (SC) allowing plasmid selection as previously described [126]. For all experiments, the cells were grown to mid-log phase (~ 6 x 10^6 cells/ ml) before treatment with low concentrations of 0.4 mM H_2O_2 as previously described [130]. 25 mls of cells were collected per timepoint, washed in water, then the pellet flash frozen in liquid nitrogen. Yeast two hybrid experiments were executed as described [168]. *E. coli* cells were grown in LB

medium with selective antibiotics. For the kinase assays cells were grown initially grown in SD-Ura (1.7 g Yeast Nitrogen Base, 5 g Ammonium Sulfate, 20 g Dextrose per liter), overnight, diluted 1:100-fold into 500 ml of SD-Ura, and grown for 10–12 h. Thereafter the cells were pelleted, and resuspended in 500mL SGal-Ura (1.7 g Yeast Nitrogen Base, 5 g Ammonium Sulfate, 20 g Galactose per liter)

A1.8.3 Western blot analysis and co-immunoprecipitation

Tagged full length Med13-HA constructs were detected by using NaOH lysis of cell pellets exactly as described in [121]. To detect Med13-HA, 1 in 5000 dilutions of anti-HA antibodies (Abcam) were used. The co-immunoprecipitation analysis was performed essentially as described [128]. Anti-alpha tubulin antibodies (12G10) were obtained from the Developmental Studies Hybridoma Bank, University of Iowa. Western blot signals were detected using either goat anti-mouse or goat anti-rabbit secondary antibodies conjugated to alkaline phosphatase (Sigma) and the CDP-Star chemiluminescence kit (Thermo). Signals were quantitated by CCD camera imaging (Kodak) and standardized to the loading control. All degradation assays were performed two or three times. SEM's were generated for each point (error bars are indicated on the graphs) and the data analyzed using linear regression analysis using GraphPad Prism 7 program.

A1.8.4 Snf1 activation and kinase assays

The Snf1 activation assays were executed as follows. Cells were grown to mid log and treated with 0.4 mM H_2O_2 for the times indicated. They were then immediately boiled for 3 minutes and pellets frozen using liquid nitrogen. Protein extracts were made using the NaOH method described in [121] and analyzed by SDS-PAGE and Western blotting. Anti-phospho-Thr172–AMPK (Cell Signaling Technology; Cat. No. 2531) was used to detected

phosphorylated Snf1 and polyhistidine antibody H1029 (Sigma-Aldrich) to detect Snf1. This is possible as Snf1 ORF contains 13 contiguous histidine residues at its N terminus. The *in vitro* kinase assays were executed as follows. Wild-type yeast or *cdk8*Δ harboring myc-tagged Snf1, Snf1 kinase dead (K84R) plasmids under the control of the *GAL1-10* promotor, were first grown in SD-Ura followed by SGal-Ura as described above and then resuspended in lysis buffer (20 mM HEPES, 10 mM KCl, 1 mM EDTA, 1 mM ethylene glycol tetra-acetic acid (EGTA), 50 mM NaCl, 10% glycerol, 1 mM β-mercaptoethanol, Pierce™ Protease Inhibitor Tablets, pH 7.4 with phosphatase inhibitors). Resuspended cultures were lysed using a Microfluidics M-110P homogenizer (Microfluidics) and cell debris removed by centrifugation at 12,000 x g for 30 min. Supernatants were transferred to new tubes and incubated with 5–10µl of Myc-conjugated magnetic beads (Cell Signaling) for 2–3 h at 4°C. Beads were separated using magnetic force and washed four times with 1 ml of lysis buffer lacking the protease inhibitor. Beads containing Myc-tagged proteins were used directly for *in vitro* kinase assays without eluting. GST-Med13$^{571\text{-}650\ S608A}$ was purified from *E. coli* BL21 DE3 strain as previously described [121] and assayed for Snf1–dependent phosphorylation. In short, GST-Med13$^{571\text{-}650\ S608A}$ was incubated with the Snf1 immunoprecipitates in 30 µl of reaction buffer containing 1X Snf1 kinase buffer (50 mM Tris-HCl, 10 mM $MgCl_2$, 1 mM dithiothreitol (DTT), pH 7.5, 10 µM ATP, and 7.5 µCi of γ32P-ATP, and reactions were incubated for 35 min. Kinase assays were stopped by the addition of SDS–PAGE sample buffer and analyzed by SDS-PAGE, stained with coommassie (30 mins), destained for 2 h, dried and exposed to film.

A1.8.5 Fluorescence microscopy

Cyclin C-YFP subcellular localization and mitochondrial morphology were monitored as described previously [127, 129]. For all experiments, the cells were grown to mid-log (6 x 10^6

cells/ ml), treated with 0.4 mM H_2O_2 for the timepoints indicated, then analyzed by fluorescence microscopy. Cyclin C-YFP release analysis was performed on cells stained with DAPI in mounting medium (10 mg/ml p-phenylenediamine, 50 ng/ml 4',6-diamidino-2-phenylindole, Molecular Probes) to visualize nuclei and prevent photo bleaching. Images were obtained using a Nikon microscope (model E800) with a 100X objective with 1.2X camera magnification (Plan Fluor Oil, NA 1.3) and a CCD camera (Hamamatsu model C4742). Data were collected using NIS software and processed using Image Pro software. All images of individual cells were optically sectioned (0.2 μM slices at 0.3 μM spacing) deconvolved and the slices were collapsed to visualize the entire fluorescent signal within the cell. Cyclin C-YFP foci were scored as being cytoplasmic when 3 or more foci were observed outside of the nucleus. Mitochondrial fission assays were performed on live cells as described [127]. In brief, mitochondrial fission was scored positive if no reticular mitochondria were observed that transversed half the cell diameter. Fusion was scored when cells exhibited one or more reticular mitochondria the diameter of the cell. Fission and fusion was scored for 200 cells from three independent isolates. Statistical analysis was performed using the Student's T-test.

A1.9 Acknowledgments

We thank. S. Fields, S. Hohmann, E. Herrero, J. Nunnari, M. Schmidt and M. Solomon for strains and plasmids. We thank R. Strich for critical reading of this manuscript. This work was supported by grants from the National Institutes of Health awarded to K.F.C. (GM113196), and J.G (GM100376). The yeast two-hybrid strain was made by work supported by NIH grant P41 RR11823 awarded to T. N. Davis.

Supplemental Table A1-1 Yeast strains used in this study

Strain	Genotype*	Source
RSY10		[201]
RSY1696	*cnc1::KANMX6*	[208]
RSY1701	*med13::HIS3*	[154]
RSY1707	*mid2::HIS3 mtl1::TRP1 wsc1::KANMX4*	[130]
RSY1770	*grr1*Δ*::his5*$^{+}$	[121]
RSY1726	*cdk8*Δ*::KANMX4*	[154]
RSY1949	*gal83::KANMX4*	This study
RSY2080	*snf1::KANMX4*	This study
YPDahl17	*sak1::KANMX4*	[202]
MML1445	*sip1::natMX4 sip2:: KANMX4*	[209]
MSY557	*sip1::HIS3 sip2:: HIS3 gal83::HIS3*	[203]
JGY1		[82]
JGY4	*psk1::HIS3 psk2*Δ*:: KANMX4*	[75]
PJ69-4	*LYS2::GAL1-HIS3 GAL2-ADE2 met2::GAL7-lacZ gal4*Δ *gal80*Δ	[166]

*Genotype of all strains is *MAT***a** *ade2 ade6 can1-100 his3-11,15 leu2-3,112 trp1-1 ura3-1* except YPDahl17, MML1445, JGY1 and JGY4 which are *MAT***a** *ade2-1 can1-100 his3-11,15 leu2-3,112 trp1-1 ura3-1 and* PJ69-4 which is *MAT***a** *trp1-901 leu2-3,112 ura3-52 his3-200 gal4*Δ *gal80*Δ.

Supplemental Table A1-2 Plasmid used in this study

Plasmid Name	Gene	Epitope Tag	Marker	Promoter	2μ/ CEN	Reference
pBK38	*CNC1*	YFP	*URA3*	*ADH1*	CEN	[129]
pKC337	*CNC1*	*CNC1*	*TRP1*	*ADH1*	CEN	[126]
pKC801	*MED13*	3HA	*URA3*	*TRP1*	CEN	[121]
pLR166	*CNC1*^{S266A}	*CNC1*	*TRP1*	*TRP1*	CEN	[210]
pKC803	*MED13*	3HA	*LEU2*	*ADH1*	CEN	[121]
pKC805	*MED13*$^{571\text{-}650deg\Delta}$	3HA	*URA3*	*ADH1*	CEN	This study
pKC814	*MED13*$^{742\text{-}844deg\Delta}$	3HA	*URA3*	*ADH1*	CEN	This study
pDS8	*GAL4AD-MED13*$^{571\text{-}906}$	1HA	*LEU2*	*ADH1*	2*μ*	[121]
pDS15	*GAL4AD-MED13*$^{571\text{-}650}$	1HA	*LEU2*	*ADH1*	2*μ*	[121]
pDS16	*GAL4AD-MED13*$^{651\text{-}906}$	1HA	*LEU2*	*ADH1*	2*μ*	[121]
pDS32	*GAL4AD-MED13*$^{742\text{-}844}$	1HA	*LEU2*	*ADH1*	2*μ*	[121]
pDS44	*GAL4AD-MED13*$^{571\text{-}650\ S636}$	1HA	*LEU2*	*ADH1*	2*μ*	This study
pDS51	*GAL4AD-MED13*$^{571\text{-}650\ S636,\ S634A}$	1HA	*LEU2*	*ADH1*	2*μ*	This study
pDS55	*GAL4AD-MED13*$^{571\text{-}650\ S587A}$	1HA	*LEU2*	*ADH1*	2*μ*	This study
pDS56	*GAL4AD-MED13*$^{571\text{-}650\ S58A7,\ S636A,\ S634A}$	1HA	*LEU2*	*ADH1*	2*μ*	This study
pDS45	*NLS-Med13*$^{1\text{-}306}$	1HA	*LEU2*	*ADH1*	2*μ*	This study
pDS46	*NLS-Med13*$^{306\text{-}570}$	1HA	*LEU2*	*ADH1*	2*μ*	This study
pDS47	*NLS-Med13*$^{907\text{-}1420}$	1HA	*LEU2*	*ADH1*	2*μ*	This study
pDS52	*NLS-Med13*$^{307\text{-}570}$	1HA	*LEU2*	*ADH1*	2*μ*	This study
pDS54	*GST-Med13*$^{571\text{-}650,S608A}$	GST	*AMP*	-	-	This study
pJG1215	*HIS*$_6$*-PSK1-KD*	HIS$_6$	*AMP*	-	-	[75]
pUM504	*CDK8*	1HA	*TRP*	*GPD*	CEN	[128]
pACT2	*GAL4AD*	1HA	*LEU2*	*ADH1*	2*μ*	[211]

pAS2	*GAL4BD*	1HA	*TRP*	*ADH1*	2μ	[211]
pAS2-Grr1	*GAL4BD-GRR1*	1HA	*TRP*	*ADH1*	2μ	[168]
pAS2-Grr1ΔLΔF	*GAL4BD-GRR1Grr1ΔLΔF*	1HA	*TRP*	*ADH1*	2μ	[168]
pJG1465	*GAL4AD-MED13*$^{504-703}$	1HA	*TRP*	*ADH1*	2μ	[82]
pAS2-Psk1	*GAL4BD-PSK1*	1HA	*TRP*	*ADH1*	2μ	[82]
JG1193	Snf1	8Myc	*URA3*	*Snf1*	CEN	[206]
JG1338	Snf1^{K84R}	8Myc	*URA3*	*Snf1*	CEN	[207]
	Snf1	8Myc	*URA3*	*GAL1-10*	2μ	[207]
	Snf1^{K84R}	8Myc	*URA3*	*GAL1-10*	2μ	[207]
pNLS-HA	SV40 NLS	1HA	*LEU2*	*ADH1*	2μ	This study
Mt-Cherry	Mito-targeting	mCherry	*TRP1*	*ADH1*	CEN	This study
pRS314	-	-	*TRP1*	-	CEN	[212]
pRS316	-	-	*URA*	-	CEN	[212]

APPENDIX 2: A Complex Molecular Switch Directs Stress-induced Cyclin C Nuclear Release Through SCFGrr1 Mediated Degradation of Med13

David C. Stieg[1], Stephen D. Willis[1], Vidyaramanan Ganesan[1], Kai Li Ong[3], Joseph Scurozo[2,4], Mia Song[2], Julianne Grose[3], Randy Strich[1] and Katrina F. Cooper[1,5.]

Mol Biol Cell. 2018 Feb 1;29(3):363-375

A2.1 Author information

Running head: SCF^{Grr1} mediated degradation of Med13

[1]Department of Molecular Biology, Graduate School of Biological Sciences, Rowan University, Stratford, NJ, 08084, USA

[2]School of Osteopathic Medicine, Rowan University, Stratford, NJ, 08084, USA

[3]Department of Microbiology and Molecular Biology, Brigham Young University, Provo, UT 84602, USA

[4]Current address Lehigh Valley Health network, One City Center, 707 Hamilton St. Allentown PA 18101, USA

[5]Corresponding author: cooperka@rowan.edu Tel: (856)-566-2887, Fax: (856)-566-6366

David C. Stieg - stiegdc@rowan.edu

Stephen D. Willis - willis58@rowan.edu

Vidyaramanan Ganesan - ganesan@rowan.edu

Kai Li Ong - jkm525@go.byuh.edu

Joseph Scurozo – Joseph.scuorzo@lvhn.org

Mia Song - songm6@rowan.edu,

Julianne Grose - julianne_grose@byu.edu

Randy Strich - strichra@rowan.edu

*This work described in this chapter was been published in the journal Molecular Biology of the Cell in 2018. It has been formatted for this thesis but is otherwise unchanged.

A2.2 Abbreviations

RCD – Regulated Cell Death

ROS - Reactive Oxygen Species

SCF - Skip1, Cullin, F box E3 ligase

IDR - Intrinsic Disordered Region

MoRF - Molecular Recognition Feature

Cdk - cyclin dependent kinase

PKA - Protein Kinase A

MAPKKK - MAP Kinase Kinase Kinase

MAPK - MAP Kinase

ORF - Open Reading Frame

ßME - ß-mercaptoethanol

3-AT - 3-amino-1,2,4-triazole

CKM – cyclin C/Cdk8 kinase module

Y2H – Yeast Two Hybrid

Keywords:

Med13, cyclin C, Cdk8, Slt2, Programmed Cell Death

A2.3 Abstract

In response to oxidative stress, cells decide whether to mount a survival or cell death response. The conserved cyclin C and its kinase partner Cdk8 play a key role in this decision. Both are members of the Cdk8 kinase module that, with Med12 and Med13, associate with the core mediator complex of RNA polymerase II. In *S. cerevisiae,* oxidative stress triggers Med13 destruction, which thereafter releases cyclin C into the cytoplasm. Cytoplasmic cyclin C associates with mitochondria where it induces hyper-fragmentation and regulated cell death. In this report, we show that residues 742-844 of Med13's 600 amino acid intrinsic disordered region (IDR) both directs cyclin C-Cdk8 association and serves as the degron that mediates ubiquitin ligase SCF^{Grr1}-dependent destruction of Med13 following oxidative stress. Here, cyclin C-Cdk8 phosphorylation of Med13 most likely primes the phospho-degron for destruction. Next, pro-oxidant stimulation of the cell wall integrity pathway MAP Kinase Slt2 initially phosphorylates cyclin C to trigger its release from Med13. Thereafter, Med13 itself is modified by Slt2 to stimulate SCF^{Grr1}-mediated destruction. Taken together, these results support a model that this IDR of Med13 plays a key role in controlling a molecular switch that dictates cell fate following exposure to adverse environments.

A2.4 Introduction

Protein-protein interactions are at the heart of nearly all facets of cell physiology including transducing exogenous signals necessary for proper cell fate decisions to be adopted. For example, following exposure to cytotoxic compounds, the cell must assess the level of damage and decide whether to arrest cell division and repair the damage or execute programmed cell death. Recently, it has become apparent that intrinsic-disordered regions (IDRs) defined by a continuous stretch of disordered promoting residues, play key roles in directing protein−protein

interaction networks especially those involved in macro-molecular decisions including signaling and control pathways (reviewed in [156, 157]). This hotspot for communication is achieved in part by the ability of IDR's to contribute to the formation of large, malleable interfaces that can interact with multiple partners. These protein interactions can occur via short segments termed molecular recognition features (MoRFs) that undergo disorder-to-order transition upon binding to their cognate ligands [213]. Consistent with these domains being communication hubs, the binding of IDR's to their targets is often regulated by covalent modifications including phosphorylation, which can serve as simple biological switches [214].

In budding yeast, cyclin C and its kinase partner Cdk8 are predominantly negative regulators of a diverse set of stress response genes [126, 138-141]. Together with Med13 and Med12, they form the Cdk8 kinase module (CKM) of the multi-subunit Mediator complex which acts as an interface between DNA bound transcription factors and RNA polymerase [135-137]. In addition to its transcriptional role, cyclin C possesses another function following oxidative stress that is found in both yeast and mammalian cells [127, 129, 134, 215]. Specifically, nuclear release of cyclin C, but not Cdk8, allows its re-localization to the mitochondrial outer membrane. At this new subcellular address, cyclin C is necessary and sufficient for stress-induced mitochondrial fission and is required for MOMP dependent normal regulated cell death (RCD) execution [127, 129, 134]. This type of cell death is the reclassification of programmed cell death (PCD) passed by the international Nomenclature Committee on Cell Death in 2015 [216]. In the budding yeast, cyclin C release is dependent upon its direct phosphorylation by Slt2 MAPK [131] and the ubiquitin mediated degradation of Med13 ([154] and see Figure A2-1) In the CKM, Med13 contains a large centrally located IDR, the extent and placement of which is conserved across metazoans, plants and fungi [217]. As Med13 also bridges the CKM to the

Mediator complex [218] this centrally placed IDR may provide structural plasticity, allowing the CKM to interface with different mediator components according to the environment. Consistent with Med13 IDR being a potential communication hub, computer predictions suggest the presence of several MoRPs biased toward an alpha helical confirmation [219].

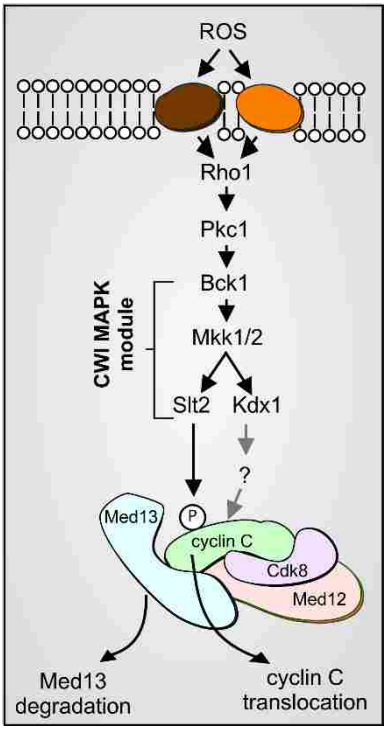

Figure A2-1 Cdk8 module (Cd8, cyclin C, Med12 and Med13) regulation by the CWI MAPK pathway H_2O_2 stimulates cell wall sensors leading to activation of the cell wall integrity (CWI) MAP kinase module. Slt2 phosphorylation triggers cyclin C translocation to the mitochondria and Med13 degradation [154]. The pseudokinase Kdx1 is also required for cyclin C nuclear release via an unknown mechanism [131]. Med12 is not required for cyclin C nuclear release [154].

In this report, we provide mechanistic details on how Med13 is targeted for destruction following oxidative stress in the budding yeast *S. cerevisiae*. We show that the Cell WalI Integrity (CWI) pathway MAPK Slt2 directly phosphorylates Med13, which is required for recognition by the SCF^{Grr1} E3 ligase complex. Consistent with other SCF targets in yeast and higher eukaryotes (reviewed in [155]), degradation of Med13 by SCF^{Grr1} also requires the phosphorylation by cyclin C-Cdk8 which most likely primes this phospho-degron. Furthermore,

this phospho-degron partly overlaps with the predicted Med13 IDR [219]. Consistent with this region serving as an interaction hub [220], this IDR directs both Cdk8 and Grr1 binding and is sufficient to retain cyclin C in the nucleus. Taken together, these results define a multi-step switch required for the cellular decision to release cyclin C from the nucleus and identifies a Med13 IDR as the communication hub that co-ordinates this pro-death decision.

A2.5 Results

A2.5.1 SCF^{Grr1} is required for Med13 H_2O_2-mediated degradation

We have previously shown that Med13 degradation is dependent upon a functional 26S proteasome indicating that a ubiquitin ligase is required [154]. In unstressed human cells, Med13 is turned over by the conserved SCF ubiquitin ligase utilizing the Fbw7 F-box recognition protein [221]. Grr1, a yeast homologue of Fbw7, is a non-essential F-box protein that utilizes a Leucine Rich Region (LRR, Fig. 2A) for substrate recognition [221, 222]. SCFGrr1 is required for degradation of the mediator component Med3 [222] as well as proteins regulating the glycolytic-gluconeogenic switch [180]. More recently it has also been shown to regulate Whi7, a repressor of Start transcriptional gene expression [223]. To determine whether SCF^{Grr1} plays a role in H_2O_2-induced Med13 degradation, we examined Med13 degradation following 0.4 mM H_2O_2 treatment in wild type and *grr1*Δ cells harboring functional Med13-HA on a single copy plasmid. This concentration of H_2O_2 has long been established to induce a MOMP dependent RCD response in yeast [169, 171, 224] as well as trigger cyclin C nuclear export [127, 129, 131]. The results (Figure A2-2B) show that Med13-HA is significantly more stable in *grr1*Δ cells. We next repeated these experiments using endogenous *MED13* tagged with the myc epitope in wild type (RSY1798) and *grr1*Δ mutant strains (RSY1771) harboring a plasmid expressing either wild-type *GRR1,* a vector control or a *GRR1* derivative deleted for the LRR domain (*grr1*Δ*L)*

[221]. Following H_2O_2 treatment, Med13-myc was again significantly more stable in *grr1*Δ cells harboring either the vector control or *grr1*Δ*L* than in wild-type cells (Figure A2-2C and A2-S1A). These results suggest that SCF^{Grr1} is the E3 ligase responsible for mediating Med13 degradation following H_2O_2 stress.

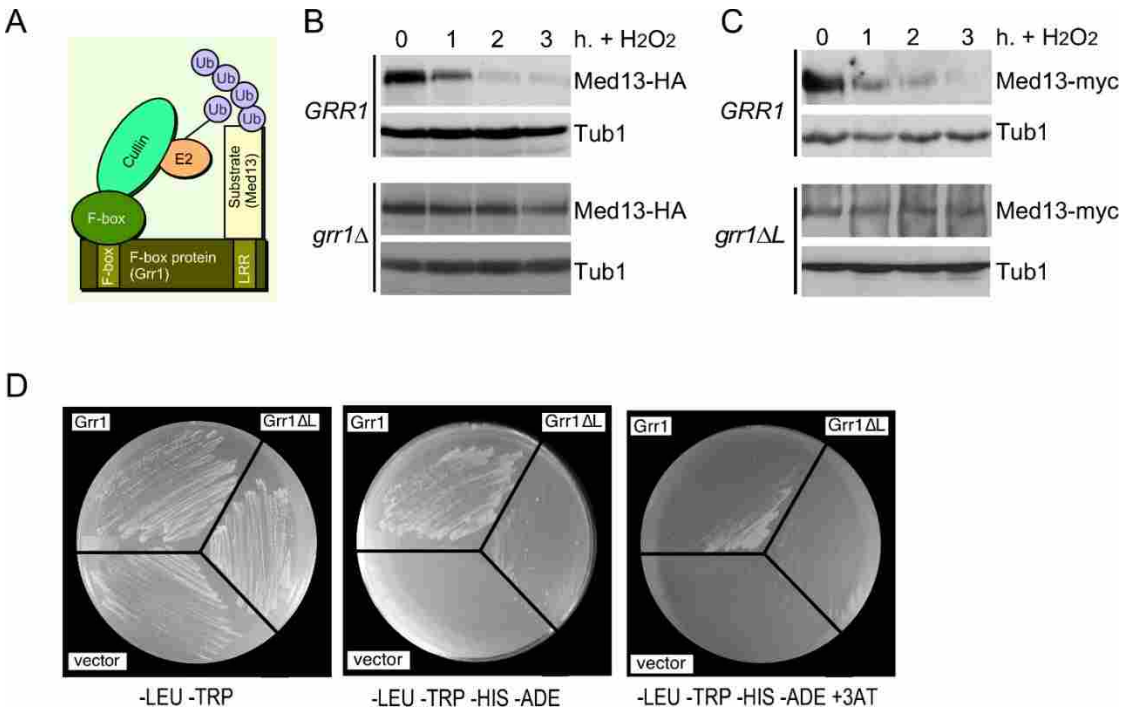

Figure A2-2 SCF^{Grr1} mediates Med13 degradation following H_2O_2 stress (A) Model of the SCF^{Grr1}. (B) Wild type (RSY10) and *grr1*Δ cells (RSY1770) harboring Med13-HA (pKC801) were treated with 0.4 mM H_2O_2 for the timepoints indicated and Med13 levels analyzed by Western blot. (C) Top panel: RSY1798 (*MED13-myc::KAN)* was treated with 0.4 mM H_2O_2 for the timepoints indicated and Med13 levels analyzed by Western blot. Tub1 levels were used as loading controls. Bottom panel: RSY1771 (*grr1*Δ*::HIS3 MED13-myc::KAN*) harboring $ADH1_{PRO}$-*grr1*Δ*L* was analyzed as for RSY1798. Tub1 levels were used as loading controls. (D) Yeast two hybrid analysis of Med13 and Grr1 derivatives. Y69a cells harboring Med13-activating domain plasmid (pKC800) and either pAS2, pAS-Grr1 or pAS2-Grr1ΔL binding domain plasmids were grown on *-LEU, -TRP* drop out medium to select for both plasmids (left panel), *-TRP, -LEU, -HIS –ADE* (middle panel) and *-TRP,-LEU, -HIS, -ADE* +3AT (right panel) to test for Med13-Grr1 interaction.

If SCF^{Grr1} is the ubiquitin ligase directing Med13 proteolysis, then Grr1 should interact with Med13. To test this possibility, Grr1 and Med13 association was assayed using a two-hybrid strategy. This approach has been previously used to both identify and confirm Grr1 substrates [167, 168]. We expressed either the wild type or *grr1ΔL* mutant *GRR1* allele fused to the Gal4 DNA binding domain bait with the full length Med13 fused to the activator domain (AD) prey. These studies revealed that Grr1 interacts with Med13 and this interaction survives addition of the histidine analog 3-amino-1,2,4-triazole (3-AT) suggesting that the *HIS3* reporter gene induction is robust (Figure A2-2D). With the *grr1ΔL* mutant bait, an interaction is detected selecting for the dual *HIS3* and *ADE2* reporter genes but colony formation is uneven (middle panel) or absent in the presence of 3-AT (right panel). Taken together with the increased stability of Med13 observed in *grr1Δ* cells, these results argue that Med13 is an SCF^{Grr1} substrate.

A2.5.2 The intrinsic disordered region of Med13 interacts with Grr1

Many SCF targets require phosphorylated substrates for F-box recognition [225]. Consistent with this model, the LRR of Grr1 specifically recognizes phosphorylated serine/threonine-proline motifs within its substrate degron [221]. In human cells, phosphorylation of T326 is required for Med13 destruction by SCF^{Fbw7} [226]. To address whether a similar mechanism directs H_2O_2-induced Med13 degradation in yeast, the requirement of the analogous threonine in yeast (T210, Fig S1B) was tested. For these studies we expressed Med13-HA from a single-copy plasmid in *med13Δ* cells. These studies revealed that both the wild type and the $Med13^{T210A}$ derivative were still degraded following 0.4 mM H_2O_2 stress (Figure A2-S1C, D and quantitated in E) indicating that T210 phosphorylation is not necessary for oxidative stress-induced destruction of Med13. Furthermore, consistent with our previously published results with endogenously tagged Med13-myc [154], Med13-HA degradation is not

dependent upon new protein synthesis as it is still observed following cycloheximide treatment (Figure A2-S1C).

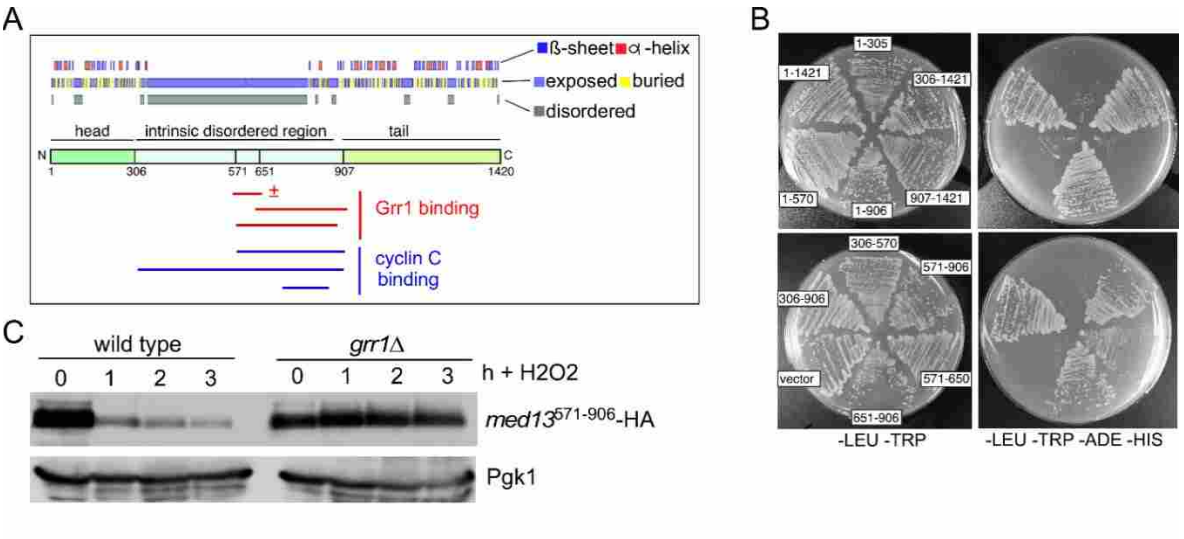

Figure A2-3 The unstructured domain of Med13 binds Grr1 (A) ProteinPredict® [227] analysis of yeast Med13. Med13 contains amino and carboxyl terminal structured domains separated by an intrinsic disordered domain (IDR). Grr1 and Med13 interaction regions are indicated below the schematic. ± = qualitatively reduced binding (B). Med13-Grr1 Y2H analysis. Y69a cells harboring pAS-Grr1 and the indicated Gal4AD-Med13 subclone were streaked on media selecting for plasmid maintenance (left) or induction of the ADE2 and HIS3 reporter genes (right) by Y2H interaction. (C) Wild type (RSY10) and grr1Δ (RSY1770) cells harboring the minimal Med13 interaction domain expression plasmid (Gal4AD-Med13571-906) were treated with 0.4 mM H2O2 for the timepoints indicated and Med13571-906 levels analyzed by Western blot. Pgk1 levels were used as a loading controls.

We next employed Y2H assays to identify the Med13 region able to interact with Grr1. Med13 has structured head and tail domains flanking a large intrinsic disordered region (IDR) [219] (Figure A2-3A). A series of Gal4AD-Med13 constructs that span the length of Med13 were built and tested for their ability to interact with Gal4BD-Grr1. The results revealed that the Grr1 interaction domain lies within the unstructured domain, between amino acids 571 and 906 (Figure A2-3B, summarized in Figure A2-3A). To confirm that the Med13 degron lies within this region, we performed a classical degron assay. The levels of the prey Gal4AD-Med13$^{571\text{-}906}$ fusion protein were monitored following 0.4 mM H_2O_2 stress in wild type and *grr1*Δ cells. The results indicated that Med13$^{571\text{-}906}$ was destroyed following oxidative stress in a Grr1-dependent

manner (Figure A2-3C). Taken together, these results indicate that the SCF^{Grr1} degron lies within the IDR.

A2.5.3 The Med13 IDR binds cyclin C

As cyclin C nuclear release represents an important step toward entering the cell death pathway, we next sought to identify the Med13 region that binds cyclin C using two hybrid strategies. However, the yeast cyclin C self activates when tethered to a Y2H bait protein [126]. Therefore, we used the human cyclin C as it does not self-activate two-hybrid reporter genes [228]. Using this approach, we found that the same region associating with Grr1 (amino acid residues 571-906) also bound cyclin C (Figure A2-4A, summarized in Figure A2-3A). To confirm these results, as well as to address if this interaction is direct, we used a pull down approach. We expressed a central region of the Med13 interaction domain (amino acid residues 742-844) as a Gst fusion protein. Gst-$Med13^{742-844}$ was passed over a cobalt column on which *E. coli* prepared human His_6-cyclin C was bound. Following extensive washing, bound proteins were eluted with imidazole and the presence of Gst-$Med13^{742-844}$ was determined by Western blot analysis using antibodies to 6His or human cyclin C. These results show that human cyclin C interacts with $Med13^{742-844}$ (Figure A2-4B). The experiments were repeated using yeast cyclin C (Figure A2-4C). Although the residual cleaved GST that was present in the GST-Med13 construct showed some interaction with yeast cyclin C, the full length construct showed a significantly stronger interaction. Confidence was garnered in this interaction being specific as no interaction was observed when GST alone was used in either Figure A2-4B or 4C. Interestingly, although amino acid residues 571-650 of Med13's IDR can associate with Grr1 (Figure A2-3B) this region does not associate with cyclin C (Figure A2-4D). Thus taken together

these results indicate that cyclin C binds the same region of Med13's large IDR that is recognized by SCF^{Grr1}.

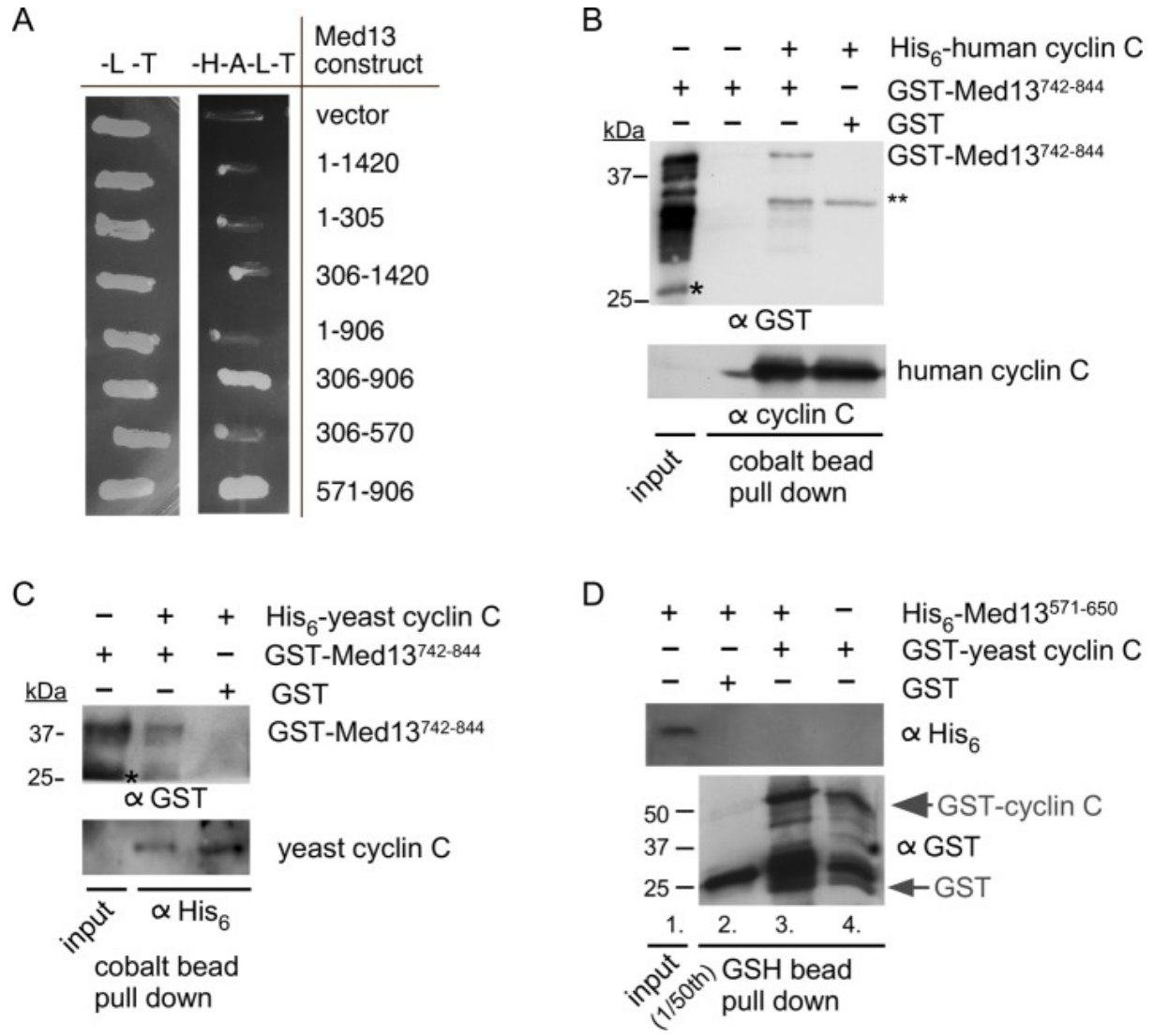

Figure A2-4 The Med13 IDR binds cyclin C (A) Y2H analysis of human cyclin C DNA binding domain plasmid (pSW108) and the indicated $Gal4^{AD}$-Med13 subclone derivatives. The numbers indicate the amino acids remaining in the activation domain plasmids. Transformants were patched onto either *-LEU, -TRP* (-L –T) or *-HIS -ADE -LEU -TRP* (-H-A-L-T) to select for plasmid maintenance or Y2H interaction, respectively. (B) Western blot analysis of pull down assays with His_6-human cyclin C and GST-$Med13^{742-844}$ (DS30). The load control contains 1/10 of the input. Single and double asterisks represent cleaved GST and cross-reaction between anti-GST antibody and human cyclin C, respectively. Molecular weight markers (kDa) are indicated. (C) As in (B) except that yeast cyclin C was used. **(**D) Western blot analysis of pull down assays with GST yeast cyclin C and 6His-$Med13^{571-650}$ (DS22). The load control contains 1/50th of the input. Molecular weight markers (kDa) are indicated.

A2.5.4 The Med13 IDR is sufficient to retain cyclin C in the nucleus

To determine whether the yeast cyclin C also associates with the same region of Med13's IDR *in vivo*, we asked if this region (Med13$^{571\text{-}906}$) is sufficient to retain cyclin C in the nucleus in the absence of stress. To address this question, mitochondrial morphology and subcellular localization of a functional cyclin C-YFP [129] was monitored in unstressed *med13*Δ cells harboring either a vector control or one of four Gal4^{AD}-Med13 fusion proteins. As expected, cyclin C was predominantly cytoplasmic and co-localized with fragmented mitochondria in the vector control (A, top row, quantitated in Figure A2-5B and see Figure A2-S2 for DAPI stained images). Similarly, expression of Gal4AD-Med13$^{571\text{-}650}$ was unable to retain cyclin C in the nucleus or prevent mitochondrial fragmentation (second row). However, cells expressing either Gal4AD-Med13$^{571\text{-}906}$ Gal4AD-Med13$^{651\text{-}906}$ or Gal4AD-Med13$^{742\text{-}844}$ exhibited both nuclear retention of cyclin C and fused mitochondria. Taken together with the pull down assays, these results suggest that Med13$^{742\text{-}844}$ is sufficient s sufficient to retain yeast cyclin C in the nucleus.

A2.5.5 Cdk8 phosphorylation primes Med13 for destruction

SCF substrates are typically recognized following phosphorylation of the degron. However, many substrates require two phosphorylation marks; one to "prime" the substrate and the other that represents the trigger for ubiquitylation (reviewed in [155]. Previous work revealed that Protein Kinase A (PKA) phosphorylates Med13 on Serine 608 and 1236 [229]. However, a derivative mutated for both phosphor acceptor sites (Med13^{S608A,S1236A}-HA) was still destroyed with similar kinetics to wild type (Figure A2-S3A) indicating that PKA phosphorylation is not required for Med13 degradation following H_2O_2 treatment. Consistent with this result, the Med13^{S608A,S1236A}-HA complements the aberrant mitochondrial morphology exhibit by *med13*Δ cells (Figure A2-S3B).

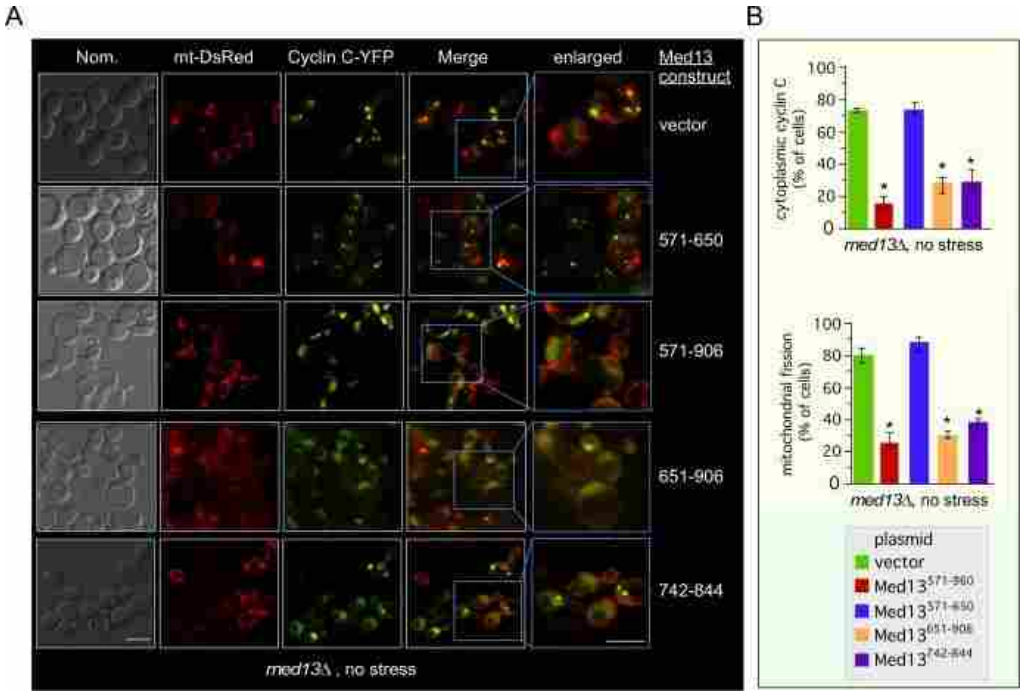

Figure A2-5 The unstructured domain of Med13 retains cyclin C in the nucleus (A) Fluorescence microscopy of mid-log phase *med13*Δ cells (RSY1701) harboring the Gal4^{AD}-Med13 construct indicated or a vector control (pACT2) and both cyclin C-YFP and DsRed mitochondrial targeting (mt-DsRed) plasmids. Blue boxes indicated enlarged regions of the image. Bar = 10 μM. (B) The percent of the population of cells in (A) displaying at least 3 cyclin C-YFP foci in the cytoplasm (top panel) or fragmented mitochondria (bottom panel) is quantified (mean ± s.e.m.). At least 200 cells were counted per timepoint from 3 individual isolates. * $p<0.05$ difference from vector control.

In addition to PKA, cyclin C-Cdk8 phosphorylates Med13 in humans [218, 230] suggesting the possibility that Cdk8 represents the priming kinase. To test this model, Med13 destruction kinetics were monitored in a *cnc1*Δ null strain transformed with either the wild type *CNC1* gene or the vector control. These experiments indicated that cyclin C-Cdk8 kinase is required for Med13 destruction (Figure A2-6A and quantified in Figure A2-S4A). Our previous studies showed that Slt2 phosphorylates cyclin C on Ser266 following H_2O_2 and this modification is required for its release from Med13 and translocation to the cytoplasm [131]. Therefore, one possibility is that cyclin C release is a prerequisite for Med13 destruction.

Consistent with this possibility, Med13 was protected from destruction in a *cnc1*Δ mutant harboring a plasmid expressing cyclin C^{S266A} (Figure A2-6A, right panel). These results indicate cyclin C phosphorylation by Slt2 is also required for Med13-HA destruction (see below).

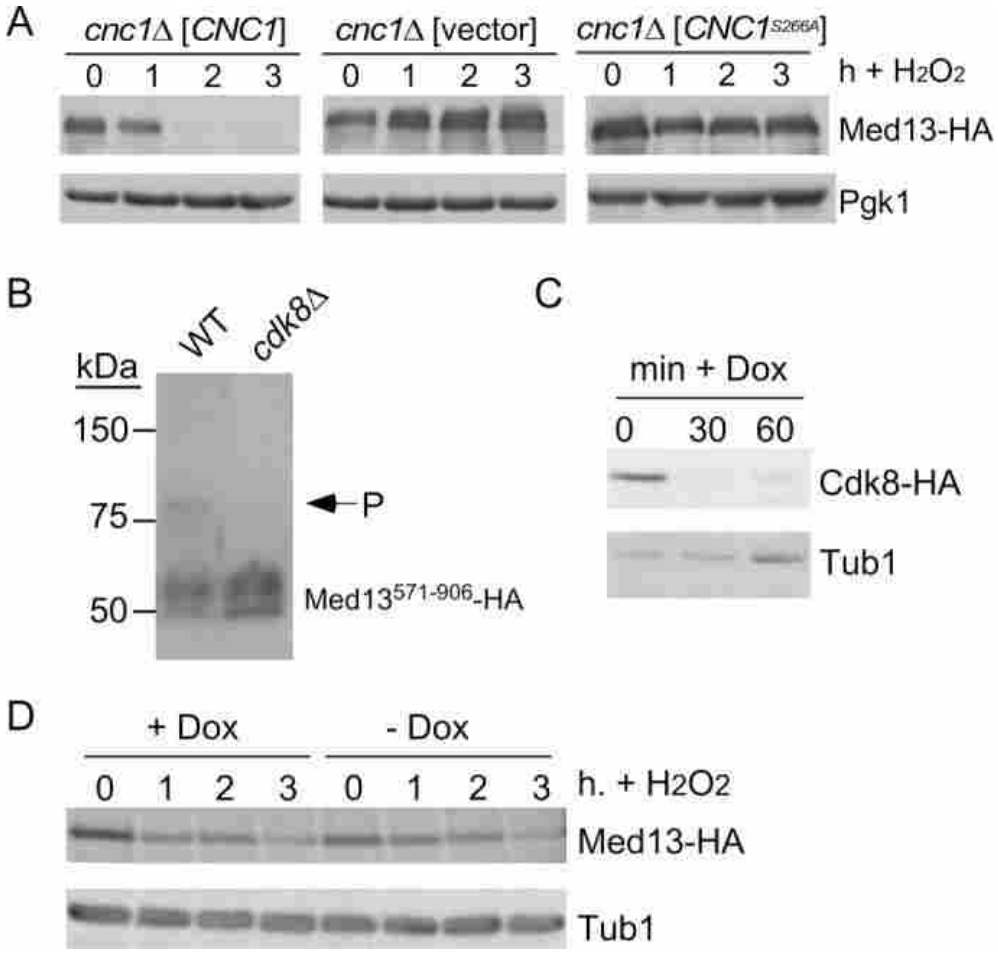

Figure A2-6 Cyclin C-Cdk8 directly stimulate Med13 proteolysis (A) Mid-log *cnc1*Δ cultures (RSY391) harboring either wild-type *CNC1* (pKC337), vector (pRS314) or $cnc1^{S266A}$ (pLR166) expression plasmids and pKC803 (CEN, Med13-HA) were subjected to an H_2O_2 timecourse experiment. Pgk1 levels were used as loading controls. (B) Phos-tag gel analysis of pDS8 ($Gal4^{AD}$-$Med13^{571-906}$) in unstressed wild type (RSY10) or *cdk8*Δ (RSY1796) cultures. Arrow indicates phosphorylated $Med13^{571-906}$ species. Molecular weight markers (kDa) are indicated. (C) RSY2066 harboring the Ubi-Ile3-Cdk8-HA expression plasmid (pCM1888) were grown to mid-log phase and doxycycline added for the indicated times. Cdk8-HA levels were monitored by Western blot analysis. Tub1 levels were monitored for loading control. (D) RSY2066 harboring pCM1888 and Med13-HA (pKC803) were grown to mid-log phase, the culture split, and doxycycline added to one for 1 hour. Both cultures were then treated with 0.8mM H_2O_2 and Med13-HA degradation monitored as previously described. Tub1p was monitored for loading control.

The results just presented indicated that the cyclin C-Cdk8 kinase is required for Med13 destruction in response to oxidative stress. Consistent with this Med13 is protected from degradation in cells harboring kinase dead *cdk8* as the only source of this enzyme [127]. As cyclin C-Cdk8 is active in unstressed cells these results suggest this kinase could prime the degron for recognition by SCF^{Grr1}. To test this model attempted to perform *in vitro* kinase assays with cyclin C-Cdk8 and $Med13^{571-906}$ as the substrate. Unfortunately, we were unable to get these assays to work. Thus we decided to ask examine the phosphorylation state of the Med13 degron derivative (GalADMed13$^{571-906}$) using the Phos-Tag™ SDS-PAGE system that severely retards the movement of a phosphorylated peptide [231]. Protein extracts prepared from unstressed wild type or *cdk8*Δ cultures harboring $GalADMed13^{571-906}$ were subjected to Phos-Tag western blot analysis. The results revealed the presence of a slower migrating band in the wild type extract that was missing in the *cdk8*Δ sample (Figure A2-6B). This indicates that Cdk8 is required for Med13 phosphorylation in unstressed cells.

To test whether cyclin C-Cdk8 activity was required before or after oxidative stress, a Cdk8-N-end rule degron was constructed. This system takes advantage of the rapid turnover of proteins that contain arginine as the amino terminal residue [232-234]. The Cdk8-N-end rule construct is under the control of a doxycycline-repressible promoter such that the administration of doxycycline coupled with the rapid turnover of the Cdk8-N-end rule fusion protein results in rapid depletion of Cdk8 from yeast cells (Figure A2-6C). To test the execution point for Cdk8 phosphorylation, a mid-log culture expressing an epitope-tagged allele of full length *MED13* (MED13-HA) and Cdk8-N-end degron was untreated or treated with doxycycline for one hour prior to H_2O_2 addition to ensure Cdk8 depletion. A timecourse was conducted and samples collected, extracts prepared and Med13-HA levels monitored by Western blot analysis. These

studies revealed that Med13-HA levels were reduced similarly in both cultures (Figure A2-6D) indicating that Cdk8 function was required before oxidative stress. Thus taken together, these results are consistent with a model that Cdk8 phosphorylation primes Med13 for degradation.

A2.5.6 The CWI pathway is required for ROS-mediated destruction of Med13

The CWI signal transduction pathway is the major MAPK pathway in yeast that transmits the reactive oxygen species (ROS) stress signal to transcription factors [235]. To facilitate cyclin C nuclear release, the CWI employs two MAPKs, Slt2 and its pseudokinase paralog Kdx1. Slt2 phosphorylates cyclin C on Serine 266 to induce cytoplasmic re-localization [129-131] while Kdx1 functions through an unknown mechanism [236]. To address if Kdx1 and/or Slt2 are required for Med13 degradation, we examined Med13-HA degradation kinetics in wild type and *slt2*Δ or *kdx1*Δ single mutant cultures following 0.4 mM H_2O_2 stress. As *slt2*Δ mutants are temperature sensitive, these experiments were conducted at 23°. The results show that Med13-HA was degraded in wild type or *kdx1*Δ cells but stable in the *slt2*Δ mutant (Figure A2-7A, quantified in Figure A2-S4B). These results indicate that unlike cyclin C, only Slt2 but not Kdx1, is required for Med13 destruction. Repeating this experiment with cells expressing a kinase dead version of *SLT2* (*slt2*^{K54R}) produced similar results (Figure 7B) indicating the Slt2 kinase activity is required for Med13 proteolysis. To investigate whether the role of Slt2 in Med13 degradation was direct, *in vitro* kinase assays were performed using activated Slt2-HA or the kinase dead derivative (Slt2^{K54R}-HA) [149] immunoprecipitated from yeast extracts. The immunoprecipitate was incubated with the *E. coli* prepared Med13 degron (amino acids 571-906) described above. These experiments revealed enhanced phosphorylation of Med13$^{571-906}$ above background that was dependent upon a functional kinase (Figure A2-7C) indicating that Slt2 directly regulates Med13 stability. Finally, we asked whether Slt2 activation was sufficient to induce Med13

destruction or whether another stress signal was required. To address this question, Med13-HA levels were monitored in an unstressed culture expressing a constitutively active allele of the upstream MAPKKK *BCK1* (*BCK1-20*). Mid-log cultures expressing *BCK1-20* exhibited dramatically reduced Med13-HA levels compared to vector control (Figure A2-7D). These results indicate that the CWI pathway is both necessary and sufficient to induce Med13 destruction. Finally, to test the epistatic relationship between *BCK1-20* and *cdk8*Δ alleles, the experiment just described was repeated in a *cdk8*Δ background. Western blot analysis revealed that Cdk8 was required for *BCK1-20* induced Med13 destruction in unstressed cells (Figure A2-6D). Taken together, these results indicate that Slt2 activation is necessary for H_2O_2-mediated Med13-HA degradation and that this signal requires Cdk8 activity. These results are consistent with a three-step model for initiating the Med13 destruction pathway (see Discussion).

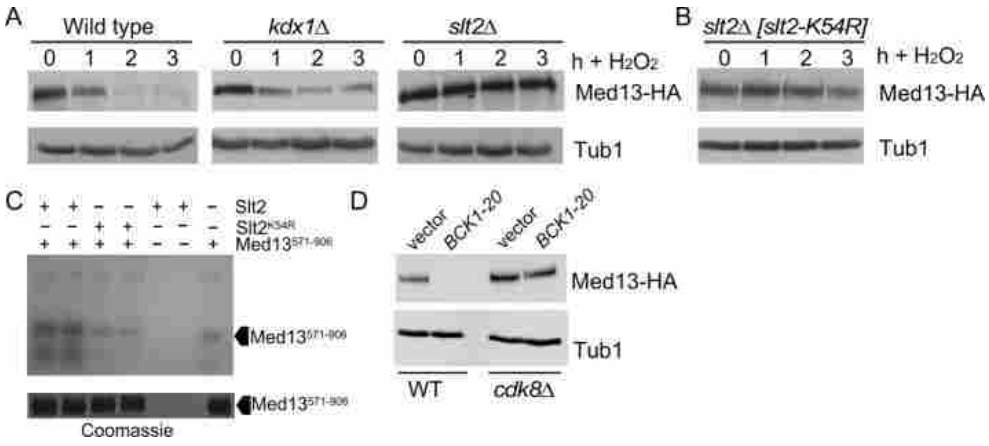

Figure A2-7 Slt2 directly stimulates Med13 destruction (A) Wild type (RSY10), *kdx1*Δ (RSY1736) and *slt2*Δ (RSY1006) cultures expressing pKC801 (CEN, Med13-HA) were grown to mid-log phase (0 hr) then treated with 0.4 mM H_2O_2 for the indicated times. Med13-HA levels were determined by Western blot analysis. (B) As in A except that the *slt2*Δ cells expressed a kinase dead *SLT2* mutant (*slt2*^{K54R}) plasmid. (C) Upper panel: Slt2-HA or Slt2^{K54R}-HA (kinase dead) was immunoprecipitated from extracts prepared from cells treated for 60 min with 5mM sodium orthovanadate was mixed with Med13$^{571-906}$ and radioactive ATP as indicated. All reactions were conducted in duplicate then separated by SDS PAGE and subject to autoradiography. Med13$^{571-906}$ is indicated by the arrowhead. Lower panel: Coomassie stained gel showing the Med13$^{571-906}$ input used in the kinase assays. (D) Wild-type (RSY10) or *cdk8*Δ (RSY1796) mutant cells expressing either an empty vector control or the hyperactive allele of *BCK1* (*BCK1-20*) and *MED13*-HA (pKC803) were grown to mid-log and Med13-HA levels determined by western blot analysis. Tub1 served as a loading control.

A2.5.7 Slt2 and Cdk8 phosphorylation of the IDR region is required for Med13 destruction

IDR regions confer conformational flexibility to proteins that are often targets of post-translational modifications [190]. Notably IDR's are enriched for phosphorylation sites raising the possibility that they are substrates for multiple kinases [192]. As our data indicate that Cdk8 and Slt2 are required for Med13 degradation, we next asked if the sites they phosphorylate lie within the same IDR region of Med13 that associates with Grr1 and cyclin C (amino acids 651-906). Slt2 and Cdk8 are both proline directed kinases that preferentially phosphorylate the consensus sequences PX(S/T)P or S/T-P-X-K/R (where X is any amino acid), respectively. They also can phosphorylate the minimal consensus sequence S/T-P [188]. Med13$^{651-906}$ contains a conserved Slt2 consensus sequence at position 748 that has been identified as potential phosphorylation site in two genomic screens [181, 237] well as four additional TP sites (Figure A2-8A). Thus, to address if these kinases phosphorylate the five S/T-P sites in Gal4^{AD}-Med13$^{651-906}$ fusion protein, its degradation was monitored following H_2O_2 stress in wild type, *slt2*Δ and *cdk8*Δ cells. The results show that Gal4AD-Med13$^{651-906}$ fusion protein is stable in either *slt2*Δ or *cdk8*Δ cells (Figure A2-8B). These results are consistent with a model that the Med13 phospho-degron is targeted by both Cdk8 and Slt2. Consistent with the Y2H data presented in Figure A2-3B, the phopho-degron is stable in *grr1*Δ cells (Figure A2-8C). If the Med13 phospho-degron is regulated by two kinases, then two separate S/T-P sites within the degron should stabilize the protein. To test this, wild-type cells harboring either a wild type Gal4AD-Med13$^{742-844}$ fusion protein or mutant derivatives were subjected to 0.4 mM H_2O_2 stress and analyzed as described above. As anticipated, the smaller Gal4AD-Med13$^{742-844}$ fusion protein that contains all 5 S/T-P sites was still degraded in wild-type cells (Figure A2-8C). Interestingly,

the S748A, T781A and T803A mutants were also degraded with the same kinetics as wild type (Figure A2-S4C). In addition, the double mutants (T781A T803A and S748A T781A) were also degraded with wild-type kinetics (Figure A2-8D and E). However, the T835A, T837A double mutant was significantly more stable than wild type (Figure A2-8C and E) suggesting that these sites are required for Med13 degradation. Taken together, these results suggest that both kinases have to be active in order for SCF^{Grr1} to recognize this 100 amino acid phospho-degron, at position T835 and T837.

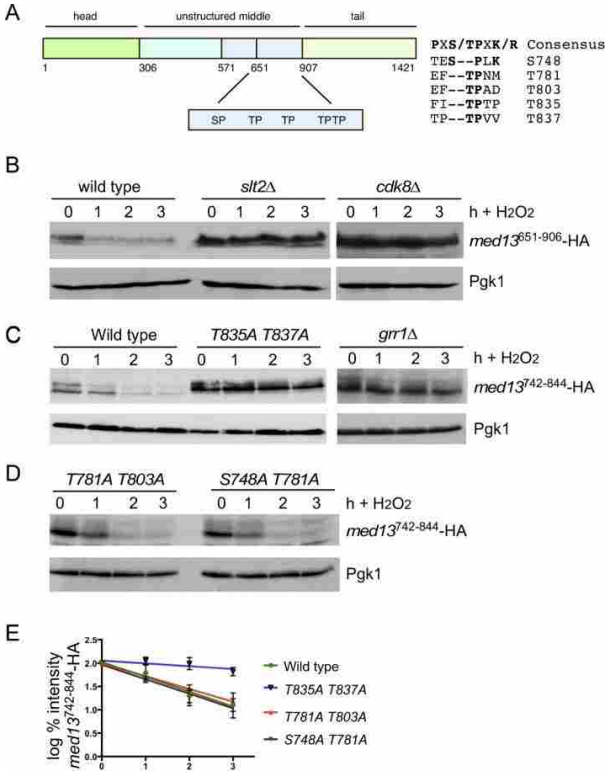

Figure A2-8 The Med13 IDR contains the phospho-degron (A) Map of Med13 showing the location of potential Cdk and MAPK sites within the IDR. (B) Wild type (RSY10), *slt2*Δ (RSY1737) and *cdk8*Δ (RSY1796) cultures expressing pDS16 ($Gal4^{AD}$-$Med13^{651-906}$) were grown to mid-log phase (0 hr) then treated with 0.4 mM H_2O_2 for the indicated times. $Med13^{651-906}$-HA levels were determined by Western blot analysis. Pgk1 levels were used as a loading control. (C) (D) Wild type (RSY10) cultures harboring wild type Gal4AD-$Med13^{742-844}$ (pDS32) or various point mutations as indicated were grown to mid-log phase (0 hr) then treated with 0.4 mM H_2O_2 for the indicated times. Med13-HA levels were determined by Western blot analysis. Pgk1 levels were used as a loading control. The Gal4AD-$Med13^{742-844}$ levels were also monitored in the *grr1*Δ strain. (E) Degradation kinetics of the Gal4AD-$Med13^{742-844}$ constructs shown in C and D.

A2.6 Discussion

Communication between organelles is critical to coordinate the cellular response to a variety of external or internal signals including oxidative stress. The data presented here and in previous publications [126, 127, 129-131, 134, 154, 228, 236] has revealed that the Cdk8 module (cyclin C, Cdk8, Med12 and Med13) of the mediator complex plays a key role in both yeast and mammalian cells. Previously, we reported that the cyclin C, but not Cdk8, translocates from the nucleus to the mitochondria following oxidative stress in both yeast and mammalian cells. At the mitochondria, cyclin C associates with the fission machinery to induce fragmentation and directs programmed cell death [127, 129, 134]. Therefore, releasing cyclin C from the nucleus represents an important step determining whether the cell initiates the RCD pathway or not. Importantly, we found that the nuclear anchor for cyclin C, Med13, is destroyed in response to oxidative stress providing a mechanism for how cyclin C nuclear release was orchestrated [154]. Interestingly, Med12, is neither required for this response [154] nor destroyed following H_20_2 stress (Figure A2-S4D). In this report, we provide the molecular details of how Med13 destruction is triggered to operate this important molecular switch in yeast. First, Med13 proteolysis is mediated by the ubiquitin ligase SCF and the specificity factor Grr1. Several studies in yeast and higher eukaryotes found that SCF substrates require a complex interplay between multiple kinases to generate the requisite phospho-degron on the substrate (reviewed in [155]). For example, Cdk1 acts as a priming kinase for Cdc5 [238, 239] whereas Cdc5 acts as a priming kinase for Wee1 [240]. In all cases, the priming kinase first phosphorylates the substrate, while the second kinase completes the formation of the phospho-degron by modifying residues that are recognized by the SCF. This has led to the current model that priming phosphorylations create docking sites for downstream kinases. Moreover, local structural disorder most likely

facilitates how multiple kinases regulate a protein within a small region. We identified a small region (amino acids 742-844) within the intrinsic-disordered region (IDR) of Med13 that acts as a communication hub. This region is sufficient to retain cyclin C in the nucleus, associates with Grr1, and contains the Med13 phospho-degron that is primed by Cdk8 and activated by Slt2 following oxidative stress exposure. This dual kinase requirement provides the cell with a mechanism to integrate multiple input signals into a single read out.

A2.6.1 The Med13 phospho-degron activation requires a three-step process

Our results indicate that cyclin C-Cdk8 provides the priming signal for Med13 destruction (Figure A2-9, Step 1). Although technical reasons prevented us from addressing whether this activity is direct or indirect, four independent experiments support a model that this is a direct phosphorylation event. 1. The observation that Med13$^{651\text{-}906}$ was not destroyed following H_2O_2 stress in *cdk8*Δ cells (Figure A2-8B). 2. Observation of a slower migrating band seen in Phos-Tag™ SDS-PAGE analysis of unstressed in wild type extracts that was missing in the *cdk8*Δ sample (Figure A2-6B). 3. The end-N rule experiments conducted in Figure A2-6C and D also revealed that Med13-HA levels were reduced regardless of the presence of Cdk8 after stress. 4. Lastly, *in vitro* evidence revealed that cyclin C directly interacts with this region of Med13 (Figure A2-4B and 4C) which would position the kinase with direct access to the Med13 degron. Thus taken together, these results suggest that Cdk8 phosphorylation primes Med13 for degradation, most likely by a direct event. Consistent with this, human Cdk8 directly phosphorylates human Med13 on S749, which lies in the intrinsic disorder domain in what appears to be a non-conserved residue compared to yeast [230]. This requirement may be necessary to inform the cell that Med13 is in the Cdk8 module and its destruction will lead to cyclin C release and Cdk8 inactivation. Slt2 activation by oxidative stress provides the trigger

mechanism that commits the cell to destroying Med13 and releasing cyclin C from the nucleus (Step 3). This event accomplishes two goals. First, removing cyclin C and destroying Med13 inhibits the repressor activity of Cdk8 for several stress responsive genes including chaperones (e.g., *SSA1*), anti-oxidants such as catalase (*CTT1*) and the multi-stress responsive gene *DDR2* [126, 129, 139]. In addition, Slt2 activation stimulates several transcription factors, such as Rlm1 that is required for the transcriptional arm of the stress response [148, 151, 241]. Therefore, Slt2 activation both stimulates transcriptional activators and inhibits repressors. By releasing cyclin C, the cell is able to transmit the stress signal to the rest of the cell including the mitochondria. We have previously demonstrated that cyclin C-induced fission alone is not sufficient to induce cell death but does make cells hypersensitive to oxidative stress [154]. Therefore, cyclin C release poises the cell to initiate RCD but additional regulatory layers exist. Unlike other priming/trigger two-kinase degron phosphorylation switches, we have identified an additional step in the system regulating Med13. Specifically, Slt2 also modifies cyclin C on S266, which promotes its dissociation from Med13 [131]. Our finding that the S266A mutation protects Med13 from destruction is consistent with a model that S266 modification disrupts cyclin C-Med13 interaction (Step 2) allowing Slt2 access to the phospho-degron. Taken together, our model predicts a three-step system that controls Med13 stabilityand cyclin C nuclear release.

If cyclin C phosphorylation is sufficient to initiate cyclin C nuclear release, then why would it be important to completely destroy Med13? First, our results indicate that S266 phosphorylation is capable of stimulating only partial release of cyclin C in unstressed cells [131]. Therefore, Med13 destruction may be necessary for complete cyclin C release. Not exclusive of this model, another possibility is that Med13 destruction prevents the reaccumulation of cyclin C in the nucleus after its cytoplasmic translocation. In this model,

Med13 proteolysis fixes the decision of cyclin C release thus directing a complete transcriptional and mitochondrial response to oxidative stress.

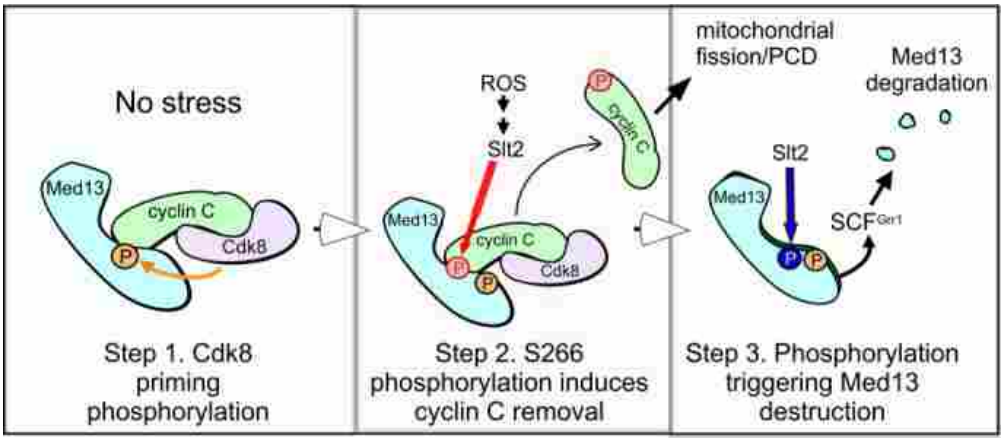

Figure A2-9 Three-step model of cyclin C release from Med13 following H_2O_2 stress Step 1. Cdk8-Cyclin C kinase phosphorylates Med13 in unstressed cells to provide the priming modification for this degron. Step 2 requires stress-activated Slt2 that phosphorylates cyclin C on S266 leading to disassociation of cyclin C from Med13. This event allows Slt2 access to the phospho-degron to deliver the trigger modification leading to Med13 recognition by SCF^{Grr1} and its destruction.

A2.6.2 Med13 Intrinsic disordered Region (IDR) is a communication hub

It has recently been suggested that IDR's play important roles in protein:protein communication as they provide a flexible interaction surface to multiple partners [189]. Using protein two different structure prediction algorithms IUPred/ANCHOR and Phyre^2 [242-244] Med13 has a large IDR spanning the middle of the protein (amino acids residues 307-906 and Figure A2-S5A and B). Although not conserved in amino acid sequence, it is notable that the position and presence of Med13's IDR is conserved throughout three kingdoms [217]. Also conserved is the observation that Med13 is the CKM member that brings this kinase module in contact with the Mediator complex [218]. This suggests a model in which the IDR of Med13 provides conformational plasticity to the CKM, which is important for bringing the kinase and other proteins in contact with different mediator members on a "*pro re nata"* basis. This idea is consistent with the results presented here in which we show that the IDR of Med13 can bind to

cyclin C before stress and Grr1 after. Although speculative, taken together this suggests a model in which Med13 IDR is conserved functionally and may contain signature motifs that are important for protein binding. Consistent with this idea is the observation that two other conserved proteins that regulate transcription (CCR4-NOT4 and TFIIS) also bind to the IDR region of yeast Med13 but in a different location (Fig S5, [245, 246]. Such a signature could be a MoRF, which is defined as a short binding region located within longer intrinsically disordered regions that bind to protein partners via disorder-to-order transitions [247]. ANCHOR analysis [243] predicts that the IDR of Med13 has many such domains, with two lying within the cyclin C binding region (residues 742-844 - Figure A2-S5A). As additional factors are identified that bind the Med13 IDR, the rules that govern these interactions may become better understood.

The need to understand the role Med13 IDR plays in protein communication has become important in the last decade as in humans truncating or loss of function mutations in MED13L, a paralogue of MED13 [248], results in *MED13L* haploinsufficiency syndrome. This syndrome is complex and presents with either complex congenital heart and neurodevelopmental defects or severe neurocognitive deficiencies and facial dysmorphism [249-252]. Interestingly many of these mutations lie in the IDR region of MED13L [252]. In yeast, a hallmark of *med13*Δ cells is that they are respiratory deficient which is dependent upon cyclin C nuclear export [154]. Thus it would be anticipated that a strain deleted for Med13 residues 742-844 would have a similar phenotype. Taken together, these studies emphasize the need for further analysis of both yeast and human Med13 IDR's to understand the molecular details of how this region contributes to Med13 function.

A2.6.3 Role of SCF^{Fbw7} and Med13 in higher eukaryotes following stress

Our previous studies described the conserved role of cyclin C in stressed and unstressed cells [127, 134]. However, differences are observed in cyclin C regulation between yeast and humans. In yeast, all of cyclin C is released into the cytoplasm followed by its destruction by the Not1 ubiquitin ligase. Conversely, only about 10% of total cyclin C is released from the nucleus in mammalian cells following oxidative stress and we do not detect any significant changes in its overall protein levels [134]. Steady state turnover of the human Med13 is directed by the analogous SCF ubiquitin ligase by a homologue of Grr1, called Fbw1 [226]. As Med13 tethers the Cdk8 module to the Mediator complex [218], Med13 turnover determines the promoter residency of the module and therefore impacts transcriptional regulation. However, we found that the phospho-degron directing the turnover of Med13 in human cells (T326) is not required for stress-induced destruction of Med13 in yeast. These results suggest that either a different degron system is employed in these two systems or that stress-induced destruction is regulated differently than that observed under normal growth conditions. Consistent with this is the observation that Cdk substrates are often clustered in regions of intrinsic disorder (reviewed in [253]). However, similar to other intrinsic disordered regions, their exact position in the protein is often poorly conserved in evolution, indicating that precise positioning of phosphorylation may not be required to permit a shared function (reviewed in [253]). Thus, it is possible that following oxidative stress in human cells, a similar two-kinase mechanism could regulate Med13 degradation. In support of this model, phosphorylation by two kinases of has been observed for other SCF^{Fbw1} substrates [254] including oncogenic transcription factors. This has led to classifying Fbw1 as a tumor suppressor (reviewed in [255]). Fbw7 degrades numerous oncogenic transcription factors (e.g., Myc, Notch, and Jun) as well as other proteins that contribute to

carcinogenesis. As cyclin C has also recently been given this tumor suppressor designation [256], it is imperative to understand the relationship between these proteins following stress in higher eukaryotes.

A2.7 Materials and methods

A2.7.1 Yeast strains and plasmids

All experiments, except the yeast two-hybrid assays (Y2H), were performed in *S. cerevisiae* W303 strain RSY10 [201] and are listed in Table S1. The Y2H assays were performed in PJ69-4a [166]. In accordance with the Mediator nomenclature unification effort [204], cyclin C (*SSN8*/*UME3*/*SRB11*) and Cdk8 (*SSN3*/*UME5*/*SRB10*) will use *CNC1* and *CDK8* gene designations, respectively. The *cnc1*Δ*, cdk8*Δ*, med13*Δ*, slt2*Δ, *kdx1*Δ and *kdx1 slt2*Δ and strains have been previously described [126, 127, 131, 228]. The *grr1*Δ strain RSY1770 and myc tagged Med12 strain (RSY18787) were constructed using gene replacement methodology as described [205]. The *MED13*-13myc allele was generated in this strain to create RSY1771 using the same methodology. RSY2066 was made by integrating pMK634 [234] into the *CDK8* locus of RSY10. The strain was then transformed with pCM188 [257] which contains the TET activator on a plasmid. The yeast two hybrid strain PJ69-4a was obtained from the Yeast Resource center, courtesy of a gift from S. Fields. All cells were grown at 30°C apart from *slt2*Δ and *slt2*Δ *kdx1*Δ which were grown at 23°C.

All plasmids used in this study are listed in Table S2. The wild-type epitope tagged plasmids pHY1066 (*MED13*-HA*,* 2*μ*), pKC337 (*ADH1*$_{Pro}$-cyclin C-myc), pUM511 (*GPD1*$_{Pro}$-*CDK8*-HA) and pBK38 (*ADH1*$_{Pro}$-*CNC1*-YFP) are functional and have been previously described [126, 129, 130, 229, 258]. pLR141 was made by cloning the *ADH1*$_{Pro}$-*CNC1*-myc, CYC$_{Term}$ from pKC337 into pRS426. The 2μ *MED13*-HA plasmids (PHY1066 and PHY1089)

and were a gift from P. Herman [229]. The wild-type *MED13* centromere based plasmids pKC801 and pKC803 were made by PCR cloning the *ADH1* promoter, *MED13*-3HA ORF, and *MED13* terminator from PHY1022 into pRS316 and pRS315 respectively. Site directed mutagenesis (New England Bio-Rad Q5) was used to create plasmids harboring amino acid mutations except for DS36 which was made using the Change-IT^{TM} kit by Affymetrix. The *CNC1*^{S266A} and the *SLT2*^{K54R} (a gift from D. Levin) have been previously described [131, 149]. The *MED13* Y2H plasmids were constructed by PCR cloning from pHY1022 into the *Xho*1 site of the Gal4 activating domain plasmid pACT2. Likewise the human cyclin C Y2H Gal4 binding domain plasmid pSW108 was made by PCR cloning of cyclin C cDNA amplified from pEGFP-cyclin C [259] into *Nco*1 digested pAS2. The GST-*MED13* fusion plasmid was made by PCR cloning from PHY1022 into pGEX4T-1. Oligonucleotide sequences were used to make plasmids and strains are available upon request. In short, all constructs were amplified from plasmid DNA using Phusion Taq (Thermo) digested using NEB fast digest restriction enzymes and ligated using Thermo fast ligase into their respective vectors. All protein fusion constructs were sequenced (Eurofins Genomics). Other plasmids that were used in this study that have been previously described are listed in Table S2.

A2.7.2 Cell growth

Yeast cells were grown in either rich, non-selective medium (YPDA) or synthetic minimal medium (SC) allowing plasmid selection as previously described [126]. For all experiments the cells were grown to mid-log phase (~ 6 x 10^6) before treatment with low concentrations of 0.4 mM H_2O_2 as previously described [130]. 25 mls of cells were collected per timepoint, washed in water, then the pellet flash frozen in liquid nitrogen. Yeast two hybrid experiments were executed as described [168]. 10 mM 3-amino-1,2,4-triazole (3-AT) was added

to the selective plates to increase the stringency of the interactions. *E. coli* cells were grown in LB medium with selective antibiotics. The degron experiments described in Figure A2-5D and E were executed as follows. In Figure A2-5D, cells (RSY2066) were grown to mid log and samples removed at the timepoints shown for analysis of Ubi-isoleucine::3HA-Cdk8 degradation after the addition of 2 µg/ml doxycycline. In Figure A2-5E, RSY2066 was transformed with Med13-3HA plasmid (pKC803), grown to mid-log, split and into one flask 2 µg/ml doxycycline added. After 60 minutes, 0.8 mM H_2O_2 was added to both sets of cells and samples taken for NaOH lysis and Western analysis as described below.

A2.7.3 Western blot analysis

Tagged Med13 constructs were detected by using NaOH lysis of cell pellets as basically described by [260]. In short, the frozen cell pellets were defrosted on ice, resuspended in 2M LiOAc on ice for 5 minutes, centrifuged and then resuspended in 0.4 M NaOH for a further 5 minutes on ice. Thereafter, the pellets were finally resuspended in 100 µl 2X SDS loading dye [126], boiled for 5 minutes and 15µl loaded onto a 6% SDS-PAGE gel (Novagen). For the phos-tag gel (Figure A2-9B), proteins were prepared as just described and analyzed on an 7.5% polyacrylamide gel containing 7.5 µM phos-tag (Wako Laboratory Chemicals) and 15 µM $MnCl_2$. The proteins were transferred to a nylon membrane (Millipore) using 10% methanol, 0.02% SDS and 10X running buffer [126]. To detect Med13-myc, Med12-myc and Med13-HA, 1 in 5000 dilutions of either anti-myc (Roche) or anti-HA antibodies (Clontech) were used. Tub1 and Pgk1 were visualized as previously described [261] except that anti-alpha tubulin antibodies (12G10) were obtained from the Developmental Studies Hybridoma Bank, University of Iowa. Western blot signals were detected using either goat anti-mouse or goat anti-rabbit secondary antibodies conjugated to alkaline phosphatase (Sigma) and the CDP-Star

chemiluminescence kit (Tropix). Signals were quantitated by CCD camera imaging (Kodak Inc.). All degradation assays were performed more than once. S.E.M. were generated for each point and error bars are indicated on the graphs which were generated using GraphPad Prism 7 program.

A2.7.4 Fluorescence microscopy

YFP-cyclin C subcellular localization and mitochondrial morphology was monitored as described previously [127, 129]. For all experiments, the cells were grown to mid-log (6 x 10^6 cells/ml), treated with 0.4 mM H_2O_2 for the timepoints indicated, then analyzed by fluorescence microscopy. Cyclin C-YFP export analysis was performed on cells fixed with 4% paraformaldehyde/3.4% sucrose for 1 h at room temperature. The cells were washed three times in water and prepared for fluorescence microscopy as described previously [262] using mounting medium (10 mg/ml p-phenylenediamine, 50 ng/ml 4',6-diamidino-2-phenylindole) to visualize nuclei and prevent photo bleaching. Images were obtained using a Nikon microscope (model E800) with a 100X objective with 1.2X camera magnification (Plan Fluor Oil, NA 1.3) and a CCD camera (Hamamatsu model C4742). Data were collected using NIS software and processed using Image Pro software. All images of individual cells were optically sectioned (0.2 μM slices at 0.3 μM spacing) deconvolved and the slices were collapsed to visualize the entire fluorescent signal within the cell. Cyclin C-YFP foci were scored as being cytoplasmic when 3 or more foci were observed outside of the nucleus. Mitochondrial fission assays were performed on live cells as described [127]. In brief, mitochondrial fission was scored positive if no reticular mitochondria were observed that transversed half the cell diameter. Fusion was scored when cells exhibited one or more reticular mitochondria the diameter of the cell. Fission and fusion

was scored for 200 cells from three independent isolates. Statistical analysis was performed using the Student's T-test with $p<0.05$ used to indicate significant differences.

A2.7.5 Pull down assays and kinase assays

Purified proteins that were used in the pull down assay (Figure A2-4B) were made as follows. The GST constructs (DS30, GST hCCNC and GST alone) were transformed into BL21 DE3 *E. coli* strain and expression induced with 0.5 M IPTG at 37°C for 3 h. Cell pellets were resuspended in 50 mL GST lysis buffer (150 mM KCl, 50 mM HEPES, pH 7.5, 1mM ßME), sonicated (25 x 10 sec. bursts) and the supernatant recovered by centrifugation at 40000xg for 30 minutes. The supernatant was then added to 1mL of washed glutathione beads (LifeTech) rotated at 4°C for 1 hr. The unbound fraction was removed from the beads by gravity flow. The beads were washed twice with lysis buffer and the bound protein was eluted in five 1mL fractions with the elution buffer (lysis buffer supplemented with 10 mM reduced Glutathione). The protein containing fractions were pooled and then desalted using 4 mL Zebra7K desalting columns that had been pre-equilibrated with the lysis buffer. The protein fraction was supplemented with glycerol to a final concentration of 10% and stored at -80 °C in small aliquots. 6His tagged human or yeast cyclin C was purified the same way with the following exceptions. The lysis buffer (buffer A) was 500 mM KCl, 50mM HEPES pH7.5, 1mM ßME, 20mM imidazole. Talon beads (Clontech,) were used and washed with buffer B (150mM KCl, 50mM HEPES pH7.5, 1mM BME, 20 mM imidazole) and the bound protein was eluted in elution buffer (150 mM KCl, 50mM HEPES pH7.5, 1 mM BME, 500 mM imidazole). The desalting columns were pre-equilibrated with the B buffer without Imidazole. The concentrations of all the recombinant proteins were determined by Bradford assay. The pull down assays in Figure A2-4B and C were performed using His-tagged human or yeast cyclin C respectively as bait and GST-tagged

Med13$^{742-844}$ (DS30) as target. 500nM cyclin C was mixed with 1uM of Med13$^{742-844}$ in a final reaction volume of 250 µL with B buffer and incubated for 1hr at room temperature. Bound protein was precipitated with 100 µL of washed Talon beads and eluted using 500mM imidazole. The protein mixture was resolved using SDS-PAGE and Western blotting with either anti-GST (Abcam), anti-His (Bethal) or anti human cyclin C antibodies (Bethal). Controls with only the target protein and no bait protein were included in all the experiments. The pull down assays in Figure A2-4D were performed using 500 nM of either GST, GST-tagged yeast cyclin C and 1µM 6His-Med13$^{571-660}$ (DS22). The proteins were incubated together in GST lysis buffer and incubated at RT for 1hr. Then 100uL of GSH beads (pre-equilibrated with GST wash/lysis buffer) was added to the protein mixture and incubated with rotation for 1hr. The beads were centrifuged for 30sec washed twice with 500uL of GST wash/lysis buffer. The protein mixture was resolved using SDS-PAGE and Western blotting with either anti-GST or anti-His antibodies

The *in vitro* kinase assays were executed basically as described [75]. Slt2-HA and Slt2^{K54R}-HA kinases were immunoprecipitated from cells treated with 5mM sodium orthovanadate for 60 minutes which activates Slt2 [263]. In short, yeast extracts harboring the respective plasmids were made by resuspending cells in lysis buffer (20 mM HEPES, 10 mM KCl, 1 mM EDTA, 1 mM ethylene glycol tetraacetic acid [EGTA], 50 mM NaCl, 10% glycerol, 1 mM β-mercaptoethanol, cOmplete Protease Inhibitor Cocktail Tablet, pH 7.4, with phosphatase inhibitors for Cdk8-HA purification) and protein immunoprecipitation was conducted as previously described [75]. with anti-HA magnetic beads (PierceTM)/ anti-myc magnetic beads (Cell Signaling). Med13$^{571-906}$ was purified from *E. coli* BL21 DE3 strain induced with 0.5 mM IPTG for 5 hours at 37ºC using 6X His-tagged purification method previously described [75]. The Slt2 *in vitro* kinase assay was conducted as previously described

[264] by resuspending Slt2 beads in kinase buffer (20 mM HEPES, 10 mM $MgCl_2$, 100 μM Na_3VO_4, pH 7.5), with 20uM ATP, 5 uCi of 32P-ATP and purified $Med13^{571-907}$. Reactions were incubated at 30ºC for 30 minutes.

A2.8 Acknowledgments

We thank C. Wittenburg, S. Fields, P. Herman, D. Levin and M. Solomon for strains and plasmids. We also thank A. Sardallah and S. Khakhina for help in making Med13 plasmids and the Med12-myc strain respectively. We thank members of the Cooper, Strich and Grose laboratories for critical reading of this manuscript. This work was supported by grants from the National Institutes of Health awarded to K.F.C. (GM113196), R.S. (GM113052), J.G (GM100376) and the New Jersey Cancer Commission (DHFS16PPC067) to V. G. The yeast two-hybrid strain was made by work supported by NIH grant P41 RR11823 awarded to T. N. Davis.

A2.9 Supplementary materials

Supplemental Table A2-1 Yeast strains used in this study

Strain	Genotype*	Source
RSY10	-	[201]
RSY1006	*slt2Δ::his5*$^{+}$	[228]
RSY1696	*cnc1Δ::KANMX6*	[208]
RSY1701	*med13Δ::HIS3*	[154]
RSY1706	*med13Δ:: KANMX6*	[154]
RSY1726	*cdk8Δ:: KANMX6*	[154]
RSY1736	*kdx1Δ::KANMX6*	[131]
RSY1737	*kdx1Δ::KANMX6 slt2Δ::his5*$^{+}$	[131]
RSY1798	*Med13-myc::KANMX4*	[154]
RSY1770	*grr1Δ::his5*$^{+}$	This study
RSY1771	*grr1Δ::his5+ MED13-13Myc:: KANMX6*	This study
RSY1787	*Med12-myc::KANMX4*	This study
RSY2066	*PTetO7-Ubi-Ile::3HA-Cdk8::NatMX4*	This study
PJ69-4a	*LYS2::GAL1-HIS3 GAL2-ADE2 met2::GAL7-lacZ gal4Δ gal80Δ*	[166]

*Genotype of all strains is MATa ade2 ade6 can1-100 his3-11,15 leu2-3,112 trp1-1 ura3-1 except PJ69-4alpha which is MATa trp1-901 leu2- 3,112 ura3-52 his3-200 gal4Δ gal80Δ

Supplemental Table A2-2 Plasmids used in this study.

Plasmid Name	Gene	Epitope Tag	Marker	Promoter	2µ/ CEN/ int	Reference
pBK38	*CNC1*	GFP	*URA3*	*ADH1*	CEN	[129]
pKC337	*CNC1*	1myc	*TRP1*	*ADH1*	CEN	[126]
pKC800	*GAL4AD-MED13*	1HA	*LEU2*	*ADH1*	CEN	This study
pKC801	*MED13*	3HA	*URA3*	*ADH1*	CEN	This study
pKC802	*MED13*^{T210A}	3HA	*URA3*	*ADH1*	CEN	This study
pKC803	*MED13*	3HA	*LEU2*	*ADH1*	CEN	This study
pLR106	*BCK1-20*	None	*HIS3*	*ADH1*	CEN	[228]
pLR141	*CNC1*	1 myc	*URA*	*ADH1*	2µ	This study
pLR166	*CNC1*^{S266A}	1 myc	*TRP1*	*ADH1*	CEN	[131]
pDS2	*GAL4AD -MED13*$^{1-305}$	1HA	*LEU2*	*ADH1*	CEN	This study
pDS4	*GAL4AD-MED13*$^{907-1421}$	1HA	*LEU2*	*ADH1*	CEN	This study
pDS5	*GAL4AD-MED13*$^{306-906}$	1HA	*LEU2*	*ADH1*	CEN	This study
pDS6	*GAL4AD-MED13*$^{1-906}$	1HA	*LEU2*	*ADH1*	CEN	This study
pDS7	*GAL4AD-MED13*$^{306-570}$	1HA	*LEU2*	*ADH1*	CEN	This study
pDS8	*GAL4AD-MED13*$^{571-906}$	1HA	*LEU2*	*ADH1*	CEN	This study
pDS10	*6HIS- MED13*$^{571-906}$	-	-	-		This study
pDS15	*GAL4AD-MED13*$^{571-650}$	1HA	*LEU2*	*ADH1*	CEN	This study
pDS16	*GAL4AD-MED13*$^{651-906}$	1HA	*LEU2*	*ADH1*	CEN	This study
pDS30	*GST-MED13*$^{742-844}$	GST	-	-	-	This study
pDS22	6His-*MED13*$^{571-650}$	6His	-	-	-	This study
pDS32	*GAL4AD-MED13*$^{742-844}$	1HA	*LEU2*	*ADH1*	2µ	This study
pDS33	*GAL4AD-MED13*$^{742-844\ S748A}$	1HA	*LEU2*	*ADH1*	2µ	This study
pDS34	*GAL4AD-MED13*$^{742-844\ T781A}$	1HA	*LEU2*	*ADH1*	2µ	This study
pDS36	*GAL4AD-MED13*$^{742-844\ T835A, T837A}$	1HA	*LEU2*	*ADH1*	2µ	This study
pDS40	*GAL4AD-MED13*$^{742-844\ T801A}$	1HA	*LEU2*	*ADH1*	2µ	This study
pDS41	*GAL4AD-MED13*$^{742-844\ T781A, T801A}$	1HA	*LEU2*	*ADH1*	2µ	This study
pDS42	*GAL4AD-MED13*$^{742-844\ S748A, T781A}$	1HA	*LEU2*	*ADH1*	2µ	This study

pSW108	*hCCNC1-GAL4^{BD}*	1HA	*TRP1*	*ADH1*	2µ	This study
GST-yCNC1	*GST-yCNC1*	GST	-	-	-	[259]
6His-hCNC1	6His-hCNC1	6His	-	-	-	This study
6His-	6His-yCNC1	6His	-	-	-	This study
pACT2	*GAL4AD*	1HA	*LEU2*	*ADH1*	CEN	[211]
pAS2	*GAL4BD*	1HA	*TRP*	*ADH1*	CEN	[211]
pAS2-Grr1	*GAL4BD-GRR1*	1HA	*TRP*	*ADH1*	CEN	[168]
pAS2-Grr1ΔL	*GAL4BD-GRR1$^{\Delta L}$-*	1HA	*TRP*	*ADH1*	CEN	[168]
pGrr1	*Grr1*	1HA	*TRP*	*ADH1*		[221]
pGrr1ΔL	*Grr1ΔL*	1HA	*TRP*	*ADH1*		[221]
Mt-dsRed	Mito-targeting	dsRed	*URA3*	*ADH1*	CEN	[265]
pHY1022	*MED13*	3HA	*URA3*	*ADH1*	2µ	[229]
pHY1089	*MED13*^{S608A,S1236A}	3HA	*URA3*	*ADH1*	2µ	[229]
Slt2	*SLT2*	3HA	*LEU2*	*SLT2*	2µ	[149]
Slt2^{K54R}	*SLT2^{K54R}*	3HA	*LEU2*	*SLT2*	2µ	[149]
pCM188	*TET*	-	*URA3*	*ADH1-Tet02*	CEN	[257]
pMK634	*Ubi-lLe-3HA*		*NAT-MX4*	*ADH1*	Int.	[234]

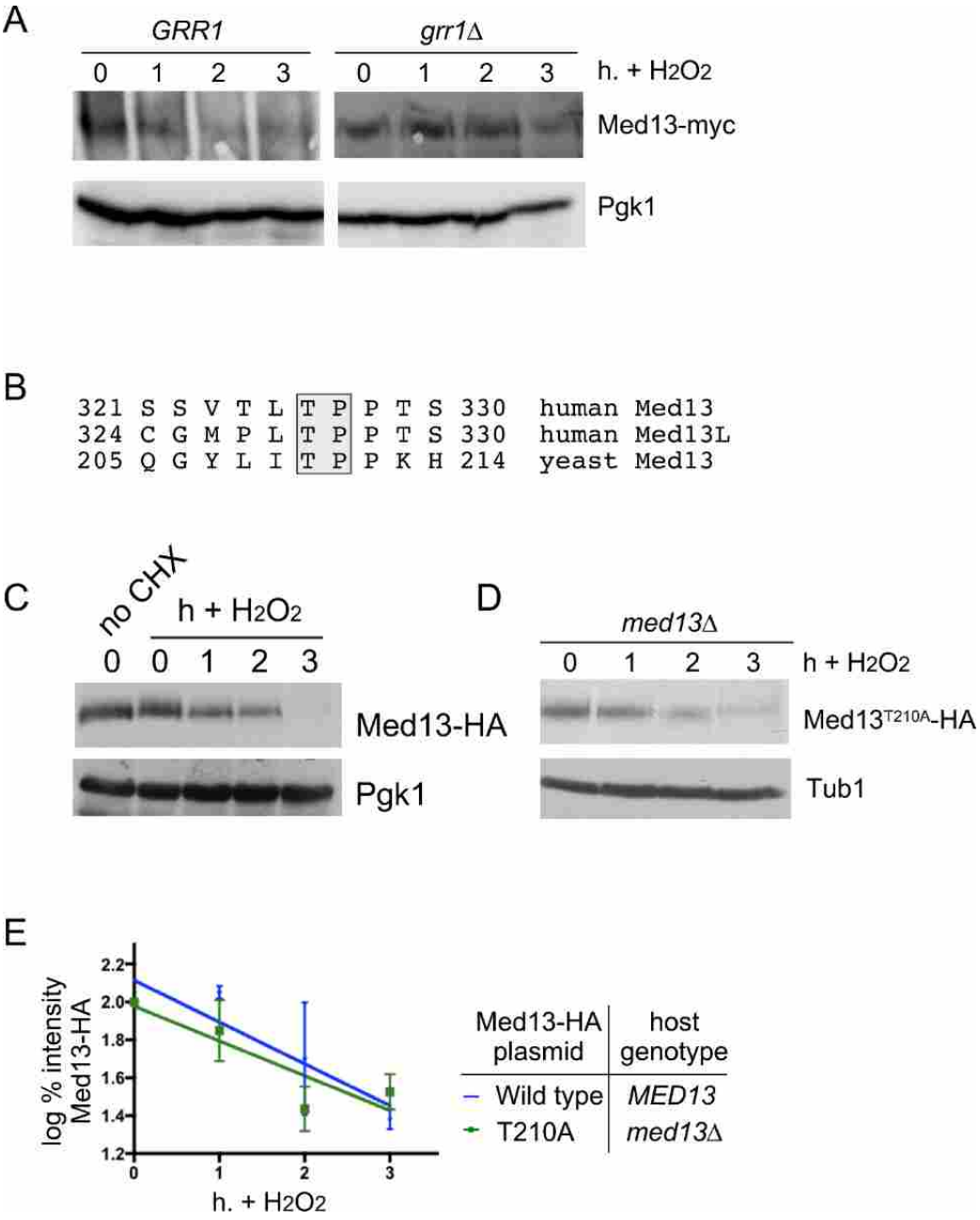

Figure A2-S1 The human Fbw7 degron on Med13 is not required for Med13 degradation (A) RSY1771 (*grr1*Δ*::HIS3 MED13-myc::KAN*) harboring either *ADH1*$_{PRO}$*-GRR1* or a vector control were treated with 0.4 mM H_2O_2 for the timepoints indicated and Med13 levels analyzed by Western blot. Tub1 levels were used as loading controls. (B) Conservation of the human Med13 SCF^{Fbw7} degron in yeast. (C) Degradation of Med13-HA after treatment of the cells with cycloheximide. Wild type cells (RSY10) harboring Med13-HA (pKC801) were treated with cycloheximide as previously described [131] and Med13-HA degradation analyzed as described. Pgk1 was used as a loading control. (D) *med13*Δ cells (RSY1701) harboring Med13^{T210A} as the only copy of Med13 were treated with 0.4 mM H_2O_2 for the timepoints indicated and Med13 levels analyzed by Western blot. Tub1 levels were used as a loading control. (E) Quantification of Med13-HA degradation from C and D.

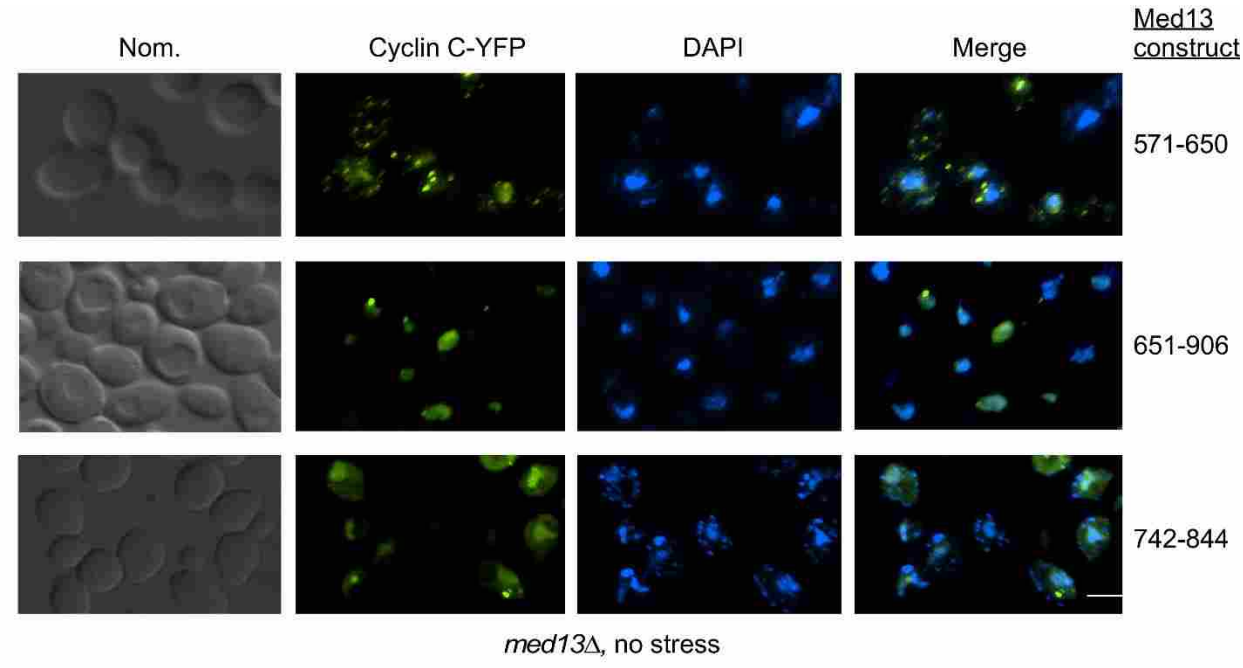

Figure A2-S2 Fluorescence microscopy of mid-log phase *med13*Δ cells (Y1701) harboring the Gal^{AD}-Med13 fusion constructs shown and cyclin C-YFP (pBK38) Cells were stained with Dapi to visualize the nucleus. Bar = 10μM

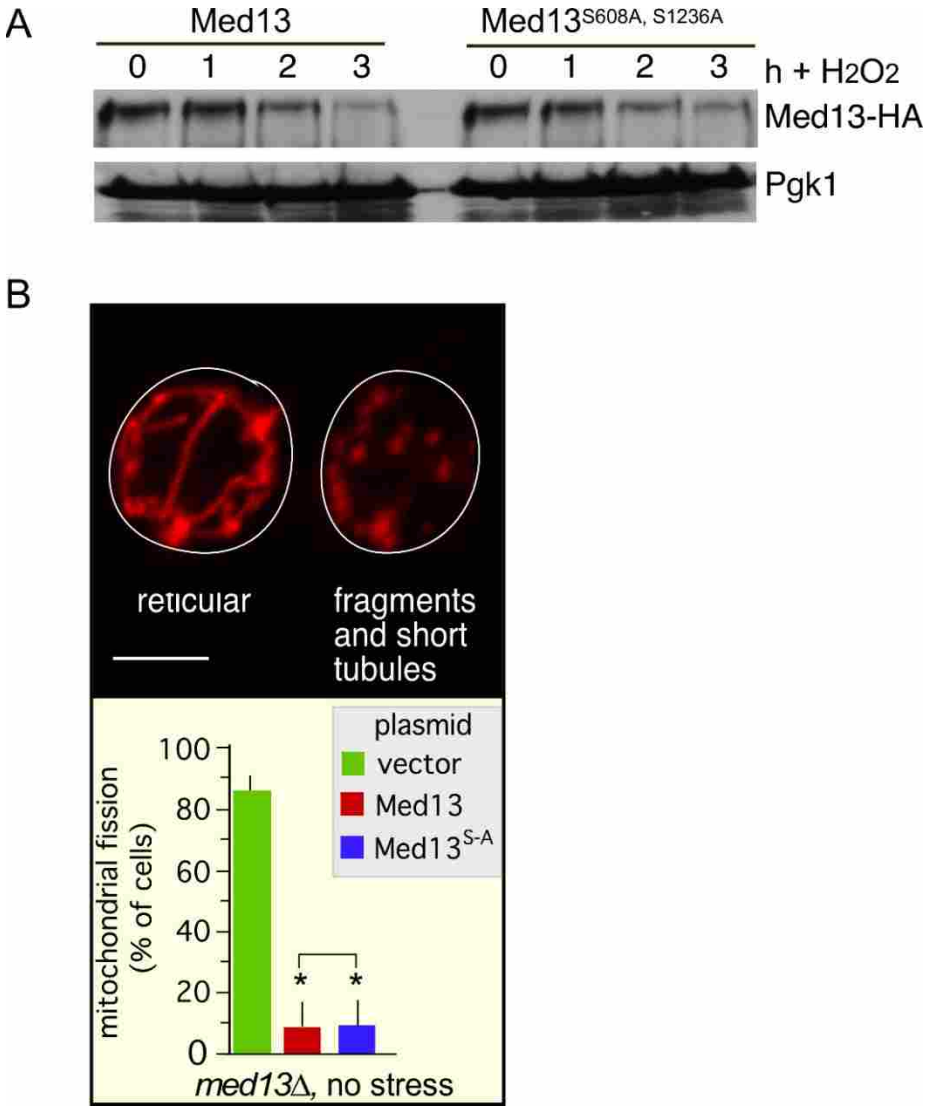

Figure A2-S3 PKA mediated phosphorylation of Med13 is not required for its degradation following H_2O_2 stress (A) Wild type (RSY10) cultures expressing either PHY1066 (2μ Med13-HA) or PHY2081 (2μ Med13-HA plasmid with PKA sites, S608 and S1236 mutated to alanine) were grown to mid-log phase (0 hr) then treated with 0.4 mM for the indicated times. Med13-HA levels were determined by Western blot analysis. Tub1 levels were used as a loading control. (B) The Med13S808A, S1236A mutant complements med13Δ mitochondrial morphology. med13Δ cells (RSY1701) expressing either PHY1066, PHY2081 or a vector and the DsRed mitochondrial targeting plasmid (mt-DsRed) were grown to mid-log. Mitochondrial morphology was examined using fluorescence microscopy of living cells. The left hand panel shows representative images of reticular or fragmented mitochondria are shown. Bar = 10μM. The percent of cells (mean ± s.e.m.) within the population displaying mitochondrial fission is given * $p<0.05$ difference from wild type.

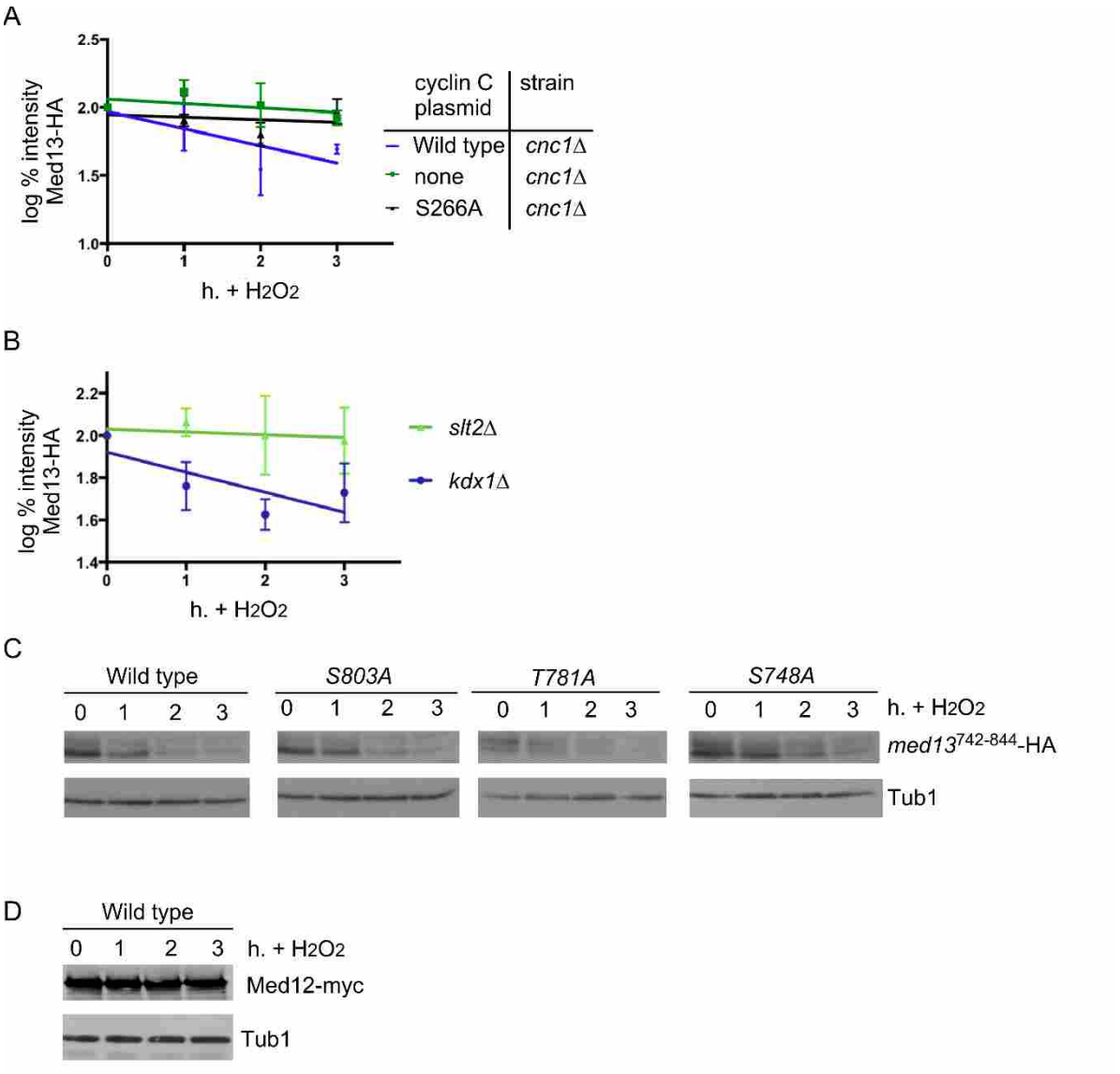

Figure A2-S4 (A) Quantification of Med13-HA degradation following 0.4mM H_2O_2 stress for the experiments shown in Figure A2-6 (A) and Figure A2-7 (B) (C) Wild type (RSY10) cultures harboring either wild type Gal4AD-Med13$^{742-844}$ or the various point mutations indicated were grown to mid-log phase (0 hr) then treated with 0.4 mM H_2O_2 for the indicated times. Med13-HA levels were determined by Western blot analysis. Tub1 levels were used as a loading control. (D) Med12 is not destroyed in H_2O_2 stress. A strain harboring endogenous Med12-myc (RSY1787) was treated with 0.4 mM H_2O_2 for the timepoints indicated and Med12 levels analyzed by Western blot. Tub1 levels were used as loading controls.

A

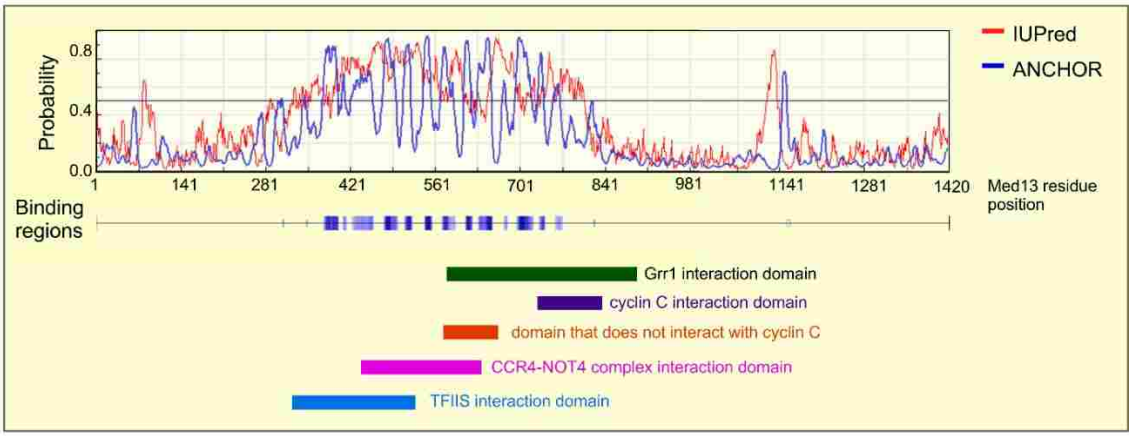

B

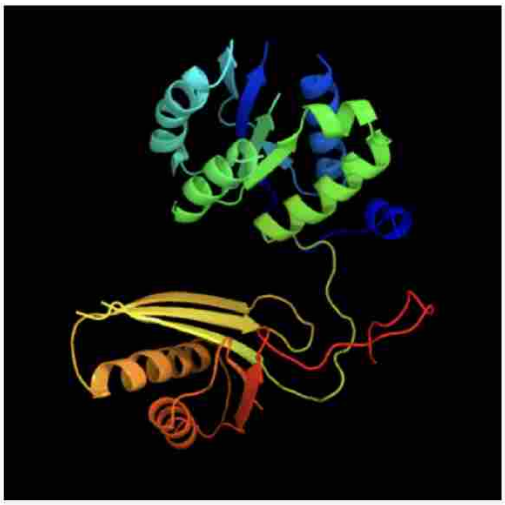

Figure A2-S5 (A) IUPred and ANCHOR plot analysis of Med13 These programs generates a plot with the profiles calculated by IUPred [242], a general disorder prediction method (in red), and ANCHOR [243], a prediction of disordered binding regions (in blue). Underneath the profile, predicted binding regions are indicated by the horizontal bars. The bar is shaded according to the prediction score. Regions that are filtered out are marked by empty bars. Grr1 and cyclin C binding domains identified in this work are also shown. In addition, the domain of Med13 that does not interact with cyclin C is marked as well as the CCR4-NOT4 complex and TFIIS interaction domains [245, 246]. (B) Phyre2 [244] plot analysis of yeast Med13.

REFERENCES

1. Mitchell, P., *Coupling of phosphorylation to electron and hydrogen transfer by a chemi-osmotic type of mechanism.* Nature, 1961. **191**: p. 144-8.

2. Liu, X., et al., *Induction of apoptotic program in cell-free extracts: requirement for dATP and cytochrome c.* Cell, 1996. **86**(1): p. 147-57.

3. Vaux, D.L., S. Cory, and J.M. Adams, *Bcl-2 gene promotes haemopoietic cell survival and cooperates with c-myc to immortalize pre-B cells.* Nature, 1988. **335**(6189): p. 440-2.

4. Sena, L.A. and N.S. Chandel, *Physiological roles of mitochondrial reactive oxygen species.* Mol Cell, 2012. **48**(2): p. 158-67.

5. Wellen, K.E. and C.B. Thompson, *A two-way street: reciprocal regulation of metabolism and signalling.* Nat Rev Mol Cell Biol, 2012. **13**(4): p. 270-6.

6. Rizzuto, R., et al., *Mitochondria as sensors and regulators of calcium signalling.* Nat Rev Mol Cell Biol, 2012. **13**(9): p. 566-78.

7. Lan, B., et al., *The roles of mitochondria-associated membranes in mitochondrial quality control under endoplasmic reticulum stress.* Life Sci, 2019: p. 116587.

8. Haynes, C.M., C.J. Fiorese, and Y.F. Lin, *Evaluating and responding to mitochondrial dysfunction: the mitochondrial unfolded-protein response and beyond.* Trends Cell Biol, 2013. **23**(7): p. 311-8.

9. Youle, R.J. and A.M. van der Bliek, *Mitochondrial fission, fusion, and stress.* Science, 2012. **337**(6098): p. 1062-5.

10. Toyama, E.Q., et al., *Metabolism. AMP-activated protein kinase mediates mitochondrial fission in response to energy stress.* Science, 2016. **351**(6270): p. 275-281.

11. Gomes, L.C., G. Di Benedetto, and L. Scorrano, *During autophagy mitochondria elongate, are spared from degradation and sustain cell viability.* Nat Cell Biol, 2011. **13**(5): p. 589-98.

12. Rambold, A.S., et al., *Tubular network formation protects mitochondria from autophagosomal degradation during nutrient starvation.* Proc Natl Acad Sci U S A, 2011. **108**(25): p. 10190-5.

13. Patron, M., et al., *The mitochondrial calcium uniporter (MCU): molecular identity and physiological roles.* J Biol Chem, 2013. **288**(15): p. 10750-8.

14. Boengler, K., et al., *Mitochondria and ageing: role in heart, skeletal muscle and adipose tissue.* J Cachexia Sarcopenia Muscle, 2017. **8**(3): p. 349-369.

15. Srinivasan, S., et al., *Mitochondrial dysfunction and mitochondrial dynamics-The cancer connection.* Biochim Biophys Acta Bioenerg, 2017. **1858**(8): p. 602-614.

16. Bratic, I. and A. Trifunovic, *Mitochondrial energy metabolism and ageing.* Biochim Biophys Acta, 2010. **1797**(6-7): p. 961-7.

17. de Moura, M.B., L.S. dos Santos, and B. Van Houten, *Mitochondrial dysfunction in neurodegenerative diseases and cancer.* Environ Mol Mutagen, 2010. **51**(5): p. 391-405.

18. Panel, M., B. Ghaleh, and D. Morin, *Mitochondria and aging: A role for the mitochondrial transition pore?* Aging Cell, 2018. **17**(4): p. e12793.

19. Hwang, A.B., D.E. Jeong, and S.J. Lee, *Mitochondria and organismal longevity.* Curr Genomics, 2012. **13**(7): p. 519-32.

20. Calabrese, M.F., et al., *Structural basis for AMPK activation: natural and synthetic ligands regulate kinase activity from opposite poles by different molecular mechanisms.* Structure, 2014. **22**(8): p. 1161-1172.

21. Stapleton, D., et al., *Mammalian AMP-activated protein kinase subfamily.* J Biol Chem, 1996. **271**(2): p. 611-4.

22. Thornton, C., M.A. Snowden, and D. Carling, *Identification of a novel AMP-activated protein kinase beta subunit isoform that is highly expressed in skeletal muscle.* J Biol Chem, 1998. **273**(20): p. 12443-50.

23. Cheung, P.C., et al., *Characterization of AMP-activated protein kinase gamma-subunit isoforms and their role in AMP binding.* Biochem J, 2000. **346 Pt 3**: p. 659-69.

24. Ross, F.A., C. MacKintosh, and D.G. Hardie, *AMP-activated protein kinase: a cellular energy sensor that comes in 12 flavours.* FEBS J, 2016. **283**(16): p. 2987-3001.

25. Hardie, D.G., D. Carling, and S.J. Gamblin, *AMP-activated protein kinase: also regulated by ADP?* Trends Biochem Sci, 2011. **36**(9): p. 470-7.

26. Gowans, G.J., et al., *AMP is a true physiological regulator of AMP-activated protein kinase by both allosteric activation and enhancing net phosphorylation.* Cell Metab, 2013. **18**(4): p. 556-66.

27. Ross, F.A., T.E. Jensen, and D.G. Hardie, *Differential regulation by AMP and ADP of AMPK complexes containing different gamma subunit isoforms.* Biochem J, 2016. **473**(2): p. 189-99.

28. Herzig, S. and R.J. Shaw, *AMPK: guardian of metabolism and mitochondrial homeostasis.* Nat Rev Mol Cell Biol, 2018. **19**(2): p. 121-135.

29. Garcia-Roves, P.M., et al., *Gain-of-function R225Q mutation in AMP-activated protein kinase gamma3 subunit increases mitochondrial biogenesis in glycolytic skeletal muscle.* J Biol Chem, 2008. **283**(51): p. 35724-34.

30. Jager, S., et al., *AMP-activated protein kinase (AMPK) action in skeletal muscle via direct phosphorylation of PGC-1alpha.* Proc Natl Acad Sci U S A, 2007. **104**(29): p. 12017-22.

31. Wu, Y., et al., *Activation of AMPKalpha2 in adipocytes is essential for nicotine-induced insulin resistance in vivo.* Nat Med, 2015. **21**(4): p. 373-82.

32. Mihaylova, M.M., et al., *Class IIa histone deacetylases are hormone-activated regulators of FOXO and mammalian glucose homeostasis.* Cell, 2011. **145**(4): p. 607-21.

33. Czubryt, M.P., et al., *Regulation of peroxisome proliferator-activated receptor gamma coactivator 1 alpha (PGC-1 alpha) and mitochondrial function by MEF2 and HDAC5.* Proc Natl Acad Sci U S A, 2003. **100**(4): p. 1711-6.

34. Canto, C., et al., *AMPK regulates energy expenditure by modulating NAD+ metabolism and SIRT1 activity.* Nature, 2009. **458**(7241): p. 1056-60.

35. Ljubicic, V. and B.J. Jasmin, *AMP-activated protein kinase at the nexus of therapeutic skeletal muscle plasticity in Duchenne muscular dystrophy.* Trends Mol Med, 2013. **19**(10): p. 614-24.

36. Peralta, S., et al., *Sustained AMPK activation improves muscle function in a mitochondrial myopathy mouse model by promoting muscle fiber regeneration.* Hum Mol Genet, 2016. **25**(15): p. 3178-3191.

37. Marcinko, K., et al., *The AMPK activator R419 improves exercise capacity and skeletal muscle insulin sensitivity in obese mice.* Mol Metab, 2015. **4**(9): p. 643-51.

38. Mounier, R., et al., *Expanding roles for AMPK in skeletal muscle plasticity.* Trends Endocrinol Metab, 2015. **26**(6): p. 275-86.

39. Bujak, A.L., et al., *AMPK activation of muscle autophagy prevents fasting-induced hypoglycemia and myopathy during aging.* Cell Metab, 2015. **21**(6): p. 883-90.

40. Ducommun, S., et al., *Motif affinity and mass spectrometry proteomic approach for the discovery of cellular AMPK targets: identification of mitochondrial fission factor as a new AMPK substrate.* Cell Signal, 2015. **27**(5): p. 978-88.

41. Otera, H., et al., *Mff is an essential factor for mitochondrial recruitment of Drp1 during mitochondrial fission in mammalian cells.* J Cell Biol, 2010. **191**(6): p. 1141-58.

42. Tondera, D., et al., *SLP-2 is required for stress-induced mitochondrial hyperfusion.* Embo j, 2009. **28**(11): p. 1589-600.

43. Rambold, A.S., S. Cohen, and J. Lippincott-Schwartz, *Fatty acid trafficking in starved cells: regulation by lipid droplet lipolysis, autophagy, and mitochondrial fusion dynamics.* Dev Cell, 2015. **32**(6): p. 678-92.

44. Chan, D.C., *Fusion and fission: interlinked processes critical for mitochondrial health.* Annu Rev Genet, 2012. **46**: p. 265-87.

45. Egan, D.F., et al., *Phosphorylation of ULK1 (hATG1) by AMP-activated protein kinase connects energy sensing to mitophagy.* Science, 2011. **331**(6016): p. 456-61.

46. Alers, S., et al., *Role of AMPK-mTOR-Ulk1/2 in the regulation of autophagy: cross talk, shortcuts, and feedbacks.* Mol Cell Biol, 2012. **32**(1): p. 2-11.

47. Weerasekara, V.K., et al., *Metabolic-stress-induced rearrangement of the 14-3-3zeta interactome promotes autophagy via a ULK1- and AMPK-regulated 14-3-3zeta interaction with phosphorylated Atg9.* Mol Cell Biol, 2014. **34**(24): p. 4379-88.

48. Kim, J., et al., *Differential regulation of distinct Vps34 complexes by AMPK in nutrient stress and autophagy.* Cell, 2013. **152**(1-2): p. 290-303.

49. Zhang, B.B., G. Zhou, and C. Li, *AMPK: an emerging drug target for diabetes and the metabolic syndrome.* Cell Metab, 2009. **9**(5): p. 407-16.

50. Li, W., et al., *Targeting AMPK for cancer prevention and treatment.* Oncotarget, 2015. **6**(10): p. 7365-78.

51. Carlson, M., B.C. Osmond, and D. Botstein, *Mutants of yeast defective in sucrose utilization.* Genetics, 1981. **98**(1): p. 25-40.

52. Woods, A., et al., *LKB1 is the upstream kinase in the AMP-activated protein kinase cascade.* Curr Biol, 2003. **13**(22): p. 2004-8.

53. Hawley, S.A., et al., *Complexes between the LKB1 tumor suppressor, STRAD alpha/beta and MO25 alpha/beta are upstream kinases in the AMP-activated protein kinase cascade.* J Biol, 2003. **2**(4): p. 28.

54. Shaw, R.J., et al., *The tumor suppressor LKB1 kinase directly activates AMP-activated kinase and regulates apoptosis in response to energy stress.* Proc Natl Acad Sci U S A, 2004. **101**(10): p. 3329-35.

55. Hedbacker, K. and M. Carlson, *SNF1/AMPK pathways in yeast.* Front Biosci, 2008. **13**: p. 2408-20.

56. Amodeo, G.A., M.J. Rudolph, and L. Tong, *Crystal structure of the heterotrimer core of Saccharomyces cerevisiae AMPK homologue SNF1.* Nature, 2007. **449**: p. 492.

57. Celenza, J.L. and M. Carlson, *Cloning and genetic mapping of SNF1, a gene required for expression of glucose-repressible genes in Saccharomyces cerevisiae.* Mol Cell Biol, 1984. **4**(1): p. 49-53.

58. Celenza, J.L. and M. Carlson, *A yeast gene that is essential for release from glucose repression encodes a protein kinase.* Science, 1986. **233**(4769): p. 1175-80.

59. Celenza, J.L. and M. Carlson, *Structure and expression of the SNF1 gene of Saccharomyces cerevisiae.* Mol Cell Biol, 1984. **4**(1): p. 54-60.

60. Jiang, R. and M. Carlson, *The Snf1 protein kinase and its activating subunit, Snf4, interact with distinct domains of the Sip1/Sip2/Gal83 component in the kinase complex.* Mol Cell Biol, 1997. **17**(4): p. 2099-106.

61. Jiang, R. and M. Carlson, *Glucose regulates protein interactions within the yeast SNF1 protein kinase complex.* Genes Dev, 1996. **10**(24): p. 3105-15.

62. McCartney, R.R. and M.C. Schmidt, *Regulation of Snf1 kinase. Activation requires phosphorylation of threonine 210 by an upstream kinase as well as a distinct step mediated by the Snf4 subunit.* J Biol Chem, 2001. **276**(39): p. 36460-6.

63. Schmidt, M.C. and R.R. McCartney, *beta-subunits of Snf1 kinase are required for kinase function and substrate definition.* EMBO J, 2000. **19**(18): p. 4936-43.

64. Vincent, O., et al., *Subcellular localization of the Snf1 kinase is regulated by specific beta subunits and a novel glucose signaling mechanism.* Genes Dev, 2001. **15**(9): p. 1104-14.

65. Hedbacker, K., S.P. Hong, and M. Carlson, *Pak1 protein kinase regulates activation and nuclear localization of Snf1-Gal83 protein kinase.* Mol Cell Biol, 2004. **24**(18): p. 8255-63.

66. Yang, X., R. Jiang, and M. Carlson, *A family of proteins containing a conserved domain that mediates interaction with the yeast SNF1 protein kinase complex.* EMBO J, 1994. **13**(24): p. 5878-86.

67. Wiatrowski, H.A., et al., *Mutations in the gal83 glycogen-binding domain activate the snf1/gal83 kinase pathway by a glycogen-independent mechanism.* Mol Cell Biol, 2004. **24**(1): p. 352-61.

68. Ashrafi, K., et al., *Sip2p and its partner snf1p kinase affect aging in S. cerevisiae.* Genes Dev, 2000. **14**(15): p. 1872-85.

69. McCartney, R.R., E.M. Rubenstein, and M.C. Schmidt, *Snf1 kinase complexes with different beta subunits display stress-dependent preferences for the three Snf1-activating kinases.* Curr Genet, 2005. **47**(6): p. 335-44.

70. Mitchelhill, K.I., et al., *Mammalian AMP-activated protein kinase shares structural and functional homology with the catalytic domain of yeast Snf1 protein kinase.* J Biol Chem, 1994. **269**(4): p. 2361-4.

71. Woods, A., et al., *Yeast SNF1 is functionally related to mammalian AMP-activated protein kinase and regulates acetyl-CoA carboxylase in vivo.* J Biol Chem, 1994. **269**(30): p. 19509-15.

72. Wilson, W.A., S.A. Hawley, and D.G. Hardie, *Glucose repression/derepression in budding yeast: SNF1 protein kinase is activated by phosphorylation under derepressing conditions, and this correlates with a high AMP:ATP ratio.* Curr Biol, 1996. **6**(11): p. 1426-34.

73. Adams, J., et al., *Intrasteric control of AMPK via the gamma1 subunit AMP allosteric regulatory site.* Protein Sci, 2004. **13**(1): p. 155-65.

74. Coccetti, P., R. Nicastro, and F. Tripodi, *Conventional and emerging roles of the energy sensor Snf1/AMPK in Saccharomyces cerevisiae.* Microb Cell, 2018. **5**(11): p. 482-494.

75. DeMille, D., et al., *PAS kinase is activated by direct SNF1-dependent phosphorylation and mediates inhibition of TORC1 through the phosphorylation and activation of Pbp1.* Mol Biol Cell, 2015. **26**(3): p. 569-82.

76. Zhang, D.D., et al., *Per-Arnt-Sim Kinase (PASK): An Emerging Regulator of Mammalian Glucose and Lipid Metabolism.* Nutrients, 2015. **7**(9): p. 7437-50.

77. Hao, H.X., et al., *PAS kinase is required for normal cellular energy balance.* Proc Natl Acad Sci U S A, 2007. **104**(39): p. 15466-71.

78. da Silva Xavier, G., J. Rutter, and G.A. Rutter, *Involvement of Per-Arnt-Sim (PAS) kinase in the stimulation of preproinsulin and pancreatic duodenum homeobox 1 gene expression by glucose.* Proc Natl Acad Sci U S A, 2004. **101**(22): p. 8319-24.

79. DeMille, D., et al., *The Regulation of Cbf1 by PAS Kinase Is a Pivotal Control Point for Lipogenesis Versus Respiration in Saccharomyces cerevisiae.* G3 (Bethesda), 2018.

80. Semache, M., et al., *Per-Arnt-Sim kinase regulates pancreatic duodenal homeobox-1 protein stability via phosphorylation of glycogen synthase kinase 3beta in pancreatic beta-cells.* J Biol Chem, 2013. **288**(34): p. 24825-33.

81. Smith, T.L. and J. Rutter, *Regulation of glucose partitioning by PAS kinase and Ugp1 phosphorylation.* Mol Cell, 2007. **26**(4): p. 491-9.

82. DeMille, D., et al., *A comprehensive protein-protein interactome for yeast PAS kinase 1 reveals direct inhibition of respiration through the phosphorylation of Cbf1.* Mol Biol Cell, 2014. **25**(14): p. 2199-215.

83. Friis, R.M.N., et al., *Rewiring AMPK and mitochondrial retrograde signaling for metabolic control of aging and histone acetylation in respiratory-defective cells.* Cell Rep, 2014. **7**(2): p. 565-574.

84. Beh, C.T., et al., *Overlapping functions of the yeast oxysterol-binding protein homologues.* Genetics, 2001. **157**(3): p. 1117-40.

85. Lehto, M., et al., *The OSBP-related protein family in humans.* J Lipid Res, 2001. **42**(8): p. 1203-13.

86. Taylor, F.R., et al., *Correlation between oxysterol binding to a cytosolic binding protein and potency in the repression of hydroxymethylglutaryl coenzyme A reductase.* J Biol Chem, 1984. **259**(20): p. 12382-7.

87. de Saint-Jean, M., et al., *Osh4p exchanges sterols for phosphatidylinositol 4-phosphate between lipid bilayers.* J Cell Biol, 2011. **195**(6): p. 965-78.

88. Ghai, R., et al., *ORP5 and ORP8 bind phosphatidylinositol-4, 5-biphosphate (PtdIns(4,5)P 2) and regulate its level at the plasma membrane.* Nat Commun, 2017. **8**(1): p. 757.

89. Im, Y.J., et al., *Structural mechanism for sterol sensing and transport by OSBP-related proteins.* Nature, 2005. **437**(7055): p. 154-8.

90. Maeda, K., et al., *Interactome map uncovers phosphatidylserine transport by oxysterol-binding proteins.* Nature, 2013. **501**(7466): p. 257-61.

91. Pietrangelo, A. and N.D. Ridgway, *Bridging the molecular and biological functions of the oxysterol-binding protein family.* Cell Mol Life Sci, 2018. **75**(17): p. 3079-3098.

92. Beh, C.T., et al., *A detour for yeast oxysterol binding proteins.* J Biol Chem, 2012. **287**(14): p. 11481-8.

93. Olkkonen, V.M. and T.P. Levine, *Oxysterol binding proteins: in more than one place at one time?* Biochem Cell Biol, 2004. **82**(1): p. 87-98.

94. Raychaudhuri, S. and W.A. Prinz, *The diverse functions of oxysterol-binding proteins.* Annu Rev Cell Dev Biol, 2010. **26**: p. 157-77.

95. Du, X., A.J. Brown, and H. Yang, *Novel mechanisms of intracellular cholesterol transport: oxysterol-binding proteins and membrane contact sites.* Curr Opin Cell Biol, 2015. **35**: p. 37-42.

96. Tian, S., et al., *Oxysterol-binding protein homologs mediate sterol transport from the endoplasmic reticulum to mitochondria in yeast.* J Biol Chem, 2018. **293**(15): p. 5636-5648.

97. Mesmin, B., et al., *A four-step cycle driven by PI(4)P hydrolysis directs sterol/PI(4)P exchange by the ER-Golgi tether OSBP.* Cell, 2013. **155**(4): p. 830-43.

98. Chung, J., et al., *INTRACELLULAR TRANSPORT. PI4P/phosphatidylserine countertransport at ORP5- and ORP8-mediated ER-plasma membrane contacts.* Science, 2015. **349**(6246): p. 428-32.

99. Moser von Filseck, J., et al., *INTRACELLULAR TRANSPORT. Phosphatidylserine transport by ORP/Osh proteins is driven by phosphatidylinositol 4-phosphate.* Science, 2015. **349**(6246): p. 432-6.

100. Babst, M., et al., *Endosomal transport function in yeast requires a novel AAA-type ATPase, Vps4p.* EMBO J, 1997. **16**(8): p. 1820-31.

101. Babst, M., et al., *The Vps4p AAA ATPase regulates membrane association of a Vps protein complex required for normal endosome function.* EMBO J, 1998. **17**(11): p. 2982-93.

102. Davies, B.A., I.F. Azmi, and D.J. Katzmann, *Regulation of Vps4 ATPase activity by ESCRT-III.* Biochem Soc Trans, 2009. **37**(Pt 1): p. 143-5.

103. Wang, P., et al., *AAA ATPases regulate membrane association of yeast oxysterol binding proteins and sterol metabolism.* EMBO J, 2005. **24**(17): p. 2989-99.

104. Galmes, R., et al., *ORP5/ORP8 localize to endoplasmic reticulum-mitochondria contacts and are involved in mitochondrial function.* EMBO Rep, 2016. **17**(6): p. 800-10.

105. Jones, D.T., W.R. Taylor, and J.M. Thornton, *The rapid generation of mutation data matrices from protein sequences.* Comput Appl Biosci, 1992. **8**(3): p. 275-82.

106. Felsenstein, J., *Confidence Limits on Phylogenies: An Approach Using the Bootstrap.* Evolution, 1985. **39**(4): p. 783-791.

107. Kumar, S., et al., *MEGA X: Molecular Evolutionary Genetics Analysis across Computing Platforms.* Mol Biol Evol, 2018. **35**(6): p. 1547-1549.

108. Zhang, J., L. Olsson, and J. Nielsen, *The beta-subunits of the Snf1 kinase in Saccharomyces cerevisiae, Gal83 and Sip2, but not Sip1, are redundant in glucose derepression and regulation of sterol biosynthesis.* Mol Microbiol, 2010. **77**(2): p. 371-83.

109. Vincent, O. and M. Carlson, *Gal83 mediates the interaction of the Snf1 kinase complex with the transcription activator Sip4.* EMBO J, 1999. **18**(23): p. 6672-81.

110. Kanki, T., D. Kang, and D.J. Klionsky, *Monitoring mitophagy in yeast: the Om45-GFP processing assay.* Autophagy, 2009. **5**(8): p. 1186-9.

111. Fukuda, T. and T. Kanki, *Mechanisms and Physiological Roles of Mitophagy in Yeast.* Mol Cells, 2018. **41**(1): p. 35-44.

112. Bergthorsson, U., D.I. Andersson, and J.R. Roth, *Ohno's dilemma: evolution of new genes under continuous selection.* Proc Natl Acad Sci U S A, 2007. **104**(43): p. 17004-9.

113. Morin, A., A.W. Moores, and M. Sacher, *Dissection of Saccharomyces cerevisiae asci.* J Vis Exp, 2009(27).

114. Wach, A., et al., *New heterologous modules for classical or PCR-based gene disruptions in Saccharomyces cerevisiae.* Yeast, 1994. **10**(13): p. 1793-808.

115. Taylor, E.B., et al., *Endurance training increases LKB1 and MO25 protein but not AMP-activated protein kinase kinase activity in skeletal muscle.* American Journal of Physiology-Endocrinology and Metabolism, 2004. **287**(6): p. E1082-E1089.

116. Pape, J.A., et al., *Per-Arnt-Sim Kinase (PASK) Deficiency Increases Cellular Respiration on a Standard Diet and Decreases Liver Triglyceride Accumulation on a Western High-Fat High-Sugar Diet.* Nutrients, 2018. **10**(12).

117. da Silva Xavier, G., et al., *Per-arnt-sim (PAS) domain-containing protein kinase is downregulated in human islets in type 2 diabetes and regulates glucagon secretion.* Diabetologia, 2011. **54**(4): p. 819-27.

118. Semplici, F., et al., *Human mutation within Per-Arnt-Sim (PAS) domain-containing protein kinase (PASK) causes basal insulin hypersecretion.* J Biol Chem, 2011. **286**(51): p. 44005-14.

119. Fontes, G., et al., *Involvement of Per-Arnt-Sim Kinase and extracellular-regulated kinases-1/2 in palmitate inhibition of insulin gene expression in pancreatic beta-cells.* Diabetes, 2009. **58**(9): p. 2048-58.

120. MacDonald, P.E. and P. Rorsman, *Per-arnt-sim (PAS) domain kinase (PASK) as a regulator of glucagon secretion.* Diabetologia, 2011. **54**(4): p. 719-21.

121. Stieg, D.C., et al., *A complex molecular switch directs stress-induced cyclin C nuclear release through SCF(Grr1)-mediated degradation of Med13.* Mol Biol Cell, 2018. **29**(3): p. 363-375.

122. Willis, S.D., et al., *Snf1 cooperates with the CWI MAPK pathway to mediate the degradation of Med13 following oxidative stress.* Microb Cell, 2018. **5**(8): p. 357-370.

123. Grose, J.H., et al., *Yeast PAS kinase coordinates glucose partitioning in response to metabolic and cell integrity signaling.* Embo j, 2007. **26**(23): p. 4824-30.

124. DeMille, D., et al., *PAS kinase is activated by direct SNF1-dependent phosphorylation and mediates inhibition of TORC1 through the phosphorylation and activation of Pbp1.* Molecular Biology of the Cell, 2015. **26**(3): p. 569-582.

125. Cardon, C.M., et al., *PAS kinase promotes cell survival and growth through activation of Rho1.* Sci Signal, 2012. **5**(209): p. ra9.

126. Cooper, K.F., *Stress and developmental regulation of the yeast C-type cyclin Ume3p (Srb11p/Ssn8p).* The EMBO Journal, 1997. **16**(15): p. 4665-4675.

127. Cooper, Katrina F., et al., *Stress-Induced Nuclear-to-Cytoplasmic Translocation of Cyclin C Promotes Mitochondrial Fission in Yeast.* Developmental Cell, 2014. **28**(2): p. 161-173.

128. Cooper, K.F., M.J. Mallory, and R. Strich, *Oxidative Stress-Induced Destruction of the Yeast C-Type Cyclin Ume3p Requires Phosphatidylinositol-Specific Phospholipase C and the 26S Proteasome.* Molecular and Cellular Biology, 1999. **19**(5): p. 3338-3348.

129. Cooper, K.F., et al., *Oxidative-stress-induced nuclear to cytoplasmic relocalization is required for Not4-dependent cyclin C destruction.* Journal of Cell Science, 2012. **125**(4): p. 1015-1026.

130. Jin, C., et al., *The Cell Wall Sensors Mtl1, Wsc1, and Mid2 Are Required for Stress-Induced Nuclear to Cytoplasmic Translocation of Cyclin C and Programmed Cell Death in Yeast.* Oxidative Medicine and Cellular Longevity, 2013. **2013**: p. 1-15.

131. Jin, C., R. Strich, and K.F. Cooper, *Slt2p phosphorylation induces cyclin C nuclear-to-cytoplasmic translocation in response to oxidative stress.* Molecular Biology of the Cell, 2014. **25**(8): p. 1396-1407.

132. Krasley, E., et al., *Regulation of the Oxidative Stress Response Through Slt2p-Dependent Destruction of Cyclin C in Saccharomyces cerevisiae.* Genetics, 2005. **172**(3): p. 1477-1486.

133. Stieg, D.C., et al., *A complex molecular switch directs stress-induced cyclin C nuclear release through SCFGrr1-mediated degradation of Med13.* Molecular Biology of the Cell, 2018. **29**(3): p. 363-375.

134. Wang, K., et al., *Cyclin C mediates stress-induced mitochondrial fission and apoptosis.* Molecular Biology of the Cell, 2015. **26**(6): p. 1030-1043.

135. Allen, B.L. and D.J. Taatjes, *The Mediator complex: a central integrator of transcription.* Nature Reviews Molecular Cell Biology, 2015. **16**(3): p. 155-166.

136. Bourbon, H.-M., *Comparative genomics supports a deep evolutionary origin for the large, four-module transcriptional mediator complex.* Nucleic Acids Research, 2008. **36**(12): p. 3993-4008.

137. Yin, J.w. and G. Wang, *The Mediator complex: a master coordinator of transcription and cell lineage development.* Development, 2014. **141**(5): p. 977-987.

138. Chi, Y., *Negative regulation of Gcn4 and Msn2 transcription factors by Srb10 cyclin-dependent kinase.* Genes & Development, 2001. **15**(9): p. 1078-1092.

139. Holstege, F.C.P., et al., *Dissecting the Regulatory Circuitry of a Eukaryotic Genome.* Cell, 1998. **95**(5): p. 717-728.

140. Surosky, R.T., R. Strich, and R.E. Esposito, *The yeast UME5 gene regulates the stability of meiotic mRNAs in response to glucose.* Molecular and Cellular Biology, 1994. **14**(5): p. 3446-3458.

141. van de Peppel, J., et al., *Mediator Expression Profiling Epistasis Reveals a Signal Transduction Pathway with Antagonistic Submodules and Highly Specific Downstream Targets.* Molecular Cell, 2005. **19**(4): p. 511-522.

142. Uversky, V.N., *Multitude of binding modes attainable by intrinsically disordered proteins: a portrait gallery of disorder-based complexes.* Chem. Soc. Rev., 2011. **40**(3): p. 1623-1634.

143. Vega, M., et al., *Hexokinase 2 Is an Intracellular Glucose Sensor of Yeast Cells That Maintains the Structure and Activity of Mig1 Protein Repressor Complex.* Journal of Biological Chemistry, 2016. **291**(14): p. 7267-7285.

144. Jendretzki, A., et al., *How do I begin? Sensing extracellular stress to maintain yeast cell wall integrity.* European Journal of Cell Biology, 2011. **90**(9): p. 740-744.

145. Heinisch, J.J. and R. Rodicio, *Protein kinase C in fungi—more than just cell wall integrity.* FEMS Microbiology Reviews, 2017. **42**(1).

146. Levin, D.E., *Regulation of Cell Wall Biogenesis in Saccharomyces cerevisiae: The Cell Wall Integrity Signaling Pathway.* Genetics, 2011. **189**(4): p. 1145-1175.

147. Lee, K.S., et al., *A yeast mitogen-activated protein kinase homolog (Mpk1p) mediates signalling by protein kinase C.* Molecular and Cellular Biology, 1993. **13**(5): p. 3067-3075.

148. Jung, U.S., et al., *Regulation of the yeast Rlm1 transcription factor by the Mpk1 cell wall integrity MAP kinase.* Molecular Microbiology, 2002. **46**(3): p. 781-789.

149. Kim, K.Y., A.W. Truman, and D.E. Levin, *Yeast Mpk1 Mitogen-Activated Protein Kinase Activates Transcription through Swi4/Swi6 by a Noncatalytic Mechanism That Requires Upstream Signal.* Molecular and Cellular Biology, 2008. **28**(8): p. 2579-2589.

150. Kim, K.-Y. and David E. Levin, *Mpk1 MAPK Association with the Paf1 Complex Blocks Sen1-Mediated Premature Transcription Termination.* Cell, 2011. **144**(5): p. 745-756.

151. Watanabe, Y., et al., *Characterization of a serum response factor-like protein in Saccharomyces cerevisiae, Rlm1, which has transcriptional activity regulated by the*

Mpk1 (Slt2) mitogen-activated protein kinase pathway. Molecular and Cellular Biology, 1997. **17**(5): p. 2615-2623.

152. Yurko, N., et al., *MPK1/SLT2 Links Multiple Stress Responses with Gene Expression in Budding Yeast by Phosphorylating Tyr1 of the RNAP II CTD.* Molecular Cell, 2017. **68**(5): p. 913-925.e3.

153. Shah, N., et al., *Tyrosine-1 of RNA Polymerase II CTD Controls Global Termination of Gene Transcription in Mammals.* Molecular Cell, 2018. **69**(1): p. 48-61.e6.

154. Khakhina, S., K.F. Cooper, and R. Strich, *Med13p prevents mitochondrial fission and programmed cell death in yeast through nuclear retention of cyclin C.* Molecular Biology of the Cell, 2014. **25**(18): p. 2807-2816.

155. Ang, X.L. and J. Wade Harper, *SCF-mediated protein degradation and cell cycle control.* Oncogene, 2005. **24**(17): p. 2860-2870.

156. Dyson, H.J. and P.E. Wright, *Intrinsically unstructured proteins and their functions.* Nature Reviews Molecular Cell Biology, 2005. **6**(3): p. 197-208.

157. Fuxreiter, M., et al., *Disordered Proteinaceous Machines.* Chemical Reviews, 2014. **114**(13): p. 6806-6843.

158. Hedbacker, K., *SNF1/AMPK pathways in yeast.* Frontiers in Bioscience, 2008. **13**(13): p. 2408.

159. Hong, S.-P. and M. Carlson, *Regulation of Snf1 Protein Kinase in Response to Environmental Stress.* Journal of Biological Chemistry, 2007. **282**(23): p. 16838-16845.

160. Hedbacker, K. and M. Carlson, *Regulation of the Nucleocytoplasmic Distribution of Snf1-Gal83 Protein Kinase.* Eukaryotic Cell, 2006. **5**(12): p. 1950-1956.

161. Hedbacker, K., S.P. Hong, and M. Carlson, *Pak1 Protein Kinase Regulates Activation and Nuclear Localization of Snf1-Gal83 Protein Kinase.* Molecular and Cellular Biology, 2004. **24**(18): p. 8255-8263.

162. Vincent, O., *Subcellular localization of the Snf1 kinase is regulated by specific beta subunits and a novel glucose signaling mechanism.* Genes & Development, 2001. **15**(9): p. 1104-1114.

163. McCartney, R.R. and M.C. Schmidt, *Regulation of Snf1 Kinase.* Journal of Biological Chemistry, 2001. **276**(39): p. 36460-36466.

164. Nath, N., R.R. McCartney, and M.C. Schmidt, *Purification and Characterization of Snf1 Kinase Complexes Containing a Defined β Subunit Composition.* Journal of Biological Chemistry, 2002. **277**(52): p. 50403-50408.

165. Sutherland, C.M., et al., *Elm1p Is One of Three Upstream Kinases for the Saccharomyces cerevisiae SNF1 Complex.* Current Biology, 2003. **13**(15): p. 1299-1305.

166. James, P., J. Halladay, and E.A. Craig, *Genomic libraries and a host strain designed for highly efficient two-hybrid selection in yeast.* Genetics, 1996. **144**(4): p. 1425-36.

167. Gonzalez, D., et al., *Suppression of Mediator is regulated by Cdk8-dependent Grr1 turnover of the Med3 coactivator.* Proceedings of the National Academy of Sciences, 2014. **111**(7): p. 2500-2505.

168. Wang, R. and M.J. Solomon, *Identification of She3 as an SCFGrr1 Substrate in Budding Yeast.* PLoS ONE, 2012. **7**(10): p. e48020.

169. Carmona-Gutierrez, D., et al., *Apoptosis in yeast: triggers, pathways, subroutines.* Cell Death & Differentiation, 2010. **17**(5): p. 763-773.

170. Galluzzi, L., et al., *Programmed Necrosis*, in *International Review of Cell and Molecular Biology*. 2011, Elsevier. p. 1-35.

171. Madeo, F., et al., *Oxygen Stress: A Regulator of Apoptosis in Yeast.* The Journal of Cell Biology, 1999. **145**(4): p. 757-767.

172. Rutter, J., et al., *PAS kinase: An evolutionarily conserved PAS domain-regulated serine/threonine kinase.* Proceedings of the National Academy of Sciences, 2001. **98**(16): p. 8991-8996.

173. DeMille, D., et al., *A comprehensive protein–protein interactome for yeast PAS kinase 1 reveals direct inhibition of respiration through the phosphorylation of Cbf1.* Molecular Biology of the Cell, 2014. **25**(14): p. 2199-2215.

174. Grose, J.H., et al., *Yeast PAS kinase coordinates glucose partitioning in response to metabolic and cell integrity signaling.* The EMBO Journal, 2007. **26**(23): p. 4824-4830.

175. Lubitz, T., et al., *Network reconstruction and validation of the Snf1/AMPK pathway in baker's yeast based on a comprehensive literature review.* npj Systems Biology and Applications, 2015. **1**(1).

176. Estruch, F. and M. Carlson, *Increased dosage of theMSN1gene restores invertase expression in yeast mutants defective in the SNF1 protein kinase.* Nucleic Acids Research, 1990. **18**(23): p. 6959-6964.

177. Hong, S.P. and M. Carlson, *Regulation of snf1 protein kinase in response to environmental stress.* J Biol Chem, 2007. **282**(23): p. 16838-45.

178. Shashkova, S., N. Welkenhuysen, and S. Hohmann, *Molecular communication: crosstalk between the Snf1 and other signaling pathways.* FEMS Yeast Research, 2015. **15**(4).

179. Backhaus, K., et al., *Mutations in SNF1 complex genes affect yeast cell wall strength.* European Journal of Cell Biology, 2013. **92**(12): p. 383-395.

180. Benanti, J.A., et al., *A proteomic screen reveals SCFGrr1 targets that regulate the glycolytic–gluconeogenic switch.* Nature Cell Biology, 2007. **9**(10): p. 1184-1191.

181. Albuquerque, C.P., et al., *A Multidimensional Chromatography Technology for In-depth Phosphoproteome Analysis.* Molecular & Cellular Proteomics, 2008. **7**(7): p. 1389-1396.

182. Kanshin, E., et al., *Machine Learning of Global Phosphoproteomic Profiles Enables Discrimination of Direct versus Indirect Kinase Substrates.* Molecular & Cellular Proteomics, 2017. **16**(5): p. 786-798.

183. Dale, S., et al., *Similar substrate recognition motifs for mammalian AMP-activated protein kinase, higher plant HMG-CoA reductase kinase-A, yeast SNF1, and mammalian calmodulin-dependent protein kinase I.* FEBS Letters, 1995. **361**(2-3): p. 191-195.

184. Mok, J., et al., *Deciphering Protein Kinase Specificity Through Large-Scale Analysis of Yeast Phosphorylation Site Motifs.* Science Signaling, 2010. **3**(109): p. ra12-ra12.

185. Kuchin, S., I. Treich, and M. Carlson, *A regulatory shortcut between the Snf1 protein kinase and RNA polymerase II holoenzyme.* Proceedings of the National Academy of Sciences, 2000. **97**(14): p. 7916-7920.

186. Chang, Y.-W., S.C. Howard, and P.K. Herman, *The Ras/PKA Signaling Pathway Directly Targets the Srb9 Protein, a Component of the General RNA Polymerase II Transcription Apparatus.* Molecular Cell, 2004. **15**(1): p. 107-116.

187. Smith, F.C., et al., *The SNF1 kinase complex from Saccharomyces cerevisiae phosphorylates the transcriptional repressor protein Mig1p in vitro at four sites within or near regulatory domain 1.* FEBS Letters, 1999. **453**(1-2): p. 219-223.

188. Nigg, E.A., *Cellular substrates of p34cdc2 and its companion cyclin-dependent kinases.* Trends in Cell Biology, 1993. **3**(9): p. 296-301.

189. Wright, P.E. and H.J. Dyson, *Intrinsically disordered proteins in cellular signalling and regulation.* Nature Reviews Molecular Cell Biology, 2014. **16**(1): p. 18-29.

190. Diella, F., *Understanding eukaryotic linear motifs and their role in cell signaling and regulation.* Frontiers in Bioscience, 2008. **Volume**(13): p. 6580.

191. Tompa, P., *The interplay between structure and function in intrinsically unstructured proteins.* FEBS Letters, 2005. **579**(15): p. 3346-3354.

192. Collins, M.O., et al., *Phosphoproteomic Analysis of the Mouse Brain Cytosol Reveals a Predominance of Protein Phosphorylation in Regions of Intrinsic Sequence Disorder.* Molecular & Cellular Proteomics, 2008. **7**(7): p. 1331-1348.

193. Trudeau, T., et al., *Structure and Intrinsic Disorder in Protein Autoinhibition.* Structure, 2013. **21**(3): p. 332-341.

194. Shevade, A., et al., *Mitochondrial Voltage-Dependent Anion Channel Protein Por1 Positively Regulates the Nuclear Localization of Saccharomyces cerevisiae AMP-Activated Protein Kinase.* mSphere, 2018. **3**(1).

195. Elbing, K., Rhonda R. McCartney, and Martin C. Schmidt, *Purification and characterization of the three Snf1-activating kinases ofSaccharomyces cerevisiae.* Biochemical Journal, 2006. **393**(3): p. 797-805.

196. Vallier, L.G. and M. Carlson, *Synergistic release from glucose repression by mig1 and ssn mutations in Saccharomyces cerevisiae.* Genetics, 1994. **137**(1): p. 49-54.

197. Treitel, M.A., S. Kuchin, and M. Carlson, *Snf1 Protein Kinase Regulates Phosphorylation of the Mig1 Repressor inSaccharomyces cerevisiae.* Molecular and Cellular Biology, 1998. **18**(11): p. 6273-6280.

198. RodrÍGuez, A., et al., *The hexokinase 2 protein regulates the expression of the GLK1, HXK1 and HXK2 genes of Saccharomyces cerevisiae.* Biochemical Journal, 2001. **355**(3): p. 625-631.

199. De Vit, M.J., J.A. Waddle, and M. Johnston, *Regulated nuclear translocation of the Mig1 glucose repressor.* Molecular Biology of the Cell, 1997. **8**(8): p. 1603-1618.

200. Fernández-García, P., et al., *Phosphorylation of Yeast Hexokinase 2 Regulates Its Nucleocytoplasmic Shuttling.* Journal of Biological Chemistry, 2012. **287**(50): p. 42151-42164.

201. Strich, R., M.R. Slater, and R.E. Esposito, *Identification of negative regulatory genes that govern the expression of early meiotic genes in yeast.* Proceedings of the National Academy of Sciences, 1989. **86**(24): p. 10018-10022.

202. Ye, T., K. Elbing, and S. Hohmann, *The pathway by which the yeast protein kinase Snf1p controls acquisition of sodium tolerance is different from that mediating glucose regulation.* Microbiology, 2008. **154**(9): p. 2814-2826.

203. Shirra, M.K., et al., *A Chemical Genomics Study Identifies Snf1 as a Repressor ofGCN4Translation.* Journal of Biological Chemistry, 2008. **283**(51): p. 35889-35898.

204. Bourbon, H.-M., et al., *A Unified Nomenclature for Protein Subunits of Mediator Complexes Linking Transcriptional Regulators to RNA Polymerase II.* Molecular Cell, 2004. **14**(5): p. 553-557.

205. Longtine, M.S., et al., *Additional modules for versatile and economical PCR-based gene deletion and modification in Saccharomyces cerevisiae.* Yeast, 1998. **14**(10): p. 953-961.

206. Simpson-Lavy, K.J. and M. Johnston, *SUMOylation regulates the SNF1 protein kinase.* Proceedings of the National Academy of Sciences, 2013. **110**(43): p. 17432-17437.

207. Strogolova, V., et al., *Mitochondrial Porin Por1 and Its Homolog Por2 Contribute to the Positive Control of Snf1 Protein Kinase in Saccharomyces cerevisiae.* Eukaryotic Cell, 2012. **11**(12): p. 1568-1572.

208. Cooper, K.F., et al., *Ama1p is a meiosis-specific regulator of the anaphase promoting complex/cyclosome in yeast.* Proceedings of the National Academy of Sciences, 2000. **97**(26): p. 14548-14553.

209. Pérez-Sampietro, M., C. Casas, and E. Herrero, *The AMPK Family Member Snf1 Protects Saccharomyces cerevisiae Cells upon Glutathione Oxidation.* PLoS ONE, 2013. **8**(3): p. e58283.

210. Huang, M., et al., *PSK1 regulates expression of SOD1 involved in oxidative stress tolerance in yeast.* FEMS Microbiol Lett, 2014. **350**(2): p. 154-60.

211. Van Criekinge, W. and R. Beyaert, *Yeast Two-Hybrid: State of the Art.* Biol Proced Online, 1999. **2**: p. 1-38.

212. Sikorski, R.S. and P. Hieter, *A system of shuttle vectors and yeast host strains designed for efficient manipulation of DNA in Saccharomyces cerevisiae.* Genetics, 1989. **122**(1): p. 19-27.

213. Fuxreiter, M., P. Tompa, and I. Simon, *Local structural disorder imparts plasticity on linear motifs.* Bioinformatics, 2007. **23**(8): p. 950-956.

214. Vuzman, D., Y. Hoffman, and Y. Levy, *MODULATING PROTEIN–DNA INTERACTIONS BY POST-TRANSLATIONAL MODIFICATIONS AT DISORDERED REGIONS*, in *Biocomputing 2012*. 2011, WORLD SCIENTIFIC.

215. Strich, R. and K. Cooper, *The dual role of cyclin C connects stress regulated gene expression to mitochondrial dynamics.* Microbial Cell, 2014. **1**(10): p. 318-324.

216. Galluzzi, L., et al., *Essential versus accessory aspects of cell death: recommendations of the NCCD 2015.* Cell Death Differ, 2015. **22**(1): p. 58-73.

217. Nagulapalli, M., et al., *Evolution of disorder in Mediator complex and its functional relevance.* Nucleic Acids Research, 2015. **44**(4): p. 1591-1612.

218. Knuesel, M.T., et al., *The human CDK8 subcomplex is a molecular switch that controls Mediator coactivator function.* Genes & Development, 2009. **23**(4): p. 439-451.

219. Tóth-Petróczy, Á., et al., *Malleable Machines in Transcription Regulation: The Mediator Complex.* PLoS Computational Biology, 2008. **4**(12): p. e1000243.

220. Uversky, V.N., *The most important thing is the tail: Multitudinous functionalities of intrinsically disordered protein termini.* FEBS Letters, 2013. **587**(13): p. 1891-1901.

221. Hsiung, Y.G., et al., *F-Box Protein Grr1 Interacts with Phosphorylated Targets via the Cationic Surface of Its Leucine-Rich Repeat.* Molecular and Cellular Biology, 2001. **21**(7): p. 2506-2520.

222. Gonzalez, D., et al., *Suppression of Mediator is regulated by Cdk8-dependent Grr1 turnover of the Med3 coactivator.* Proc Natl Acad Sci U S A, 2014. **111**(7): p. 2500-5.

223. Gomar-Alba, M., et al., *Whi7 is an unstable cell-cycle repressor of the Start transcriptional program.* Nature Communications, 2017. **8**(1).

224. Galluzzi, L., et al., *Programmed necrosis from molecules to health and disease.* Int Rev Cell Mol Biol, 2011. **289**: p. 1-35.

225. Skowyra, D., et al., *F-Box Proteins Are Receptors that Recruit Phosphorylated Substrates to the SCF Ubiquitin-Ligase Complex.* Cell, 1997. **91**(2): p. 209-219.

226. Davis, M.A., et al., *The SCF-Fbw7 ubiquitin ligase degrades MED13 and MED13L and regulates CDK8 module association with Mediator.* Genes & Development, 2013. **27**(2): p. 151-156.

227. Yachdav, G., et al., *PredictProtein—an open resource for online prediction of protein structural and functional features.* Nucleic Acids Research, 2014. **42**(W1): p. W337-W343.

228. Krasley, E., et al., *Regulation of the oxidative stress response through Slt2p-dependent destruction of cyclin C in Saccharomyces cerevisiae.* Genetics, 2006. **172**(3): p. 1477-86.

229. Chang, Y.W., S.C. Howard, and P.K. Herman, *The Ras/PKA signaling pathway directly targets the Srb9 protein, a component of the general RNA polymerase II transcription apparatus.* Mol Cell, 2004. **15**(1): p. 107-16.

230. Poss, Zachary C., et al., *Identification of Mediator Kinase Substrates in Human Cells using Cortistatin A and Quantitative Phosphoproteomics.* Cell Reports, 2016. **15**(2): p. 436-450.

231. Kinoshita, E., et al., *Phosphate-binding tag, a new tool to visualize phosphorylated proteins.* Mol Cell Proteomics, 2006. **5**(4): p. 749-57.

232. Bachmair, A., D. Finley, and A. Varshavsky, *In vivo half-life of a protein is a function of its amino-terminal residue.* Science, 1986. **234**(4773): p. 179-186.

233. Varshavsky, A., *The N-end rule.* Cell, 1992. **69**(5): p. 725-735.

234. Gnanasundram, S.V. and M. Kos, *Fast protein-depletion system utilizing tetracycline repressible promoter and N-end rule in yeast.* Mol Biol Cell, 2015. **26**(4): p. 762-8.

235. Staleva, L., A. Hall, and S.J. Orlow, *Oxidative Stress Activates FUS1 and RLM1 Transcription in the Yeast Saccharomyces cerevisiae in an Oxidant-dependent Manner.* Molecular Biology of the Cell, 2004. **15**(12): p. 5574-5582.

236. Jin, C., et al., *The MAPKKKs Ste11 and Bck1 jointly transduce the high oxidative stress signal through the cell wall integrity MAP kinase pathway.* Microbial Cell, 2015. **2**(9): p. 329-342.

237. Holt, L.J., et al., *Global Analysis of Cdk1 Substrate Phosphorylation Sites Provides Insights into Evolution.* Science, 2009. **325**(5948): p. 1682-1686.

238. Asano, S., et al., *Concerted mechanism of Swe1/Wee1 regulation by multiple kinases in budding yeast.* The EMBO Journal, 2005. **24**(12): p. 2194-2204.

239. Yoshida, S., et al., *Polo-Like Kinase Cdc5 Controls the Local Activation of Rho1 to Promote Cytokinesis.* Science, 2006. **313**(5783): p. 108-111.

240. Watanabe, N., et al., *M-phase kinases induce phospho-dependent ubiquitination of somatic Wee1 by SCF -TrCP.* Proceedings of the National Academy of Sciences, 2004. **101**(13): p. 4419-4424.

241. Dodou, E. and R. Treisman, *The Saccharomyces cerevisiae MADS-box transcription factor Rlm1 is a target for the Mpk1 mitogen-activated protein kinase pathway.* Molecular and Cellular Biology, 1997. **17**(4): p. 1848-1859.

242. Dosztanyi, Z., et al., *IUPred: web server for the prediction of intrinsically unstructured regions of proteins based on estimated energy content.* Bioinformatics, 2005. **21**(16): p. 3433-3434.

243. Dosztanyi, Z., B. Meszaros, and I. Simon, *ANCHOR: web server for predicting protein binding regions in disordered proteins.* Bioinformatics, 2009. **25**(20): p. 2745-2746.

244. Kelley, L.A., et al., *The Phyre2 web portal for protein modeling, prediction and analysis.* Nature Protocols, 2015. **10**(6): p. 845-858.

245. Liu, H.Y., et al., *Characterization of CAF4 and CAF16 reveals a functional connection between the CCR4-NOT complex and a subset of SRB proteins of the RNA polymerase II holoenzyme.* J Biol Chem, 2001. **276**(10): p. 7541-8.

246. Wery, M., et al., *Members of the SAGA and Mediator complexes are partners of the transcription elongation factor TFIIS.* The EMBO Journal, 2004. **23**(21): p. 4232-4242.

247. Kotta-Loizou, I., G.N. Tsaousis, and S.J. Hamodrakas, *Analysis of Molecular Recognition Features (MoRFs) in membrane proteins.* Biochim Biophys Acta, 2013. **1834**(4): p. 798-807.

248. Muncke, N., et al., *Missense Mutations and Gene Interruption in PROSIT240 , a Novel TRAP240 -Like Gene, in Patients With Congenital Heart Defect (Transposition of the Great Arteries).* Circulation, 2003. **108**(23): p. 2843-2850.

249. Adegbola, A., et al., *Redefining the MED13L syndrome.* European Journal of Human Genetics, 2015. **23**(10): p. 1308-1317.

250. van Haelst, M.M., et al., *Further confirmation of the MED13L haploinsufficiency syndrome.* European Journal of Human Genetics, 2014. **23**(1): p. 135-138.

251. Yamamoto, T., et al., *MED13L haploinsufficiency syndrome: A de novo frameshift and recurrent intragenic deletions due to parental mosaicism.* American Journal of Medical Genetics Part A, 2017. **173**(5): p. 1264-1269.

252. Asadollahi, R., et al., *Genotype-phenotype evaluation of MED13L defects in the light of a novel truncating and a recurrent missense mutation.* European Journal of Medical Genetics, 2017. **60**(9): p. 451-464.

253. Enserink, J.M. and R.D. Kolodner, *An overview of Cdk1-controlled targets and processes.* Cell Division, 2010. **5**(1): p. 11.

254. Akhoondi, S., et al., *FBXW7/hCDC4Is a General Tumor Suppressor in Human Cancer.* Cancer Research, 2007. **67**(19): p. 9006-9012.

255. Welcker, M. and B.E. Clurman, *FBW7 ubiquitin ligase: a tumour suppressor at the crossroads of cell division, growth and differentiation.* Nature Reviews Cancer, 2008. **8**(2): p. 83-93.

256. Li, N., et al., *Cyclin C is a haploinsufficient tumour suppressor.* Nature Cell Biology, 2014. **16**(11): p. 1080-1091.

257. Gari, E., et al., *A set of vectors with a tetracycline-regulatable promoter system for modulated gene expression in Saccharomyces cerevisiae.* Yeast, 1997. **13**(9): p. 837-48.

258. Cooper, K.F. and R. Strich, *Functional analysis of the Ume3p/ Srb11p-RNA polymerase II holoenzyme interaction.* Gene Expr, 1999. **8**(1): p. 43-57.

259. Wang, K., et al., *Thyrocyte-specific inativation of cyclin C and PTEN accelerates thyroid hyperplasia and carcinoma development.* In preperation, 2014.

260. Zhang, T., et al., *An improved method for whole protein extraction from yeast Saccharomyces cerevisiae.* Yeast, 2011. **28**(11): p. 795-798.

261. Tan, G.S., J. Magurno, and K.F. Cooper, *Ama1p-activated anaphase-promoting complex regulates the destruction of Cdc20p during meiosis II.* Molecular Biology of the Cell, 2011. **22**(3): p. 315-326.

262. Guacci, V., E. Hogan, and D. Koshland, *Centromere position in budding yeast: evidence for anaphase A.* Molecular Biology of the Cell, 1997. **8**(6): p. 957-972.

263. Martin, H., et al., *Regulatory Mechanisms for Modulation of Signaling through the Cell Integrity Slt2-mediated Pathway in Saccharomyces cerevisiae.* Journal of Biological Chemistry, 2000. **275**(2): p. 1511-1519.

264. Carmody, S.R., et al., *The Mitogen-Activated Protein Kinase Slt2 Regulates Nuclear Retention of Non-Heat Shock mRNAs during Heat Shock-Induced Stress.* Molecular and Cellular Biology, 2010. **30**(21): p. 5168-5179.

265. Naylor, K., et al., *Mdv1 interacts with assembled dnm1 to promote mitochondrial division.* J Biol Chem, 2006. **281**(4): p. 2177-83.